



Separation and determination of cadmium in water samples based on functionalized carbon nanotube by syringe filter membrane-micro solid-phase extraction

Jamshid Rakhtshah ^{a,*}

^a Department of Inorganic Chemistry, Faculty of Chemistry, University of Tabriz, Tabriz, Iran

ARTICLE INFO:

Received 19 Nov 2020
 Revised form 25 Jan 2021
 Accepted 22 Feb 2021
 Available online 28 Mar 2021

Keywords:

Cadmium,
 Separation,
 Water,
 Functionalized carbon nanotubes,
 Syringe filter membrane micro solid phase extraction,
 Atom trap flame atomic absorption spectrometry

ABSTRACT

A simple and fast separation of cadmium (Cd) based on functionalized carbon nanotubes with 2,3-dimercapto-1-propanol (CNTs@DHSP) was achieved in water samples before a determination by atom trap flame atomic absorption spectrometry (AT-FAAS). In this study, Cd(II) ions were extracted by syringe filter membrane-micro solid phase extraction procedure (SFM- μ -SPE). Firstly, 20 mg of the CNTs@DHSP as solid-phase added to 20 mL of water sample in a syringe, then dispersed for 3 min after adjusting pH up to 7 and pass through SFM very slowly. After extraction, the Cd(II) ions were back-extracted from SFM/CNTs@DHSP by 1.0 mL of eluent in acidic pH. Finally, the cadmium concentration was measured by AT-FAAS. Under the optimal conditions, the linear range (2–90 $\mu\text{g L}^{-1}$), LOD (0.75 $\mu\text{g L}^{-1}$) and enrichment factor (19.6) were obtained (RSD<1.5%). The adsorption capacity of Cd(II) with the CNTs@DHSP was obtained about 152.6 mg g⁻¹. The method was validated by certified reference materials (SRM, NIST) and ET-AAS in water samples.

1. Introduction

Cadmium (Cd) as a toxic non-essential metal release from industrial activity to water, soil, food, agricultural product and air, then, cadmium ions cause to environmental and human health hazards. Cadmium is naturally creating in the environment matrixes from agricultural and chemical industrial sources. The sources of cadmium have various applications in different industry such as PVC products in petrochemical industries, pigments in color factories, and Ni-Cd batteries [1,2]. The cadmium enters to the human body through

gastrointestinal and respiratory tract system from food, water, air pollution and smoking. The cadmium exposure causes to hepatic dysfunction, the pulmonary edema, the testicular damage, the osteoporosis and cancer in different organs such as, breast, renal, lung and pancreas [3,4]. The Cd ions absorb through the respiratory tract or the gastrointestinal tract and enters into the bloodstream via erythrocytes and accumulated in the kidneys liver [5]. Cadmium ions excrete from the human body through urine. The liver and kidneys are able to synthesize metallothioneins (MT) which protect the cells from cadmium toxicity through bonding to cadmium (Cd- MT) [6]. Mitochondria play a crucial role in the formation of ROS (reactive oxygen species) for cadmium [7]. Moreover, the different methodologies

*Corresponding Author: [Jamshid Rakhtshah](mailto:Jamshid.Rakhtshah)

Email: jamshid_rakhtshah@yahoo.com

<https://doi.org/10.24200/amecj.v4.i01.132>

such as microbial fermentation based on TiO_2 nanoparticles have been used to remove cadmium from waters efficiently [8,9]. The cytotoxic effects of cadmium cause to apoptotic effect in human which was reported by international Agency for research on cancer (IARC) [10]. *Itai itai* disease or osteomalacia is chronic cadmium poisoning was reported in Japan. The cadmium intake to the human body is about $7 \mu\text{g Cd}$ per week. This value cause to create the cadmium concentration in renal and urine between $100\text{-}200 \mu\text{g g}^{-1}$ and less than $0.5 \mu\text{g g}^{-1}$ creatinine, respectively. Blood and urinary cadmium at $0.38 \mu\text{g L}^{-1}$ and $0.67 \mu\text{g g}^{-1}$ creatinine were associated with tubular impairment. Urinary cadmium at $0.8 \mu\text{g g}^{-1}$ creatinine was associated with glomerular impairment [11]. So, the extraction and determination of Cd(II) in waters is very important, due to the environment and human health safety. Recently, various analytical techniques can be used for cadmium extraction in different water, foods and environmental samples. The various methods such as flame atomic absorption spectrometry (AAS) [12], the optical microscopy based on laser-induced photoluminescence (UV-VIS-NIR) [13], the $\text{SrFe}_{12}\text{O}_{19}$ @CTAB magnetic nanoparticles with electrothermal atomic absorption spectrometry (ET-AAS) [14-17], the colorimetric sensor [18], the electrothermal vaporization coupled with optical emission spectrometry with inductively coupled plasma (ETV-ICP-OES) [19] and laser-induced breakdown spectroscopy (LIBS) [20] were used for cadmium determination in various environmental samples. Due to the low concentration of cadmium in water samples and difficulty matrixes in wastewater samples, the pretreatment is required before the determination of cadmium by instrumental analysis. The different extraction methods such as, the ultrasound-assisted liquid-liquid spray extraction (USA-LLSE) [21], the solvent extraction [22], the liquid-liquid extraction [23], the cloud point assisted dispersive ionic liquid-liquid microextraction [24] the dispersive solid-phase extraction (DSPE) combined with ultrasound-assisted emulsification microextraction [25], solid-phase extraction (SPE) [26, 27], the coagulating homogenous dispersive micro solid-phase extraction exploiting

graphene oxide nanosheets (CHD- μSPE)[28] and graphene oxide-packed micro-column solid-phase extraction[29] were used before cadmium analysis in water samples. Recently, the membrane micro solid-phase extraction procedure (M- μSPE) was reported as micro SPE (μSPE) for separation/determination of cadmium in water samples. This method showed several advantages, such as easy and fast extraction of cadmium in water samples. The properties of adsorbents have a main role for cadmium extraction by the syringe filter membrane micro solid-phase extraction procedure (SFM- μSPE). In this study, a novel sorbent based on CNTs@DHSP was used for extraction of Cd(II) in water and wastewater samples by SFM- μSPE at pH of 7. The proposed method was validated with CRM and spike samples in waters and high recovery was obtained by AT-FAAS.

2. Experimental

2.1. Material and Methods

Atom trap flame atomic absorption spectrophotometer (GBC 932, AT-FAAS, Aus) was used for cadmium determination in water and wastewater samples. The atom trap accessory /air-acetylene controlled by *AVANTA* software which was placed on the air-acetylene burner. The cadmium determines in water and wastewater samples with 1.0 mL of the sample with LOD of 0.025 mg L^{-1} , the wavelength of 283.3 nm and 5 mA. The lower limit of quantitation (LLOQ), ULOQ and linear range for AT-FAAS was obtained $100 \mu\text{g L}^{-1}$, $1800 \mu\text{g L}^{-1}$ and $100\text{-}1800 \mu\text{g L}^{-1}$, respectively. All water samples were injected by an auto-sampler to the injector of AT-FAAS for 1-1.5 min. The electrothermal atomic absorption spectrophotometer (ET-AAS) was used for the validation of water samples in ultra-trace analysis of Cd(II). The Metrohm pH meter was used for measuring pH in water samples (E-744, Switzerland). The shaking of water samples was used based on 250 rpm speeds by vortex mixer (Thermo, USA). The standard solution of cadmium (Cd^{2+}) was purchased from Sigma Aldrich. (Germany) with a concentration of 1000 mg L^{-1} in 1 % HNO_3 . The various concentration of cadmium was daily prepared by dilution of the standard Cd

solution with DW. Ultrapure water was purchased from Millipore Company (USA) for the dilution of water samples. 2,3-Dimercapto-1-propanol (CASN:59-52-9, HOCH₂CH(SH)CH₂SH) was prepared from Sigma Aldrich, Germany. The pH was adjusted pH by 0.2 mol L⁻¹ of sodium phosphate buffer solution (Merck, Germany) for a pH of 7.0 (Na₂HPO₄/NaH₂PO₄). The analytical grade of reagents such as HNO₃, HCl, acetone, and ethanol were prepared from Merck, Germany. The syringe Whatman filter membrane (SFM) with glass microfiber pre-filter (100 nm, Anotop filters, SN: WHA68091112, D:10 mm, polypropylene housing polypropylene membrane) was purchased from Sigma Aldrich, Germany. Anotop syringe filters contain the proprietary alumina and use for difficult separation samples.

2.2. Human sample preparation

The glass analysis was washed with a HNO₃ solution (1 M) for at least 12 h and rinsed 10 times with DW. The cadmium concentrations in water and wastewater have a low concentrations less than 50 µg L⁻¹ and low contamination for sampling and determination caused to low accuracy of results. By procedure, 20 mL of the water samples were prepared from well water, drinking water and wastewater factories from Iran. Clean syringes were prepared for sample treatment. The water is prepared and stored by standard method for sampling from water by adding nitric acid to waters.

2.3. Synthesis of CNTs@DHSP adsorbent

First, the CNTs@COOH was prepared according to the acid oxidation method reported in the literature [30]. In the final step, 1 g of CNTs@COOH was added in 50 mL of methanol and maintained under ultrasonic conditions for 15 min. Sodium borohydride was also simultaneously added to the solution. Then, the mixture was stirred at room temperature for 3 h. Then, the product was washed with methanol three times and dried under vacuum. Typically, CNTs@OH (0.5 g) and dry xylene (40 mL) were sonicated for 15 minutes in a 100 mL round-bottomed flask. 3 mL of (3-chloropropyl) trimethoxysilane (CPTMS) was added to the above

mixture, drop by drop, at room temperature. After sonicating for 15 min, the resulting mixture was refluxed at 60 °C under N₂ atmosphere to remove the produced HCl. In order to obtain the CNTs@Cl, it was dried at 100 °C under vacuum. Then, 1 g of CNTs@Cl and 1 mL of DMP were mixed in 60 mL ethanol using an ultrasonic bath for 30 min. Then, a few drops of triethylamine were added to the above slurry, and the mixture was refluxed at 60 °C for three extra hours. The product was separated from the reaction mixture by a PTFE membrane filter and washed with ethanol three times and finally dried under vacuum at 100 °C.

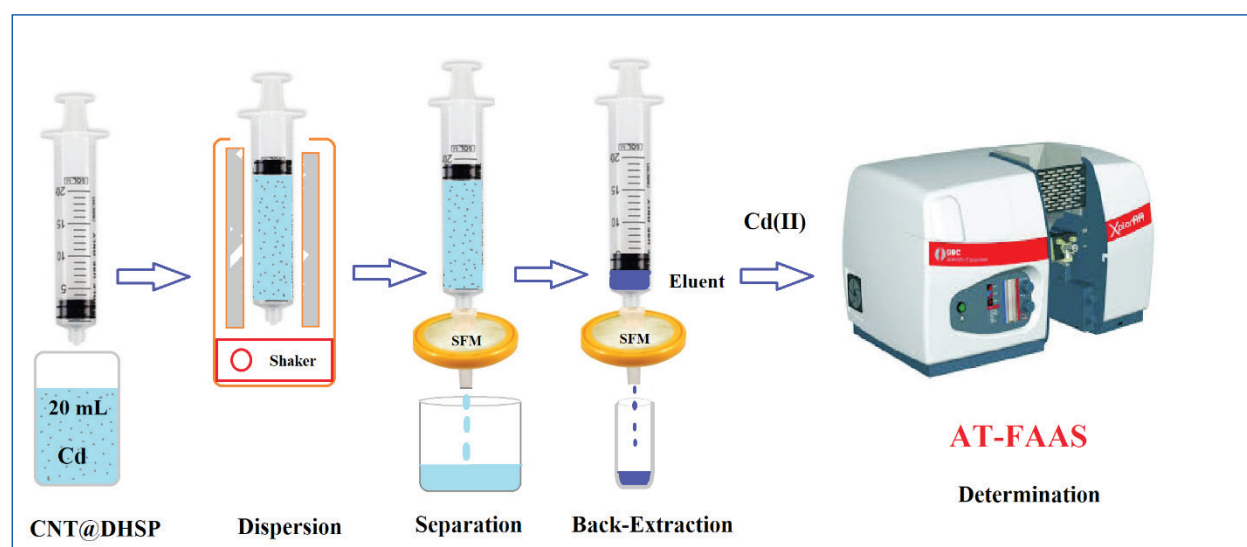
2.4. Extraction Procedure

By SFM-µ-SPE procedure, 20 mL of water and standard samples (3 µg L⁻¹ and 90 µg L⁻¹) were used for the separation and determination of cadmium ions at pH 7. Firstly, the CNTs@DHSP added to water or cadmium standard solution and shaken for 3 min at pH=7. Then, the water sample was slowly passed through SFM with glass microfiber pre-filter and the solid-phase was separated by filtering (100 nm, polypropylene housing polypropylene membrane). After shaking, the Cd(II) ions were extracted by sulfur group of CNTs@DHSP as coordination bond or dative bond at pH from 6-8 (Cd²⁺ → :SH @CNTs) and then the Cd (II) ions on SFM/CNTs@DHSP back-extracted by 0.5 mL of eluent (1.5 M, HNO₃) at pH 2. Finally, the cadmium concentration in remained solution was determined by AT-FAAS after dilution with DW up to 1 mL (Fig.1). The procedure was used for a blank solution without cadmium ten times. The calibration curve for Cd in standards solutions was prepared (3- 90 µg L⁻¹) and enrichment factor (EF) was calculated. The analytical parameters showed in Table 1. Validation of methodology was achieved by CRM for cadmium samples and ETAAS analysis. The recovery was obtained for cadmium by equation 1. The C_p and C_f is the primary and final concentration of Cd(II), which was determined by SFM-µ-SPE procedure coupled to AT-FAAS (n=10, Eq. 1).

$$\text{Re (\%)} = (C_p - C_f) / C_p \times 100 \quad (\text{Eq.1})$$

Table 1. The analytical features for determination cadmium by SFM- μ -SPE procedure

Features	value
Working pH	6-8
Amount of CNTs@DHSP (mg)	20.0
Sample volume of water (mL)	20.0
Volume of sample injection (mL)	1.0
Linear range for water ($\mu\text{g L}^{-1}$)	3.0-90
working range for water ($\mu\text{g L}^{-1}$)	3.0-170
Mean RSD %, n=10	1.5
LOD ($\mu\text{g L}^{-1}$)	0.75
Enrichment factor for water	19.6
Volume and concentration of HNO_3	1 mL, 1.5 M
Shaking time	3.0 min
Correlation coefficient	$R^2 = 0.9998$

**Fig. 1.** Cadmium extraction in water sample based on CNTs@DHSP by SFM- μ -SPE procedure

3. Results and discussion

3.1. Extraction Mechanism

The carboxylic acid-functionalized CNTs were synthesized by using the acid oxidation method. Then, for the generation of OH groups on surface CNT, these materials were treated with sodium borohydride in methanol. Afterward, hydroxyl-

functionalized CNTs were functionalized by (3-chloropropyl) trimethoxysilane (CPTMS) to provide chloroalkylsilane. Finally, thiol derivative as a DHSP was covalently immobilized on CNTs. Finally, SH group of DHSP on the surface of CNTs can be complexed with cadmium ions in a water solution (Fig.2).

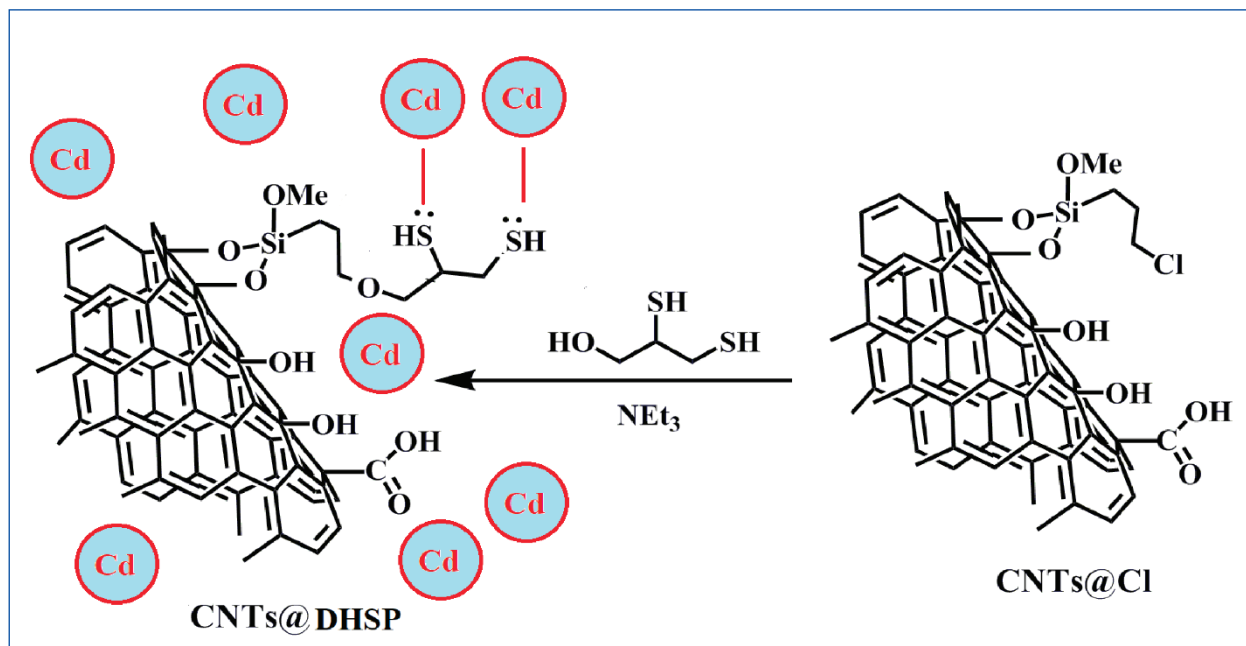


Fig. 2. The extraction mechanism of cadmium by CNTs@DHSP

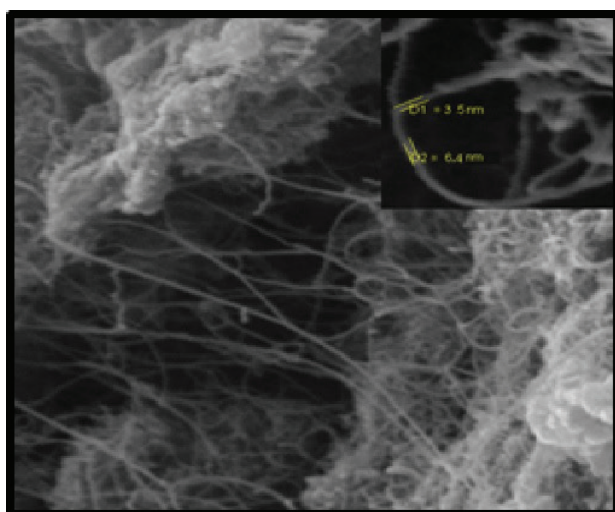


Fig.3a. SEM image of CNTs@DHSP

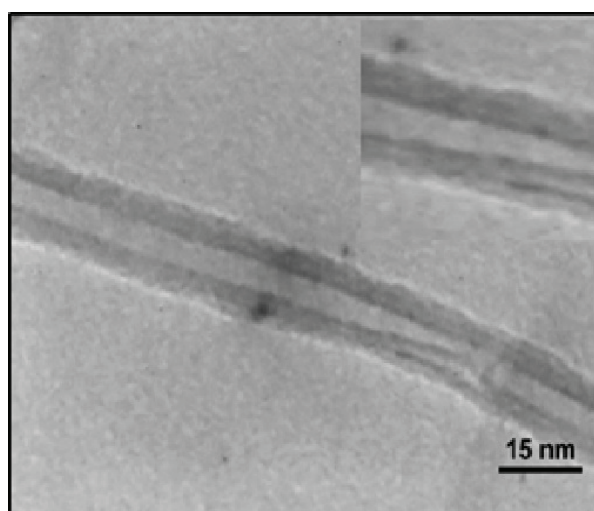


Fig.3b. TEM image of CNTs@DHSP

3.2. SEM and TEM analysis

The nanotubes of CNTs syntheses in University of Tabriz (Iran) and used for the synthesis of 2,3-dimercapto-1-propanol immobilized on CNTs (CNTs@DHSP). The Scanning Electron Microscopy (SEM) and Transmission Electron Microscopy (TEM) of CNTs@DHSP showed low nanoparticles size between 40-100 nm which was shown in Figures 3a and 3b.

3.3. Optimization of cadmium extraction SFM- μ -SPE procedure

The SFM- μ -SPE procedure based on novel CNTs@DHSP was optimized for cadmium extraction in water samples. So, different parameters such as pH, CNTs@DHSP Mass, eluent, sample volume and sonication time were studied.

3.3.1. The effect of pH

The effect of various pH was studied from 2 to 10 for Cd(II) extraction in water samples. The results showed the CNTs@DHSP can be removed cadmium ions from water samples at pH between 6 to 8. Moreover, the efficient extraction was achieved for cadmium ions at pH=7 (> 95%) and the recoveries reduced at $6 < \text{pH}$ and $\text{pH} > 8.5$. So, the pH of 7.0 was used as optimum pH for cadmium extraction in waters for further works (Fig. 4). The mechanism of cadmium extraction depended on the coordination bond or dative covalent bond of the thiol group in CNTs@DHSP adsorbent ($\text{Cd} \rightarrow \text{:SH}$). The positively charge of Cd^{2+} adsorbed on the surface of adsorbent with negative charge at optimized pH. At low pH ($\text{pH} < \text{pH}_{\text{pzc}}$), the surface of CNTs@DHSP has a positive charge. Therefore, low recovery is related to the electrostatic repulsion between Cd^{2+} and positive charge of CNTs@DHSP. In addition, at a pH of 7, the surface of CNTs@DHSP have negatively charged and absorbed Cd^{2+} . Also, in the $\text{pH} > 8.5$, the Cd ions participated as OH group and the recovery was decreased.

3.3.2. Effect of CNTs@DHSP mass

The efficient extraction was obtained by optimizing of CNTs@DHSP mass in pH=7. Therefore, the various of CNTs@DHSP mass was studied between 5-50 mg for Cd(II) extraction by SFM- μ -SPE procedure. The results showed us, a high recovery of more than 95% was achieved for 18 mg of CNTs@DHSP in water samples. So, 20 mg of CNTs@DHSP as optimum adsorbent mass was used for the experimental run. (Fig. 5). Based on Figure 6, The higher amount of CNTs@DHSP had no effect on cadmium recovery.

3.3.3. Effect of eluent and sample volume on cadmium extraction

The volume and concentration of eluent for back extraction cadmium ions from SFM/CNTs@DHSP adsorbent were optimized at pH=7. Acidic pH dissociated thiol binding to cadmium and caused to release of free cadmium ions into the eluent phase. The different acid solution such as HCl, HNO_3 , NaOH and H_2SO_4 , was selected for back-extraction of cadmium from SFM/CNTs@

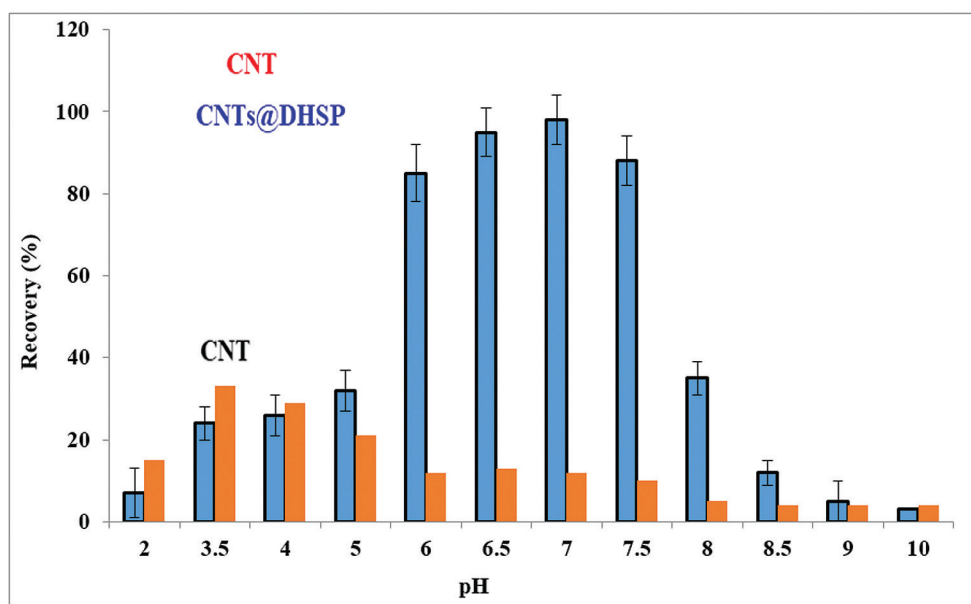


Fig. 4. The effect of pH on cadmium extraction based on CNTs@DHSP by SFM- μ -SPE procedure

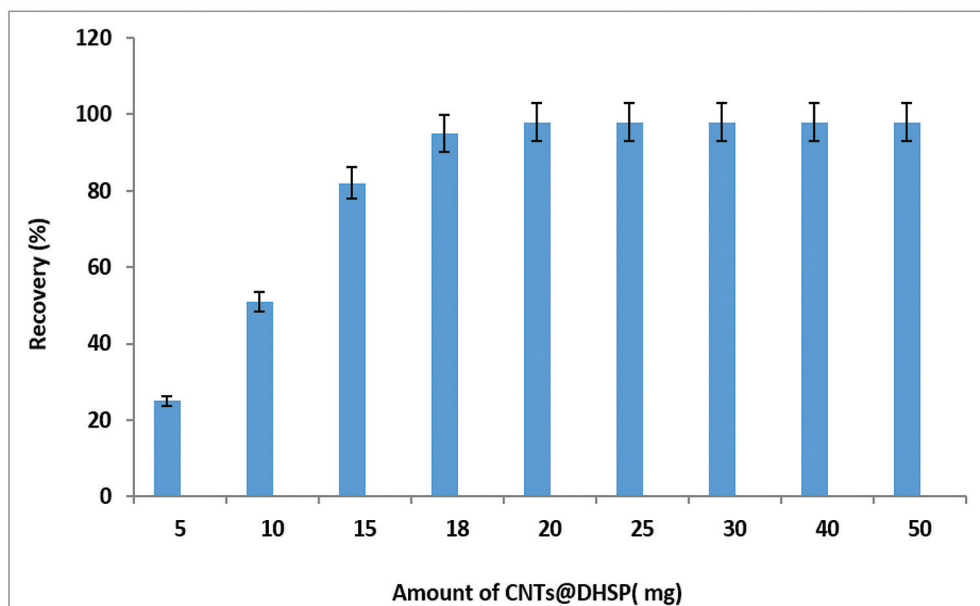


Fig. 5. The effect of CNTs@DHSP amount on cadmium extraction by SFM- μ -SPE procedure

DHSP adsorbent. The results showed that 1.5 mol L⁻¹ HNO₃ was quantitatively back-extracted the cadmium from SFM/CNTs@DHSP adsorbent. The sample volume between 1-100 mL for cadmium extraction was studied in water samples by SFM- μ -SPE procedure. For optimization, the cadmium concentration ranges (3-90 μ g L⁻¹) based on 20 mg of CNTs@DHSP adsorbent were examined by the proposed procedure. The results showed us the high recoveries were achieved 25 mL of water samples at pH=7. Therefore, 20 mL of water was used as the optimal value for further study.

3.3.4. Effect of sonication time and adsorption capacity

The extraction time depended on the dispersion of nanoparticles CNTs@DHSP adsorbent in the water samples and caused to increase interaction between HS with Cd(II) at pH=7. The effect of sonication time was studied from 0.5 to 5 min. It was observed that the sonication of 3.0 min had favorite extraction for cadmium in water samples.

The absorption capacities of cadmium for CNTs@DHSP and CNTs adsorbents were evaluated in optimized conditions. First, 20 mg of CNTs@DHSP or CNTs adsorbents added to 20 mL of water sample (standards cadmium solution: 200 mg L⁻¹) at pH 7. After sonication for 20 min, the cadmium extracted on the CNTs@DHSP or CNTs adsorbents at optimizing pH. The cadmium concentration in the liquid phase is directly determined as the final cadmium concentration after adsorption processes. The results showed the adsorption capacity for the CNTs@DHSP or CNTs adsorbents was obtained 152.6 mg g⁻¹ and 19.7 mg g⁻¹, respectively.

3.3.5. Interference of coexisting ions

The effect of interference ions on cadmium extraction based on CNTs@DHSP adsorbent in water samples was studied by SFM- μ -SPE procedure. The various interfering ions were added to 20 mL of cadmium solution (ULOQ: 90 μ g L⁻¹) at pH 7. Based on results the most of the probable concomitant ions have no effect on the extraction recovery of Cd(II) ions in optimized conditions (Table 2).

Table 2. The effect of interferences ions on cadmium extraction in water samples by SFM- μ -SPE procedure

Interfering Ions (I)	Mean ratio ($C_1/C_{Cd(II)}$)	Recovery (%)
	Cd(II)	Cd(II)
Al ³⁺ , V ³⁺	600	96.8
Zn ²⁺ , Cu ²⁺	900	08.0
I ⁻ , Br ⁻ , F ⁻ , Cl ⁻	1200	99.2
Na ⁺ , K ⁺	1000	98.4
Ca ²⁺ , Mg ²⁺	900	97.7
CO ₃ ²⁻ , PO ₄ ³⁻	1000	97.2
Co ²⁺ , Mn ²⁺ , Sn ²⁺	350	98.3
Ni ²⁺	150	96.7
NH ₄ ⁺ , NO ₃ ⁻	800	98.5
Hg ²⁺	100	97.4

3.3.6. Real samples analysis

The separation and determination of cadmium in water samples was done based on CNTs@DHSP adsorbent by the SFM- μ -SPE procedure. The results showed us, the cadmium was efficiently extracted by the thiol group of CNTs@DHSP adsorbent in water samples at pH=7. By spiking water samples, the accuracy of the results was satisfactorily validated at optimized pH and confirmed that the SFM- μ -SPE

procedure could be efficiently extracted/determined cadmium in water samples (Table 3). Due to results, the high recovery for extraction cadmium in water and wastewater samples was achieved by nanoparticles of CNTs@DHSP. Moreover, the certified reference materials (NIST; CRM) were used for validating results by the SFM- μ -SPE procedure (Table 4). Also, the results were validated by ET-AAS analysis which was compared to SFM- μ -SPE/AT-FAAS (Table 5).

Table 3. Validation of SFM- μ -SPE/AT-AAS procedure for Cd(II) determination in waters by spiking of real samples

Sample*	Added ($\mu\text{g L}^{-1}$)	*Found ($\mu\text{g L}^{-1}$)	Recovery (%)
Water A	---	4.23 \pm 0.18	---
	4.0	8.14 \pm 0.31	97.8
Water B	---	2.03 \pm 0.09	---
	2.0	3.98 \pm 0.21	97.5
Water C	---	ND	---
	2.0	1.93 \pm 0.08	96.5
Wastewater A	---	50.75 \pm 1.23	---
	40	88.83 \pm 2.64	95.2
Wastewater B	---	48.32 \pm 1.87	---
	40	89.56 \pm 3.45	103.1
Wastewater C	---	29.56 \pm 1.34	---
	30	57.95 \pm 2.08	94.6

*Mean of three determinations of samples \pm confidence interval (P = 0.95, n = 5)

Water A: Varamin River; Water B: Karaj River; Water C: drinking water Tehran; Wastewater A: Paint Factory of Karaj; Wastewater B: Petrochemical waste; Wastewater C: Chemical Factory in Industrial Varamin Co.

Table 4. Validation of SFM- μ -SPE procedure for cadmium determination by certified reference materials in waters (CRM, NIST)

Sample	conc. ($\mu\text{g L}^{-1}$)	Added	Found* ($\mu\text{g L}^{-1}$)	Recovery (%)
SRM 1643f	5.89 \pm 0.13	-----	5.82 \pm 0.16	-----
		5.0	10.79 \pm 0.25	99.4
SRM 3108	50.10 \pm 1.1	-----	48.77 \pm 1.42	-----
		40	87.64 \pm 2.61	97.2

*Mean of three determinations of samples \pm confidence interval (P = 0.95, n = 10)

SRM 3108: Certified Cadmium Mass Fraction: 10.007 mg g⁻¹ \pm 0.027 mg g⁻¹ dissolved in 1 L DW (C=10 mg L⁻¹), make by dilution DW up to 0.05 mg L⁻¹.

Table 5. Comparing of SFM- μ -SPE procedure with ET-AAS for cadmium determination in water samples

Sample	Added ($\mu\text{g L}^{-1}$)	ET-AAS* ($\mu\text{g L}^{-1}$)	AT-FAAS* ($\mu\text{g L}^{-1}$)	Recovery (%)
Water A	-----	4.18 \pm 0.17	4.06 \pm 0.13	-----
	4.0	-----	7.98 \pm 0.24	98.0
Water B	-----	2.12 \pm 0.11	2.18 \pm 0.08	-----
	2.0	-----	4.09 \pm 0.16	95.5
Water C	-----	0.25 \pm 0.02	^a ND	-----
	2.0	-----	1.97 \pm 0.09	98.5
Well water	-----	6.12 \pm 0.28	5.94 \pm 0.18	-----
	5.0	-----	11.03 \pm 0.34	101.8

*Mean of three determinations of samples \pm confidence interval (P = 0.95, n = 10)

^aND: Not Detected

4. Conclusions

A novel CNTs@DHSP nanostructure was used for cadmium extraction/separation/determination in water samples by the SFM- μ -SPE method coupled with AT-FAAS. By the proposed procedure, the efficient/easy/fast extraction for cadmium was obtained in a short time at pH=7. The CNTs@DHSP nanostructure has excellent recovery for Cd(II) extraction without any chelating ligands. The procedure had many advantages such as reusability of adsorbent, fast/easy pretreatment and a wide linear range for determination cadmium in waters. Therefore, the CNTs@DHSP nanostructure can be used as the favorite methodology for the determination and separation of cadmium in water samples by AT-FAAS.

5. Acknowledgements

The authors wish to thank from Department of Inorganic Chemistry, Faculty of Chemistry, University of Tabriz, Tabriz, Iran, for supporting this work.

6. References

- [1] L.T. Friberg, G.G. Elinder, T. Kjellstrom, G.F. Nordberg, *Cadmium and Health: A toxicological and epidemiological appraisal*, CRC Press: Boca Raton, FL, USA, Vol. 2, 2019.
- [2] M.R. Rahimzadeh, S. Kazemi, A.A. Moghadamnia, *Cadmium toxicity and treatment*, *Caspian J. Intern. Med.*, 8 (2017) 135–145.
- [3] A.A. Tinkov, T. Filippini, O.P. Ajsuvakova, M.G. Skalnaya, J. Aaseth, G. Björklundh, E.R. Gatiatulina, E.V. Popova, O.N. Nemereshina, P.T. Huang, *Cadmium and atherosclerosis: A review of toxicological mechanisms and a meta-analysis of epidemiologic studies*, *Environ. Res.*, 162 (2018) 240–260.
- [4] M.S. Sinicropi, A. Caruso, A. Capasso, C. Palladino, A. Panno, C. Saturnino, *Heavy metals: toxicity and carcinogenicity*, *Pharmacol.*, 2 (2010) 329–333.

- [5] S. Satarug, Dietary cadmium intake and its effects on kidneys, *Toxics*, 6 (2018) 15.
- [6] A.E. Nielsen, A. Bohr, M. Penkowa, The balance between life and death of cells: Roles of metallothioneins, *Biomark. Insights*, 1 (2007) 99–111.
- [7] G. Gobe, D. Crane, Mitochondria, reactive oxygen species and cadmium toxicity in the kidney, *Toxicol. Lett.*, 198 (2010) 49–55.
- [8] T. Bora, J. Dutta, Applications of nanotechnology in wastewater treatment—A review, *Nanosci. Nanotechnol.*, 14 (2014) 613–626.
- [9] L. Zhang, Q. Lei, Y. Cheng, Y. Xie, H. Qian, Y. Guo, Y. Chen, W. Yao, Study on the removal of cadmium in rice using microbial fermentation method, *J. Food Sci.*, 82 (2017) 1467–1474.
- [10] International Agency for Research on Cancer (IARC), Monographs on the evaluation of the carcinogenic risks to human's beryllium, cadmium, mercury and exposures in the glass manufacturing Industry, scientific publications: Lyon, France, pp. 119–238, 1993.
- [11] World Health Organization (WHO), Evaluation of certain food additives and contaminants, Thirty-third report of the joint FAO/WHO expert committee on food additives, technical report series 776, 1989. <http://www.who.int/ipcs/publications/jecfa/reports/en/index.html>
- [12] N. Altunay, A. Elik, Ultrasound-assisted alkanol-based nanostructured supramolecular solvent for extraction and determination of cadmium in food and environmental samples: Experimental design methodology, *Microchem. J.*, 164 (2021) 105958.
- [13] E. M. Angelin, M. Ghirardello, The multi-analytical in situ analysis of cadmium-based pigments in plastics, *Microchem. J.*, 157 (2020) 105004.
- [14] V. MortazaviNik, E. Kono, A. Feizbakhsh, A. A. M. Sharif, Simultaneous extraction of chromium and cadmium from bean samples by $\text{SrFe}_{12}\text{O}_{19}$ @CTAB magnetic nanoparticles and determination by ETAAS: An experimental design methodology, *Microchem. J.*, 159 (2020) 105588.
- [15] M. Arjomandi, H. Shirkhanloo, A review: Analytical methods for heavy metals determination in environment and human samples, *Anal. Methods Environ. Chem. J.*, 2 (2019) 97-126.
- [16] H. Shirkhanloo, S. A. H. Mirzahosseini, N. Shirkhanloo, The evaluation and determination of heavy metals pollution in edible vegetables, water and soil in the south of Tehran, province by GIS, *Arch. Environ. Prot.*, 41 (2015) 63-72.
- [17] M. Aliomrani, M.A. Sahraian, H. Shirkhanloo, M. Sharifzadeh, Blood concentrations of cadmium and lead in multiple sclerosis patients from Iran, *Iran. J. Pharm. Res.*, 15 (4), 825 2016
- [18] J. Charoensuk, J. Thonglao, B. Wichaiyo, A simple and sensitive colorimetric sensor for cadmium (II) detection based on self-assembled trimethyl tetradecyl ammonium bromide and murexide on colloidal silica, *Microchem. J.*, 160 (2021) 105666.
- [19] N. S. Medvedev, O. V. Lundovskaya, A. I. Saprykin, Direct analysis of high-purity cadmium by electrothermal vaporization-inductively coupled plasma optical emission spectrometry, *Microchem. J.*, 145 (2019) 721-755.
- [20] Y. Liu, Y. Chu, Z. Hu, S. Zhang, High-sensitivity determination of trace lead and cadmium in cosmetics using laser-induced breakdown spectroscopy with ultrasound-assisted extraction, *Microchem. J.*, 158 (2020) 105322.
- [21] H. Kaw, J. Li, X. Jin, Ultrasound-assisted liquid-liquid spray extraction for the determination of multi-class trace organic compounds in high-volume water samples, *Analyst*, 143 (2018) 4575-4584.
- [22] E. Bidari, M. Irannejad, M. Gharabaghi, Solvent extraction recovery and separation of cadmium and copper from sulphate solution, *J. Environ. Chem. Eng.*, 1 (2018) 1269–1274.
- [23] S.S. Swain, B. Nayak, N. Devi, S. Das, N. Swain, Liquid-liquid extraction of cadmium(II) from sulfate medium using phosphonium and ammonium based ionic liquids diluted in kerosene, *Hydrometallurgy*, 162 (2016) 63–70.

- [24] H. Shir Khanloo, M. Ghazaghi, M.M. Eskandari, Cloud point assisted dispersive ionic liquid-liquid microextraction for chromium speciation in human blood samples based on isopropyl 2-[(isopropoxycarbothioly) disulfanyl], *Anal. Chem. Res.*, 10 (2016) 18-27.
- [25] M. Sadeghi, E. Rostami, D. Kordestani, H. Veisi, M. Shamsipur, Simultaneous determination of ultra-low traces of lead and cadmium in food and environmental samples using dispersive solid-phase extraction (DSPE) combined with ultrasound-assisted emulsification microextraction based on the solidification of floating organic drop (UAEME-SFO) followed by GFAAS, *RSC Adv.*, 7 (2017) 27656–27667.
- [26] E. Yilmaz, I. Ocsoy, Bovine serum albumin-Cu(II) hybrid nanoflowers: An effective adsorbent for solid phase extraction and slurry sampling flame atomic absorption spectrometric analysis of cadmium and lead in water, hair, food and cigarette samples, *Anal. Chim. Acta*, 906 (2016)110-117.
- [27] H. Shir Khanloo, A. Khaligh, F. Golbabaeei, Z. Sadeghi, A. Vahid, A. Rashidi, On-line micro column preconcentration system based on amino bimodal mesoporous silica nanoparticles as a novel adsorbent for removal and speciation of chromium (III, VI) in environmental samples, *J. Environ. Health Sci. Eng.*, 13 (2015) 1-12.
- [28] M. Ghazaghi, H. Z. Mousavi, A. M. Rashidi, H. Shir Khanloo, R. Rahighi, Innovative separation and preconcentration technique of coagulating homogenous dispersive micro solid phase extraction exploiting graphene oxide nanosheets, *Anal. Chim. Acta*, 902 (2016) 33-42.
- [29] H. Shir Khanloo, A. Khaligh, H.Z. Mousavi, A. Rashidi, Graphene oxide-packed micro-column solid-phase extraction combined with flame atomic absorption spectrometry for determination of lead (II) and nickel (II) in water samples, *Int. J. Environ. Anal. Chem.*, 95 (2015) 16-32.
- [30] M. B. Hossein Abadi, H. Shir Khanloo, J. Rakhshah, The evaluation of TerphApm@MWCNTs as a novel heterogeneous sorbent for benzene removal from air by solid phase gas extraction, *Arab. J. Chem.* 13 (2020) 1741-1751.



Development of electrochemical sensor based on carbon paste electrode modified with ZnO nanoparticles for determination of chlorpheniramine maleate

Hamideh Asadollahzadeh ^{a,*}

^aDepartment of Chemistry, Faculty of Science, Kerman branch, Islamic Azad University, Kerman, Iran, P. O. Box 7635131167, Kerman, Iran

ARTICLE INFO:

Received 12 Dec 2020

Revised form 3 Feb 2021

Accepted 28 Feb 2021

Available online 28 Mar 2021

Keywords:

Chlorpheniramine maleate,
Pharmaceutical determination,
Carbon paste electrode,
Cyclic voltammetry,
ZnO nanoparticles

ABSTRACT

Zinc oxide (ZnO) nanoparticles with an average size of 60 nm have been successfully prepared by microwave irradiation. Carbon paste electrode (CPE) was modified with ZnO nanoparticles and used for the electrochemical oxidation of chlorpheniramine maleate (CPM). Cyclic voltammetry (CV) study of the modified electrode indicated that the oxidation potential shifted towards a lower potential by approximately 106 mV and the peak current was enhanced by 2 fold in comparison to the bare CPE (ZnO/CPE-CV). The electrochemical behaviour was further described by characterization studies of scan rate, pH and concentration of CPM. Under the optimal conditions the peak current was proportional to CPM concentration in the range of 8.0×10^{-7} to 1.0×10^{-3} mol L⁻¹ with a detection limit of 5.0×10^{-7} mol L⁻¹ by differential pulse voltammetry (DPV). The peak current of CPM is linear in the concentration range of 0.8 - 1000 μM (R²=0.998). The ZnO/CPE has a good reproducibility and high stability for the determination of CPM using this electrode. The proposed method was successfully applied to the determination of CPM in pharmaceutical samples. In addition, the important analytical parameters were compared with other methods which show that ZnO/CPE-CV procedure are comparable to recently reported methods.

1. Introduction

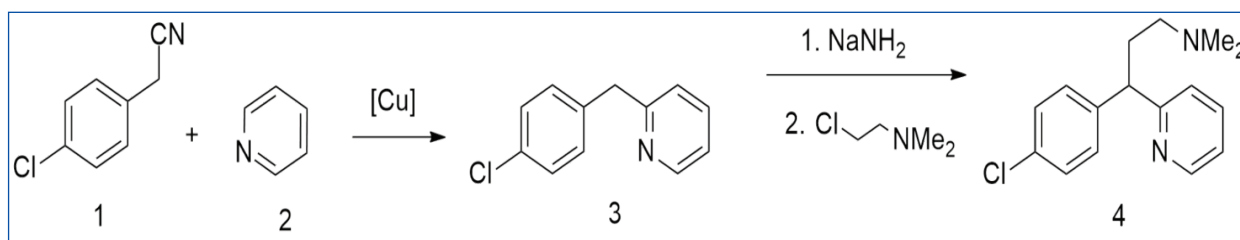
Antihistamines are a class of drugs commonly used to treat symptoms of allergies. These drugs help treat conditions caused by too much histamine, a chemical created by your body's immune system. Chlorpheniramine maleate [3-(4-chlorophenyl)-N,N-dimethyl-3-pyridin-2-yl-propan-1-amine, CPM] is an alkyl amine antihistamine. For more than 30 years, the CPM as a H₁-receptor

antagonist has been used to treat allergies such as hay fever, and other respiratory tract allergies [1]. The common side effects of chlorpheniramine (CPM, CP) include sleepiness, restlessness, and weakness dry mouth and wheeziness. CPM/CP is often combined with phenylpropanolamine to form an allergy medication with both antihistamine and decongestant properties, CPM/CP is a part of a series of antihistamines including pheniramine (Naphcon). As previous work, the CPM/CP synthesized through pyridine based on alkylation by 4-chlorophenylacetonitrile. The CPM generated by alkylating with 2-dimethylaminoethylchloride in

*Corresponding Author: [Hamideh Asadollahzadeh](mailto:Hamideh.Asadollahzadeh@iaukermans.ac.ir)

Email: asadollahzadeh90@yahoo.com

<https://doi.org/10.24200/amecj.v4.i01.130>



Schema 1. Synthesis of CPM/CP based on alkylation by pyridine

the presence of sodium amide (Schema 1). Several methods have been reported for the determination of CPM maleate including, spectrophotometry [2], liquid chromatography [3], liquid chromatography-mass spectrometry [4], gas chromatography [5], high performance liquid chromatography [6]. However, these instrumental methods have suffered some disadvantages such as time consuming, solvent-usage intensive and requires expensive devices and maintenance [7]. The electrochemical methods using chemically modified electrode have been widely used in sensitive and selective analytical methods for the detection of the trace amounts of biologically important compounds. Electrode surface may be changed with metal nanoparticles and such surfaces have found various applications within the sector of bio electrochemistry, particularly in biosensors. It's also been observed that nanoparticles can act as conductivity centers facilitating the transfer of electrons. Additionally, they provide large catalytic area. Several types of nanoparticles, including metal nanoparticles [8-10], oxide nanoparticles [11-13], semiconductor nanoparticles and even composite nanoparticles [14-16] are widely utilized in electrochemical sensors and bio sensors [17]. Some electrochemical methods are also reported for the determination of CPM by voltammetry [18-21]. Electrochemical sensors satisfy many of the requirements for such tasks particularly owing to their inherent specificity, rapid response, sensitivity and simplicity of preparation [18]. To our knowledge, no study has reported the electrocatalytic oxidation of CPM by using ZnO modified carbon paste electrode. Thus, in the present work, the ZnO nanoparticle have been

synthesized using microwave irradiation process and a modified carbon paste electrode is fabricated by using ZnO nanoparticles for the determination of CPM. All results were validated by spiking samples and compared to other methods.

2. Experimental

2.1. Chemicals and Reagents

Pure CPM, sodium dihydrogen ortho phosphate (NaH_2PO_4), disodium hydrogen phosphate (Na_2HPO_4), sodium phosphate (Na_3PO_4), orthophosphoric acid (H_3PO_4), sodium hydroxide (NaOH), hydrochloric acid (HCl), $\text{Zn}(\text{NO}_3)_2 \cdot 4\text{H}_2\text{O}$ and graphite powder were obtained from Merck. The buffer solutions were prepared from orthophosphoric acid and its salts in the pH range of 8 to 11. All the aqueous solutions were prepared by using double distilled water. High viscosity paraffin ($d = 0.88 \text{ kg L}^{-1}$) from Merck was used as the pasting liquid for the preparation of the carbon paste electrodes.

2.2. Apparatus

Electrochemical studies were performed using a Metrohm polarograph potentiostat-galvanostat (Metrohm Computrace 797-VA). The 797 VA is a voltammetric measuring stand that is connected to a PC. The computer software provided controls the measurement, records the measured data and evaluates it. Operation is most straightforward due to the well-laid-out structure of the program. The integrated potentiostat with galvanostat guarantees the highest sensitivity with reduced noise. Voltammetry system for the determination of organic additives in electroplating baths with

cyclic voltammetric stripping (CVS). Complete accessories with VA Computrace software and all electrodes for a complete measurement system: Rotating platinum disk electrode (RDE), Ag/AgCl reference electrode and Pt auxiliary electrode. Three-electrode system consisted of a bare CP and ZnO/CPE electrode as the working electrode, Ag/AgCl (3M KCl) as the reference electrode and a platinum wire as the auxiliary electrode. A Metrohm 691 pH/Ion meter was used for pH measurements. Solutions were degassed with nitrogen for ten minutes prior to recording of the voltammogram. X-ray diffraction (XRD) patterns were recorded by a Philips-X'pertpro, X-ray diffractometer using Ni-filtered Cu Ka radiation in University of Kashan-Iran. Scanning electron microscopy (SEM) images were obtained from LEO instrument model 1455VP.

2.3. Synthesis of ZnO nanoparticles

In this work, zinc acetate and graphene powders were used as the starting reagent. 0.41 mol of $\text{Zn}(\text{NO}_3)_2 \cdot 4\text{H}_2\text{O}$ was dissolved in 50 ml of deionized water under vigorous stirring. 1 ml of NaOH (1 M) was then added dropwise to the solution. Afterward, the solution was exposed by microwave irradiation with different powers and times. The microwave oven followed a working cycle of 30 s on and 70 s off (30 % power). After reaction in microwave the samples were cooled to room temperature naturally. Precipitates were washed with deionized water and ethanol, and air-dried at room temperature.

2.4. Preparation of bare carbon paste electrode and modified carbon paste electrode

The modified carbon paste electrode was prepared by hand mixing 0.1 g of ZnO nanoparticles with 0.9 g graphite powder with a mortar and pestle. Then paraffin was added to the above mixture and mixed for 30 min until a uniformly wetted paste was obtained. This paste was then packed into the end of a glass tube (ca. 3.35 mm i.d. and 10 cm

long). Electrical contact was made by forcing a copper wire down into the tube. When necessary, a new surface was obtained by pushing out an excess of paste and polishing it on weighing paper. Unmodified CPE was prepared in the same way without adding of ZnO nanoparticles.

2.5. Procedure and sample preparation

20 pieces of CPM tablet (Daro pakhsh. Iran) were powdered in a mortar. A portion equivalent to a stock solution of a concentration of about 0.01 M was accurately weighed and transferred into a 100 mL calibrated flask and completed to the volume with double distilled water. The contents of the flask were sonicated for 10 min to affect complete dissolution. Appropriate solutions were prepared by taking suitable aliquots of the clear supernatant liquid and diluting them with the phosphate buffer solutions. Also, 0.5 ml of an ampoule of CPM, according to its specifications, each ml of which contains 10 mg of the drug, was placed in a 25 ml calibrated flask and completed with a buffer at pH=10 and voltammetry was performed on it. The differential pulse voltammograms (DPV) were recorded between 0.4 and 1.2 V. The oxidation peak current of CPM was measured. The parameters for DPV were pulse width of 0.05 s, pulse increment of 4 mV, pulse period of 0.2 s, pulse amplitude of 50 mV and scan rate of 50 mVs⁻¹.

3. Results and discussion

3.1. XRD analysis

The phase type, crystal structure and purity of the product obtained are determined by the XRD method. The XRD pattern of the as obtained ZnO nanoparticles as sample number 1 was shown in [Figure 1](#). Peaks in this pattern are reported in the range of 2θ from 20 to 80 degrees. Patterns of the samples were indexed as a cubic phase. The XRD results proved the high crystallinity and purity of the products synthesized by microwave method. According to XRD data, the crystalline size (D_c) of ZnO nanoparticles can be determined by using Debye- Scherrer formula. The obtained average particle size was found to be 60 nm.

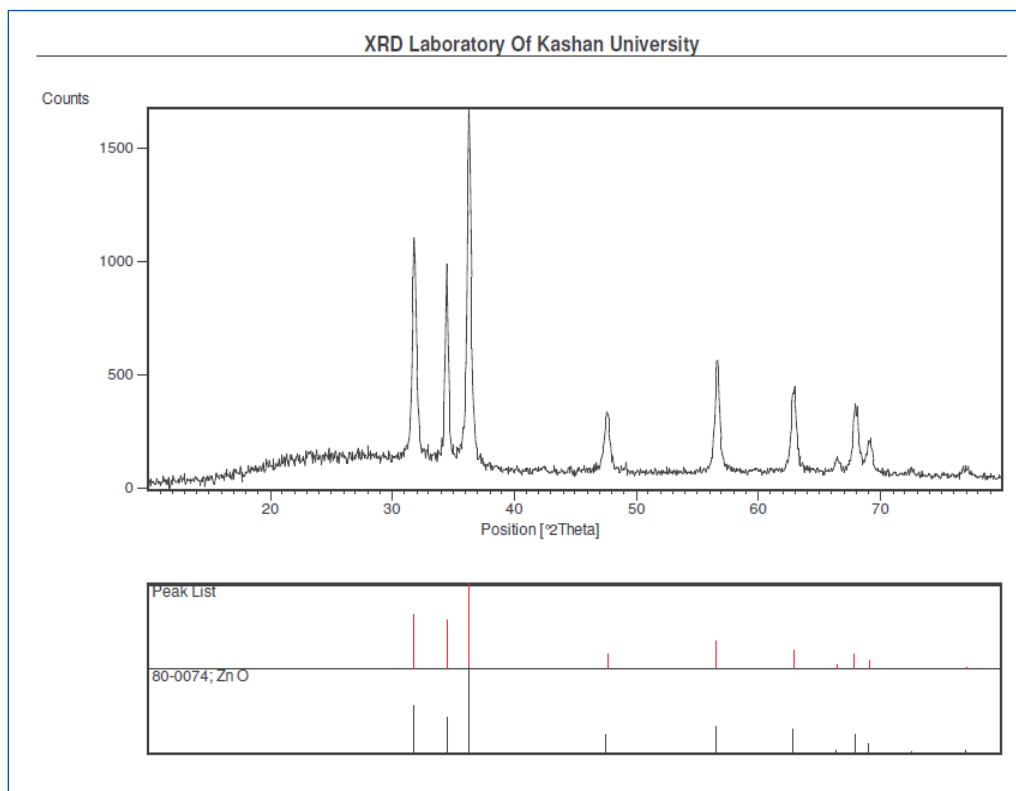


Fig. 1. XRD patterns of ZnO nanoparticles sample 1

3.2. Scanning electron microscopy

In [Figure 2](#) shows SEM image of ZnO powder obtained at 4 min and 360 W (sample no 1), at 540 W (sample no 2) and 750 W (sample no 3). As can be seen from SEM images, at 360 power, the reaction is faster due to the generation of more free radicals in solution and increased heat production due to the rotation of these active species. The formed nanoparticles have relatively smaller sizes and better distribution. At 540 and 720 W, due to the very high energy produced in these powers,

the nucleation of the particles is increased, and since the particles have a very active surface, large and cohesive masses are obtained in all test conditions. Therefore, the sample prepared in 360 W power and 4 min time due to the creation of nanoparticles in nanometer size according to the scale of images and homogeneous distribution is an optimized condition for time and power consumption to make ZnO nanoparticles. The produced ZnO nanoparticles have mean diameters of approximately 40-80 nm.

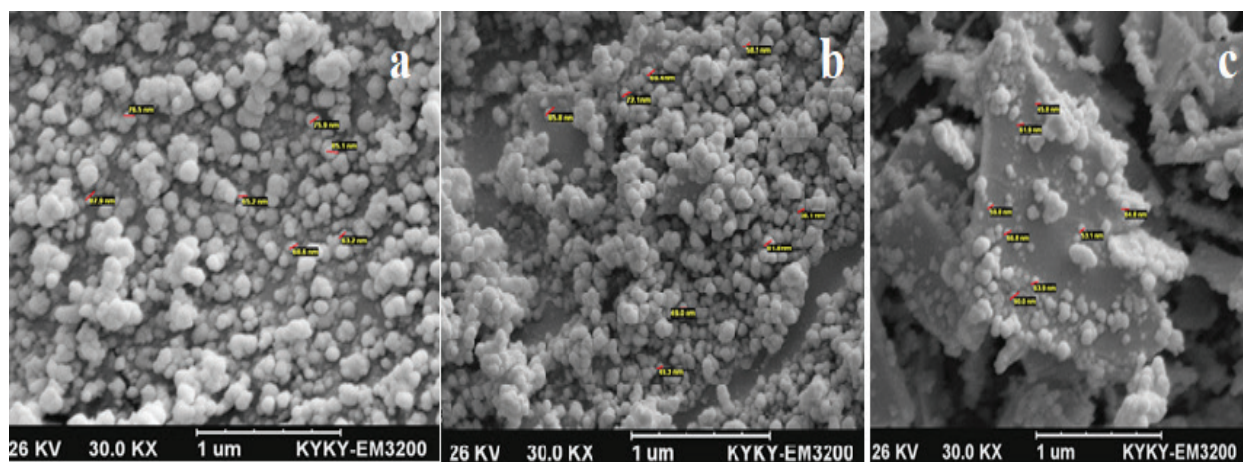


Fig. 2. SEM images of the ZnO nanoparticles for **a)** sample no. 1, **b)** sample no. 2, **c)** sample no. 3

3.3. Electrochemical behavior of CPM at the ZnO/CPE

The electrochemical behavior of CPM has been studied in two electrodes. Cyclic voltammetry (CV) was applied to investigate the electrochemical behavior of 0.4 mM CPM in 0.1 M phosphate buffer at pH 10 with a bare CPE and ZnO/CPE. Figure 3 shows the cyclic voltammograms in the CPE and ZnO/CPE electrode. As shown in this figure, in the presence of CPM, an irreversible oxidation peak at 1.093 V on the bare CPE attributed to the electrochemical oxidation of CPM. In the case of the ZnO/CPE, the oxidation peak of CPM decreased to 0.987 V and the peak current increased by 2.0 times compared with that for the bare CPE. These results suggested that ZnO obviously accelerate the electron transfer at the electrode surface and improve the electrochemical performance accordingly.

3.4. Effect of pH

The effect of pH of the solution on the electrochemical response of CPM was investigated from pH 8 to 11 (although lower pH was also examined in which the peak did not appear well). As can be seen in the Figure 4, with increasing pH, the anodic potential shifts to more negative potentials, which indicates better oxidation of the material at the electrode surface and the electrocatalytic effect. A linear relationship existed between the potential and pH in the range 8 to 11 (Fig. 5). The linear regression equation was $E = -60.5\text{pH} + 1582$ ($R^2 = 0.991$). The slope of 59 mV/pH suggests that an equal number of protons and electrons are involved in the oxidation process. Also, with increasing pH, the peak current increases to 10 and at pH = 11, the current decreases, so pH = 10 is chosen as the optimal point.

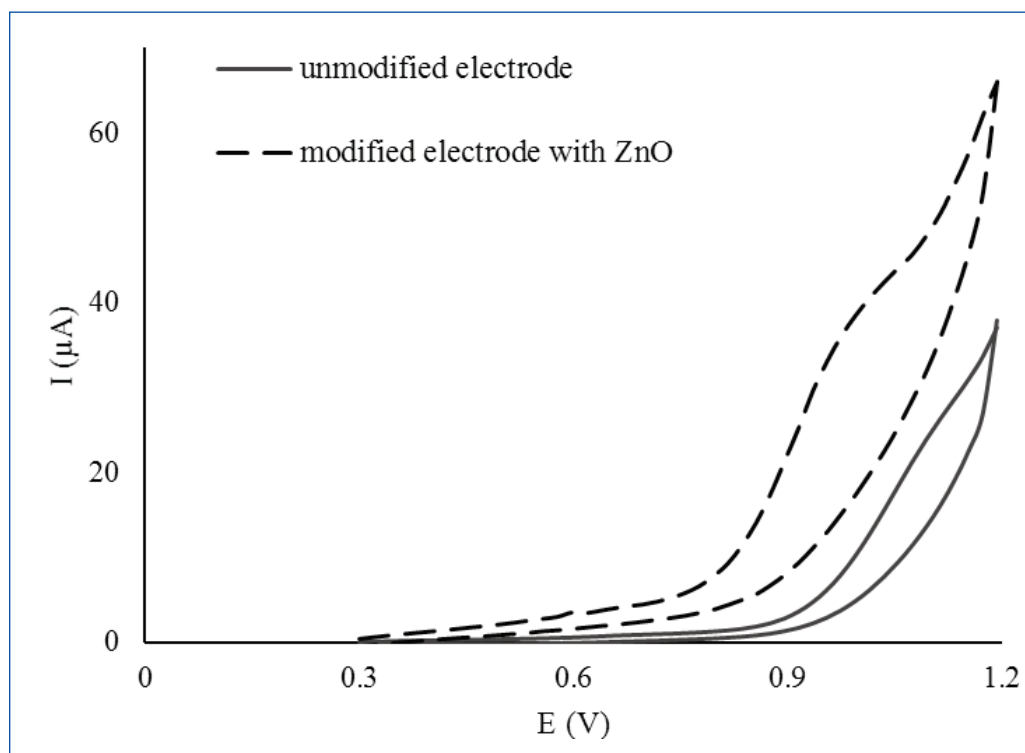


Fig. 3. Cyclic voltammograms of CPE and ZnO/CPE at presence of 0.4 mM CPM in 0.1 phosphate buffer solution (pH 10) at scan rate 50 mVs^{-1}

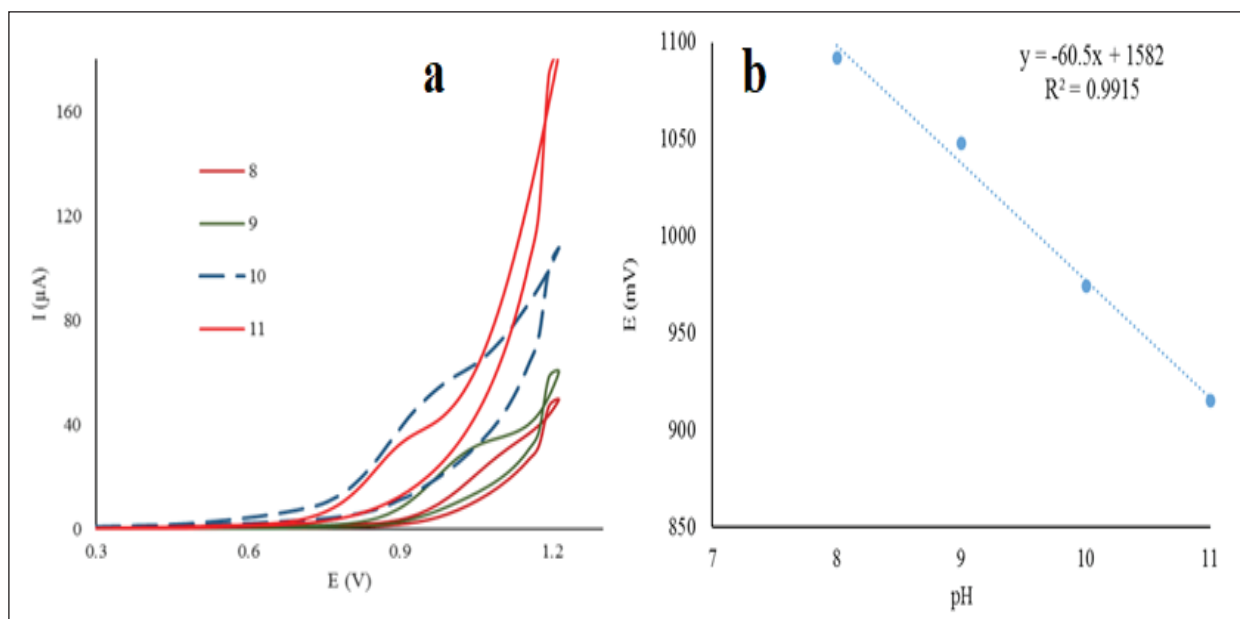


Fig.4. a) Cyclic voltammogram of CPM at different pH b) Relationship between the peak potential of CPM and pH.

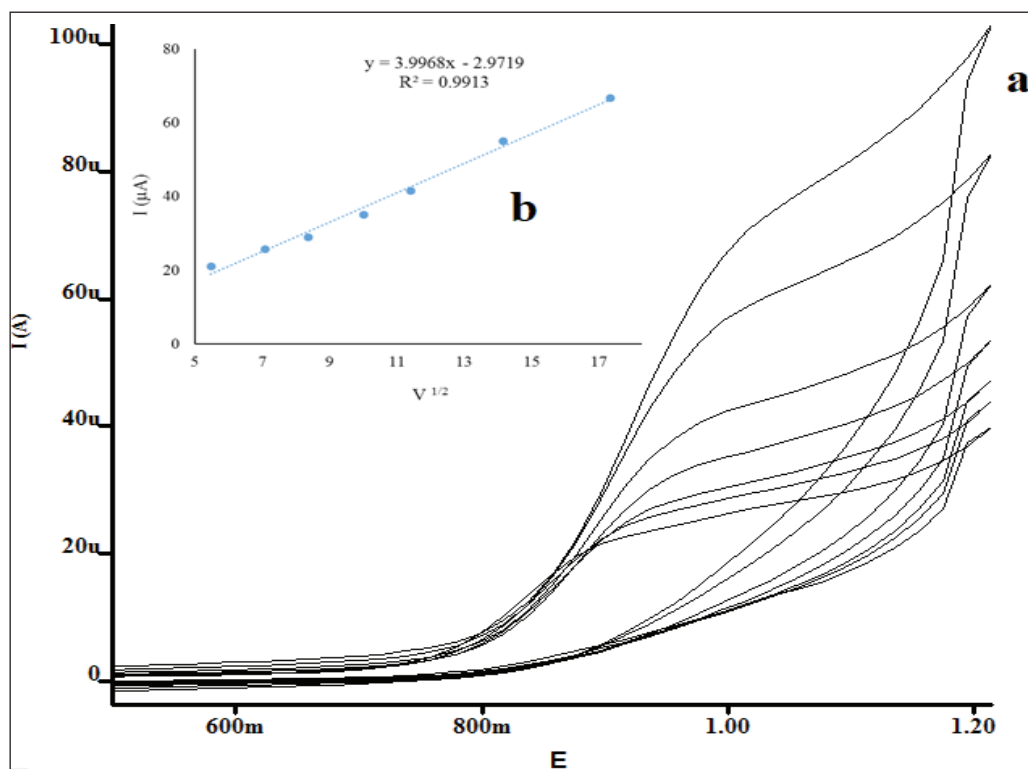


Fig. 5. Cyclic voltammograms of ZnO/CPE in the presence of 0.2 mM of CPM in 0.1 phosphate buffer solution (pH 10) at different scan rates (from inner to outer): 30, 50, 70, 100, 130, 200 and 300 mV s^{-1} . Inset: b, peak current vs. square root of scan rate ($v^{1/2}$)

3.5. Effect of scan rate

The effect of scan rate on the electrocatalytic oxidation of CPM at the ZnO /CPE was investigated by cyclic voltammetry. As can be seen in the Figure 5a, the scanning potential increases the peak CPM oxidation shifts to more positive potentials, which imposes a kinetic constraint on the electrochemical reaction. Figure 5b illustrates that a linear relationship existed between the oxidation peak currents of CPM and the square root ($v^{1/2}$) of the scan rate in the range from 30 to 300 mVs^{-1} , indicating a diffusion-controlled process. The linear regression equation was expressed as $I_{(\mu\text{A})} = 24.597v^{1/2} - 2.942$ ($R^2 = 0.991$).

3.6. Calibration curve

In order to develop a voltammetric method for determination of the drug, the DPV mode is selected, because the peaks are sharper and better defined at lower concentration of CPM than those obtained by cyclic voltammetry, with a lower background current, resulting in improved resolution. According to the obtained results, it was possible to apply this technique to the quantitative analysis

of CPM. The phosphate buffer solution of pH 10 was selected as the supporting electrolyte for the quantification of CPM as it gave maximum peak current at pH 10. DPV obtained with increasing amounts of CPM showed that the peak current increased linearly with increasing concentration, as shown in Figure 6. Using the optimum conditions described previously, linear calibration curves were obtained for CPM in the range of in range of 8×10^{-7} to 1×10^{-3} M. (Fig. 6 Inset). The linear equation $I = 0.159x + 6.99$ ($R^2 = 0.994$).

3.7. The repeatability and stability of the ZnO/CPE

Repeatability of the ZnO/CPE was examined by the determination of 0.5 mM of CPM in 0.1 M phosphate buffer solution at pH=10 with the same electrode 5 times. A relative standard deviation (RSD) value of 2.76% was observed, that indicating a good reproducibility of ZnO/CPE for CPM determination. Furthermore, the operational stability of ZnO/CPE was investigated by CV method every 2 days in 2 weeks. Only a small decrease of current (about 3.5%) for 2 mM CPM was observed, which can be attributed to the good stability of the modified electrode.

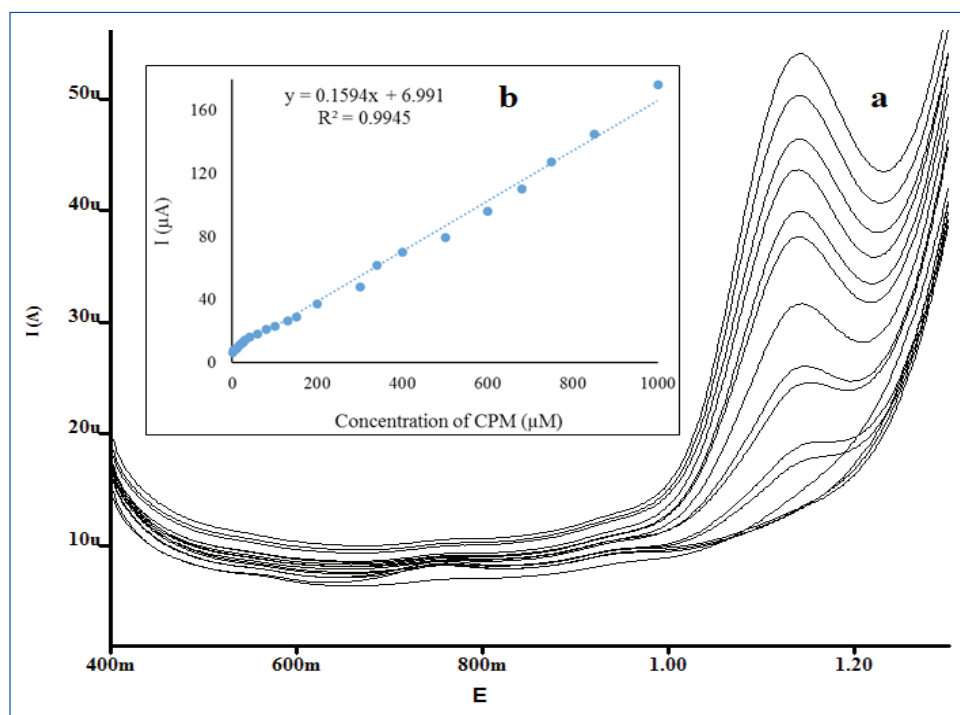


Fig. 6. DPV obtained at a ZnO/CPE for different concentrations of CPM (0.8 to 1000 μM). Inset: linear relationship between the peak current and concentration of CPM, scan rate: 50 mV s^{-1}

3.8. Analysis of real samples

In order to evaluate the applicability of the proposed method in the real sample analysis, it was used to detect CPM in tablets and ampoule (4 mg per tablet and 10 mg/mL for ampoule) (Fig. 7). The results are in good agreement with the content marked in the label. The detected content was 4.06 mg per tablet with 95% recovery and 9.76 mg/mL with 101 %recovery

for ampoule. Recovery studies were carried out after the addition of known amounts of the drug to various preanalyzed formulations of CPM. The results are listed in Table 1. Analytical parameters obtained here were compared with results obtained by other methods which show that they are comparable or better than the values reported by other groups (Table 2).

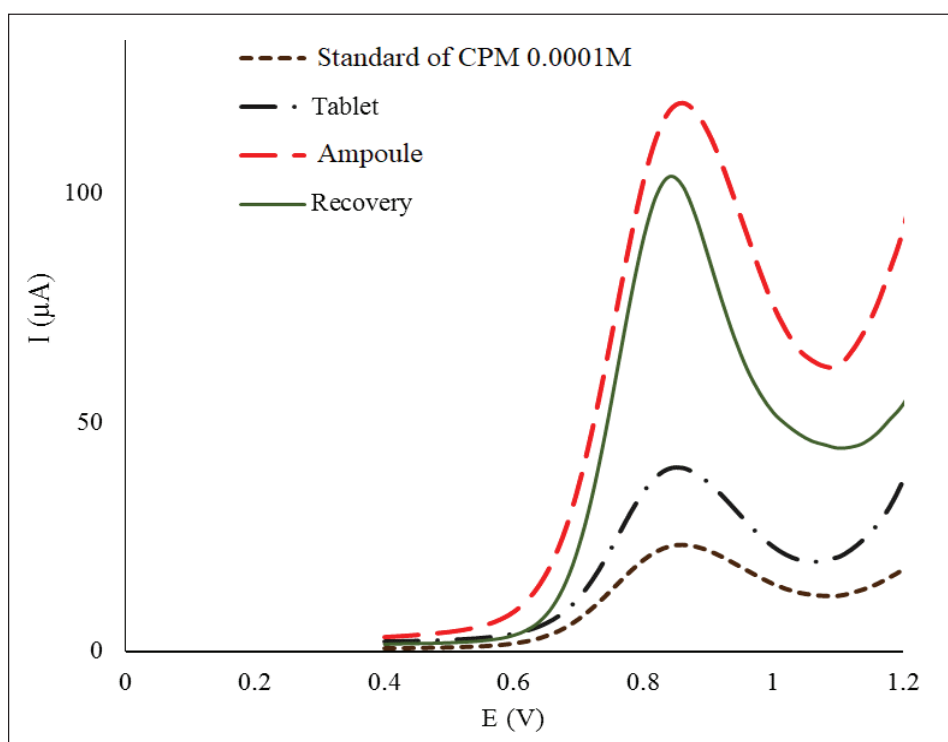


Fig.7. DPV obtained at a ZnO/CPE for standard solution 0.0001M of CPM, tablet, ampoule and standard added with tablet sample.

Table. 1. Determination of CPM in tablet and ampoule sample with ZnO/CPE by DPV method

Sample	Amount CPM in sample (mg)	Found in sample	Added (mg)	Deffected after addition (mg)	Recovery (%)
Tablet	4	4.06±0.08	2.74	2.62±0.1	95.62
Ampoule	10	9.77±0.2	3.5	3.73±0.07	106.3

Table 2. Comparison of analytical parameters for determination of CPM with different analytical methods.

Electrode	Method	LOD(μM)	LR(μM)	Ref
CPE-ion exchanger	PM	0.51	1.2-10000	[18]
CPE-SDS	DPV	1.7	1.0 – 800	[7]
Ru/Pty/GCE	CV	0.338	2.0 -45	[19]
MWCNT-modified GCE	DPV	1.63	5.0-500	[20]
CPE- CO nanostructure	DPV	0.08	0.1-10	[21]
CPE- ZnO Nanoparticle	DPV	0.50	0.8–1000	This work

4. Conclusions

ZnO/CPE was successfully fabricated and has shown electrocatalytic effect on the oxidation of CPM. In Comparison with the bare CPE, the presence of small amounts of ZnO reduced the oxidation peak potential of CPM while increased the current response of CPM. The CPM peak current is linear from a concentration range of 0.8 μM to 1000 μM with excellent R^2 value of 0.998. The detection limit of this modified electrode was found to be 0.5 μM and a good reproducibility, high stability was obtained for the determination CPM using this electrode. The content of CPM in tablet and ampoule samples was successfully determined with ZnO/CPE, which indicated the modified electrode is useable for the determination of CPM concentration in real samples.

5. Acknowledgement

The author is grateful to Islamic Azad University, Kerman Branch, for financial assistance of this work.

6. References

- [1] K. D. Tripathi, in: *Essentials of Medical Pharmacology*, Jaypee Brothers, New Delhi, p. 140, 2004.
- [2] A. K. Kaura, V. Gupta, M. Kaura, G.S.Roy, P. Bansl, Spectrophotometric determination of CPM maleate and phenylpropanolamine hydrochloride by two wavelengths method, *J. Pharm. Res.*, 7 (2013) 404-408.
- [3] N. M. Njuguna, K. O. Abuga, F. N. Kamau, G. N. Thoithi, A liquid chromatography method for simultaneous determination of diphenhydramine, promethazine, chlorpheniramine and ephedrine in cold-cough syrups, *Pharm. Chem. J.*, 51 (2017) 153–158.
- [4] X. Chen, Y. Zhang, D. Zhong, Simultaneous determination of chlorpheniramine and pseudoephedrine in human plasma by liquid chromatography–tandem mass spectrometry, *Biomed. Chromatogr.*, 18 (2004) 248-253.
- [5] M. E. Kaf Alghazal, F. Alrouh, Y. Bitar, S. Trefi, Determination of dimenhydrinate and chlorpheniramine maleate in pharmaceutical forms by new gas chromatography method, *Res. J. Pharm. Technol.*, 12 (2019) 2851-2856.
- [6] MR. Louhaichi, S. Jebali, M. H. Loueslati, N. Adhoum, L. Monser, Simultaneous determination of pseudoephedrine, pheniramine, guaifenesin, pyrilamine, chlorpheniramine and dextromethorphan in cough and cold medicines by high performance liquid chromatography, *Talanta*, 78 (2009) 991-997.
- [7] S. D. Lamani, R. N. Hegde, A. P. Savanur, S. T. Nandibewoor, Voltammetric determination of chlorpheniramine maleate based on the enhancement effect of sodium dodecyl sulfate at carbon paste electrode, *Electroanal.*, 23 (2011) 347-354.
- [8] Z. Amani-Beni, A. Nezamzadeh-Ejhieh, NiO nanoparticles modified carbon paste electrode as a novel sulfasalazine sensor, *Anal. Chim. Acta*, 1031 (2018) 47-59.

- [9] M. M. Vinay, Y. Arthoba Nayaka, Iron oxide (Fe_2O_3) nanoparticles modified carbon paste electrode as an advanced material for electrochemical investigation of paracetamol and dopamine, *J. Sci. Adv. Mater. Devices*, 49 (2019) 442-450.
- [10] N. B. Ashoka, B. E. K. Swamy, H. Jayadevappa, S. C. Sharma, Simultaneous electroanalysis of dopamine, paracetamol and folic acid using TiO_2 - WO_3 nanoparticle modified carbon paste electrode, *J. Electroanal. Chem.*, 859 (2020) 113819.
- [11] Gh. Karim-Nezhad, Z. Khorablou, M. Zamani, P. Seyed Dorraji, M. Alamgholilo, Voltammetric sensor for tartrazine determination in soft drinks using poly (*p*-aminobenzenesulfonic acid)/zinc oxide nanoparticles in carbon paste electrode, *J. Food Drug Anal.*, 25 (2017) 293-301.
- [12] O. J. D'Souza, R. J. Mascarenhas, A. K. Satpati, B. M. Basavaraja, A novel ZnO/reduced graphene oxide and Prussian blue modified carbon paste electrode for the sensitive determination of Rutin, *Sci. China Chem.*, 62 (2019) 262-270.
- [13] A. M. Fekry, M. Shehata, S. M. Azab, A. Walcarius, Voltammetric detection of caffeine in pharmacological and beverages samples based on simple nano-Co (II, III) oxide modified carbon paste electrode in aqueous and micellar media, *Sens. Actuators B*, 302 (2020) 127172.
- [14] B. Su, H. Shao, N. Li, X. Chen, Z. Cai, X. Chen, A sensitive bisphenol A voltammetric sensor relying on AuPd nanoparticles/graphene composites modified glassy carbon electrode, *Talanta*, 166 (2017) 126-132.
- [15] A. Benvidi, M. T. Nafar, Sh. Jahanbani, M. DehghanTezerjani, M. Rezaeinasab, S. Dalimasab, Developing an electrochemical sensor based on a carbon paste electrode modified with nano-composite of reduced graphene oxide and CuFe_2O_4 nanoparticles for determination of hydrogen peroxide, *Mater. Sci. Eng. C Mater. Biol. Appl.*, 75 (2017) 1435-1447.
- [16] J. Zhao, P. Yue, S. Tricard, T. Pang, Y. Yang, T. Pang, Y. Yang, J. Fang, Prussian blue (PB)/carbon nanopolyhedra/polypyrrole composite as electrode: a high performance sensor to detect hydrazine with long linear range, *Sens. Actuators B Chem.*, 251 (2017) 706-712.
- [17] E. S. Abood, A. M. Jouada, M. Mashkour, Zinc metal at a new ZnO nanoparticles modified carbon paste electrode: A cyclic voltammetric study, *Nano Biomed. Eng.*, 10 (2018) 149-155.
- [18] M. Hazem. Abu-Shawish, Potentiometric response of modified carbon paste electrode based on mixed ion-exchangers, *Electroanal.*, 20 (2008) 491-497.
- [19] E. A. Khudaish, M. Al-Hinaai, S. Al-Harthy, K. Laxman, Electrochemical oxidation of chlorpheniramine at polytyramine film doped with ruthenium (II) complex: Measurement, kinetic and thermodynamic studies, *Electrochim. Acta*, 135 (2014) 319-326.
- [20] Z. Pourghobadi, R. Pourghobadi, Electrochemical behavior and voltammetric determination of chlorpheniramine maleate by means of multiwall carbon nanotubes modified glassy carbon electrode, *Int. J. Electrochem. Sci.*, 10 (2015) 7241-7250.
- [21] M. Amiri, M. Alimoradi, K. Nekoueiian, A. Bezaatpour, Cobalt flower-like nanostructure as modifier for electrocatalytic determination of chlorpheniramine, *Ind. Eng. Chem. Res.*, 51 (2012) 14384-14389.



Novel graphite rod electrode modified with iron-functionalized nanozeolite for efficient wastewater treatment by microbial fuel cells

Mostafa Hassani^a, Mohsen Zeeb^{a*}, Amirhossein Monzavi^b, Zahra Khodadadi^a and Mohammad Reza Kalaei^{c,d}

^aDepartment of Applied Chemistry, Faculty of Science, Islamic Azad University, South Tehran Branch, Tehran, Iran

^bDepartment of Polymer and Textile Engineering, Islamic Azad University, South Tehran Branch, Tehran, Iran

^cDepartment of Polymer Engineering, Islamic Azad University, South Tehran Branch, Tehran, Iran

^dNanotechnology Research Center, Islamic Azad University, South Tehran Branch, Tehran, Iran

ARTICLE INFO:

Received 10 Nov 2020

Revised form 14 Jan 2021

Accepted 23 Feb 2021

Available online 29 Mar 2021

Keywords:

Microbial Fuel Cells (MFCs),
Graphite electrodes,
Iron-functionalized ZSM-5 nanozeolit,
Wastewater treatment

ABSTRACT

Microbial fuel cells (MFCs) are a green and efficient approach to treat wastewater and generate energy. According to the present research, a novel MFC fabricate based on graphite rod electrodes (GRE). The surface of this cathode was modified with iron-functionalized ZSM-5 nanozeolite. The characterization of Iron doping in nanozeolite structure and electrode surface modification were obtained by XRD and EDX analyzes, respectively. Chemical analysis of square wave (Sqw) and cyclic voltammetry (CV) determined for all of three graphite electrodes (G, G-Z and G-Z/Fe) with higher efficiency. Moreover, the comparison of experimental results from 72-hour fuel cell steering was evaluated and showed that the G-Z/Fe graphite electrodes has maximum efficiency and effectiveness. Thus, the efficiency of fuel cell output current and residual chemical oxygen demand removal with this electrode increased up to 21.8% and 36.9%, respectively. The effluent recovery for the modification of the graphite electrode surface was achieved due to increasing of the specific surface area, the active sites of functionalized nanozeolite and the elevation in the electrical conductivity through the presence of iron particles doped in the ZSM-5/Fe nanocatalyst structure. Therefore, the G-Z/Fe cathode can be used as a favorite electrode for the construction of MFCs based on GRE with high efficiency and economic.

1. Introduction

Microbial fuel cell (MFC) has different approach for wastewater treatment because the wastewater treatment process generates electricity or hydrogen gas instead of consuming electricity [1]. The MFC technology is depended on generating bio-electricity from bacterial biomass as the latest

method for wastewater treatment. MFCs can divided into two main categories, mediated and unmediated groups. The MFCs separated the compartments of the anode (oxidation) and the cathode (reduction). Most of MFCs use an organic electron donor that is oxidized to produce CO₂, protons, and electrons. The cathode acts by different electron acceptors such as oxygen (O₂). Other electron acceptors studied for metal treatment by reduction, nitrate reduction, and sulfate reduction in 25 °C and pH of 7 [2-4]. Microorganisms within an

*Corresponding Author: [Mohsen Zeeb](mailto:mohsen.zeeb@iaut.ac.ir)

Email: zeeb.mohsen@gmail.com

<https://doi.org/10.24200/amecj.v4.i01.133>

MFC, can be decomposed the organic matter by oxidizing, produce electrons that pass through a series of respiratory enzymes inside the cell and produce energy for the cell in the form of ATP. Then, the electrons are released towards a final electron acceptor. This receptor captures and reduces the electrons. For example, oxygen can be converted to water by the catalytic reaction of electrons with proton [5]. Previous research on electrodes used catalytic adhesives, carbon with non-platinum catalysts, flat carbon, carbon-coated tube and bio electrodes in the fabrication of carbon-based cathodes. Therefore, this study employed a carbon rod electrode coated with ZSM-5/Fe nanocatalyst [6-8]. Zeolites are tetrahedral crystalline aluminosilicates bonded with oxygen bridges. Due to their SSA, the specific channel structure, high thermal and hydrothermal stability, they are widely used in industries such as chemistry and petrochemicals, and water and wastewater treatment [9-11]. As mentioned, extensive research has been performed throughout the world to make fuel cells exploiting new electrodes. The researchers developed a cathode made of nickel-doped reduced nanographene as well as acid-hydroionized reduced nanographene to determine and evaluate the efficiency of the power output density with each of these electrodes. According to the results, the acid-hydroionized reduced nanographene showed the higher power output density (37%) than the nickel-doped reduced nanographene [12]. In another study, the researchers were developed a triple nanocomposite cathode containing graphene oxide, polyethylene dioxythiophene and iron oxide nanorods to increase the current efficiency of MFCs. Due to the large specific surface area of the electrode, high electrical conductivity as well as large sites for oxygen uptake in this electrode, the oxidation-reduction reaction occurs very quickly; as far as the power output density of the cell could be maintained for more than 600 hours [13]. By previous studies, a cathode was made of carbon nanotubes doped with titanium oxide nanoparticles aimed at enhancing the current output density and increasing the elimination of residual chemical

oxygen demand (COD). The results of this study revealed an increase in the specific surface area and the active sites for oxygen uptake, so that the maximum current output density produced was 15.16 mW m^{-2} and the COD removal efficiency was reported between 54-71% (after 10 days), which was related to the presence of active reaction sites on the electrode [14]. The results showed us, the specific surface area is a very effective factor in increasing the efficiency of MFCs.

In this study, the graphite rod as a high stability and electrical conductivity was used for wastewater treatment. So, the surface modification of graphite rod by zeolite nanocatalyst will increase the specific surface area of the electrode. On the other hand, the modification of graphite rods with zeolite nanocatalyst were compared to simple graphite rod with the low price and poor efficiency [15, 16]. Metal nanoparticles can greatly influence the oxygen reduction [17-22]. Hence, in this study the graphite rod electrodes were modified with iron particles (Fe) as a doping agent on ZSM-5 nanozeolite (G-Z/Fe/ ZSM-5) for increasing of MFC efficiency for wastewater treatment.

2. Experimental

2.1. Material

The ZSM-5 nanocatalyst powder (from the Zeolites family) was purchased from Sigma Aldrich with a crystal size of $0.5 \mu\text{m}$ and a pore size of 5.5 \AA . Ferric chloride (FeCl_3), the potassium chloride (KCl), the sodium di-hydrogen phosphate dihydrate ($\text{NaH}_2\text{PO}_4 \cdot 2\text{H}_2\text{O}$), di-sodium hydrogen phosphate dihydrate ($\text{Na}_2\text{HPO}_4 \cdot 2\text{H}_2\text{O}$), the ammonium chloride (NH_4Cl) and sulfuric acid (H_2SO_4 , %98) were also purchased from Merck Germany. Nafion117 membrane (DuPont, the USA) was used to Preparation the cell.

2.2. Preparation of ZSM-5/Fe Nanocatalyst

To Preparation the functionalized ZSM-5 nanocatalyst, first 2.5 g of ZSM-5 nanozeolite powder was placed in the furnace at a temperature of 500°C for 4 hours and calcined. Then, 0.5 g of ferric chloride (FeCl_3) powder was dissolved in

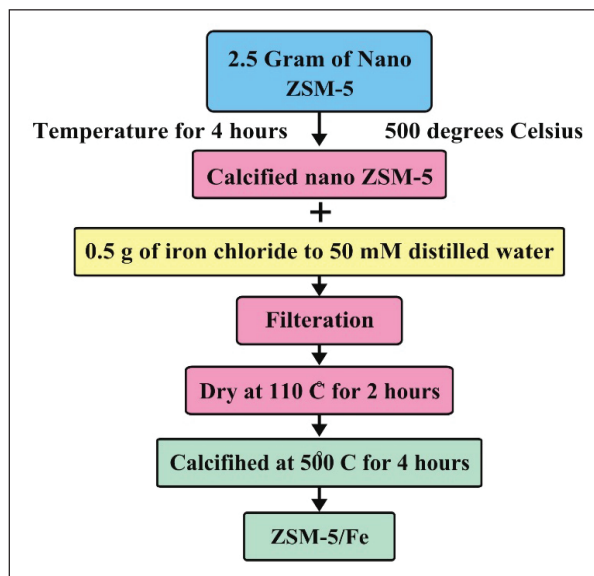


Fig.1. Schematic of the preparation process and calcination of ZSM-5/Fe nanocatalyst

distilled water twice for one hour, added to the calcined ZSM-5 nanozeolite powder and mixed for another 30 minutes, and filtered with a filter paper. The resulting powder was rinsed three times with distilled water and placed in an oven at a temperature of 80°C for 2 hours. Next, the powder was separated from the filter paper and re-calcined at a temperature of 500°C for 4 hours. The method of preparation above nanocatalyst is schematically illustrated in Figure 1.

2.3. Characterization

X-ray diffraction (XRD, STADI-P, the USA) was used to investigate ferrous (Fe) metal in the nanocatalyst structure functionalized with these

metal. Brunauer-Emmett-Teller (BET) surface area analysis (Belsorb apparatus, Japan) was used to determine the SSA of nanocatalyst particles, and energy-dispersive X-ray spectroscopy (EDX, MIRA III SAMX, Czech Republic) were applied to investigate the surface modification of the graphite electrode by each of the nanocatalysts.

2.4. Electrode Modification

To modify the graphite surface and to impregnate with the synthesized nanocatalyst powders, 0.5 g of each of the produced nanocatalysts (ZSM-5, ZSM-5/Fe) was poured into a test tube and 10 ml of ethanol was added and the graphite electrode was inserted into the test tube and placed in an

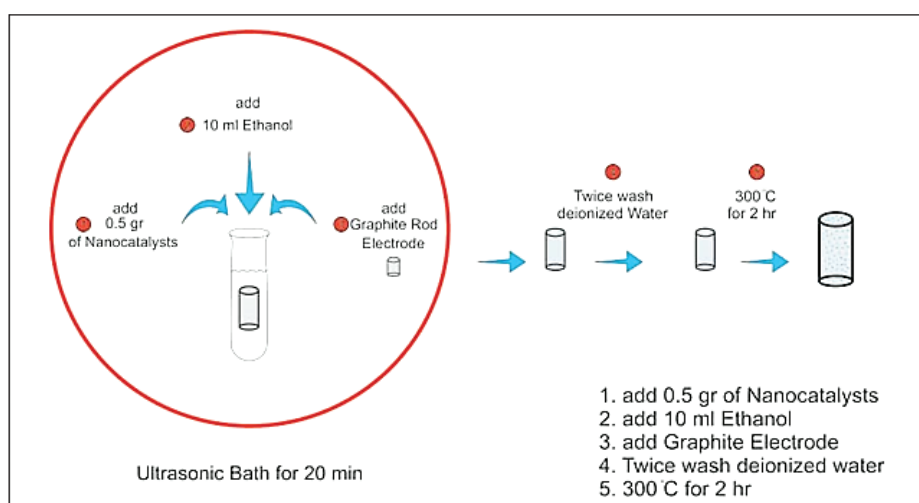


Fig. 2. Schematic of electrode surface modification by ZSM-5/Fe nanocatalyst

ultrasonic bath for 20 minutes. Then, the resulting electrode was rinsed twice with deionized water and placed in a furnace at a temperature of 300°C for 2 hours (Fig.2).

2.5. MFC construction and operation

This study applied with a separate two-part cell consisting of anaerobic anode and aerobic cathode. The chambers were made based on 500 mL pyrex glass with 75% of the volume as a working volume (375 mL). The two chambers were separated by a pyrex tube with an inner diameter of 0.8 cm and a length of 13.4 cm embedded in the middle portion with the proton exchange Nafion 117 membrane. The electrodes were made with rod graphite and heated at 3000°C with an area of 22.62 cm². In order to remove any impurities and improve membrane performance, the membrane was first boiled for an hour in 3% H₂O₂ and then washed in 1 M sulfuric acid for 1 hour. Oxygen gas was injected into the cathode with a sparger at a flow rate of 20 ml min⁻¹, and nitrogen gas was injected into the anode chamber to provide anaerobic conditions. A magnetic stirrer was used to stir the solutions inside the anode and cathode chambers, and a copper wire was used to bond the anode and the cathode electrodes. Acidification of the medium inhibits the optimal growth of the bacteria in the anode chamber, so it is necessary to use a buffer with appropriate pH in the bacterial growth medium. For

this purpose, in order to maintain the acid strength in the cell, 50 mM of phosphate buffered solution (PBS) (0.13 g L⁻¹ of potassium chloride, 3.32 g L⁻¹ of sodium di-hydrogen phosphate dihydrate, 5.13 g L⁻¹ of di-sodium hydrogen phosphate dihydrate, and 0.31 g L⁻¹ of ammonium chloride) was prepared in the cathode chamber and 375 mL was poured into the cathode chamber [23].

2.6. Microorganisms

In the anodic chamber of the fuel cell, the anaerobic wastewater prepared from the industrial town treatment plant was used as inoculum. The samples from the treatment plant were stored in stainless steel containers at 4°C, and transferred to the laboratory. The combined inoculum was inoculated into the pre-prepared culture medium containing 1 g L⁻¹ of glucose, 3 g L⁻¹ of yeast extract, 11 g L⁻¹ of peptone, 0.5 g L⁻¹ of ammonium chloride [24]. During the experiments, the cells were kept at room temperature and stirred at 50 rpm for 72 hours (Table 1).

2.7. Analytical method

A multimeter (MASTECH MS8360G, China) was used to measure the output voltage of the cell. The residual COD of the samples was measured with COD meter (Model 76133, Aqua Litik, Germany). Three-electrode systems including, anode electrode

Table.1. Anaerobic wastewater profile for anode chamber of fabricated fuel cell in the present study

Parametrs	Scale	Unit
T	22/81	°C
pH	7/13	----
SVI	1159	mg L ⁻¹
MLSS	2076	mg L ⁻¹
COD	1216	mg L ⁻¹
BODs	505	mg L ⁻¹
DO	0.6	mg L ⁻¹
Total Coliform	9000	(MPN/100 mL)

(modified electrodes), platinum wire electrode, and silver/silver chloride electrode (as the working electrode) were used to electrochemically measure the made electrodes. Cyclic voltammetry (CV) and square wave voltammetry (Sqw) with scanning rate of $5\text{mV}\cdot\text{s}^{-1}$ in 50 mM phosphate buffered solution (PBS) (PalmSense 3, the Netherlands) were used to investigate the electrochemical behaviors of the electrodes.

Spectrophotometric method was used to examine the treated wastewater. Initially, standard solutions with concentrations of 100-800 with 3 ml of digestion solution (containing potassium dichromate, sulfuric acid and silver sulfate) and 7 ml of stock solution (potassium hydrogen phthalate) are prepared and placed in an oven at $150\text{ }^{\circ}\text{C}$ for 1.5 hours was placed. After cooling, it was placed in a spectrophotometer (600nm) and the

calibration curve was drawn. It was measured by placing the absorbance of the unknown sample in the residual COD calibration equation.

3. Results and Discussion

3.1. BET characterization

By comparing the as, BET parameter as in Figure 3 and the results in Table 2, in each of the four BET analysis curves of the nanocatalysts, the highest SSA was related to the catalyst functionalized with Fe metal (ZSM-5/Fe, which was determined to be $408.41\text{ m}^2\text{ g}^{-1}$).

3.2. X-Ray Diffraction (XRD) analysis

The XRD spectrum for the ZSM-5 and the ZSM-5/Fe nanocatalyst was shown in Figure 4. The ZSM-5/Fe nanocatalyst confirms the presence of iron particles doped with silicate particles (Fig. 4).

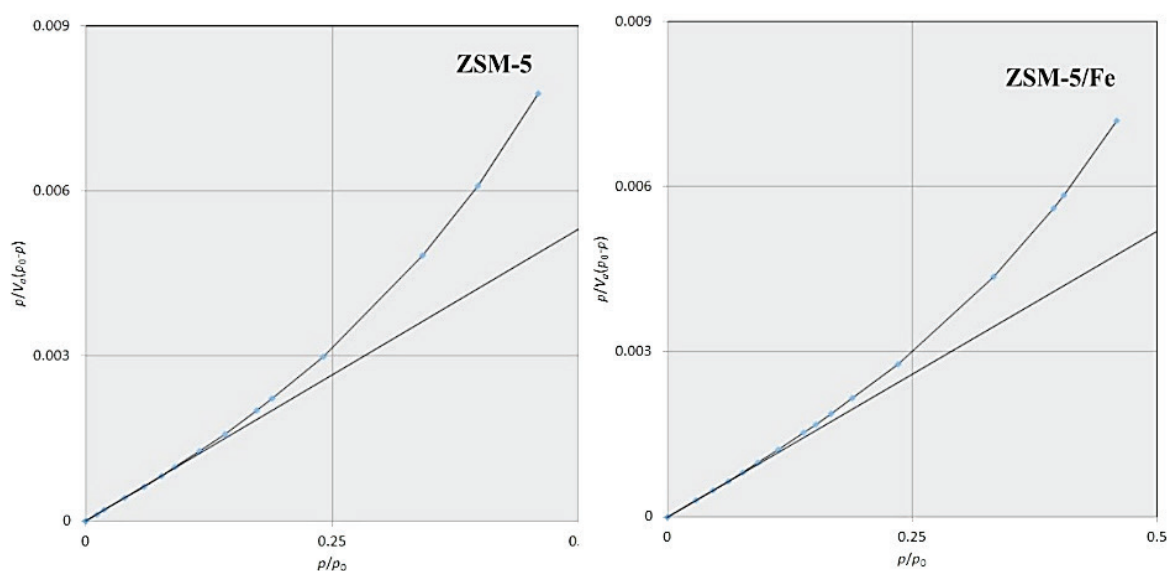


Fig.3. BET curves of prepared nanocatalysts

Table 2. specific surface area of prepared nanocatalysts

Row	Nanocatalysts	BET	Unit
1	ZSM-5	374.66	$\text{m}^2\text{ g}^{-1}$
2	ZSM-5/Fe	408.41	$\text{m}^2\text{ g}^{-1}$

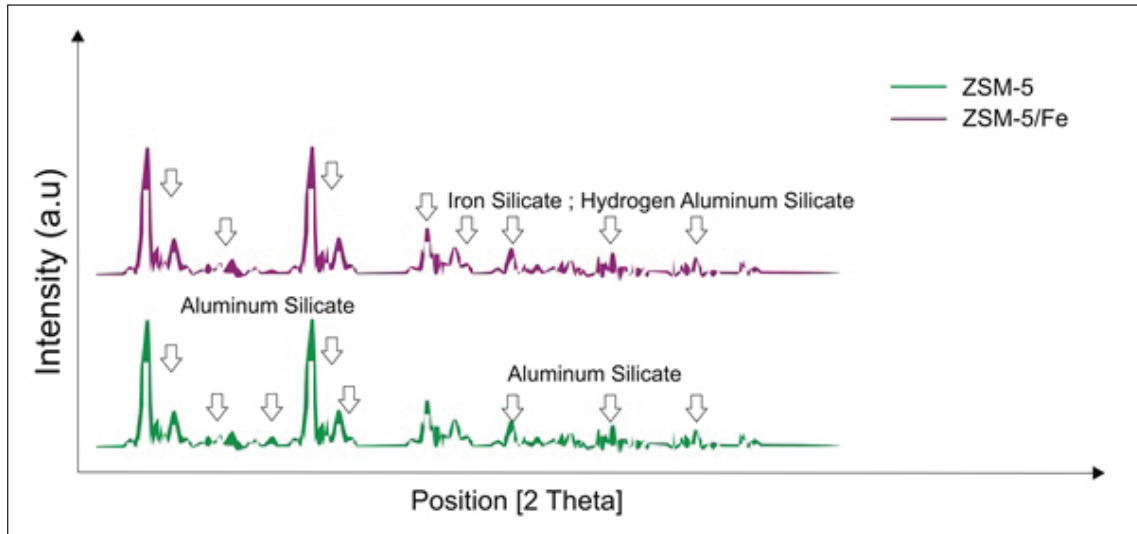


Fig. 4. X-ray diffraction (XRD) analysis of nanocatalysts, ZSM-5 and ZSM-5/Fe.

3.3. Energy dispersive X-ray spectroscopy (EDX) analysis

The curves of EDX analyzes for the surface of G-Z and G-Z/Fe electrodes compared as [Figure 5a](#) and [5b](#). The EDX analyzes showed the

presence of doped iron particles (in 1Kev area in the second curve). The presence of alumina and silicate peaks in both curves confirms that the surface of the electrodes has been covered by nanocatalysts.

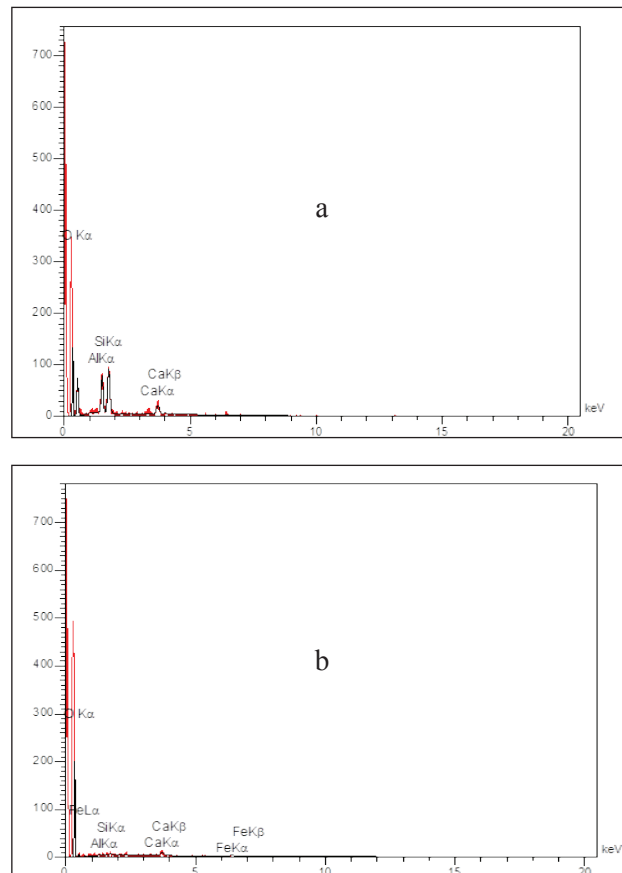


Fig.5. Energy-dispersive X-ray spectroscopy (EDX) analysis of the surface modified electrodes (a) G-Z; (b) G-Z/Fe

3.4. Electrochemical characterization

Comparing the cyclic voltammetry (CV) curves for G, G-Z and G-Z/Fe was shown in Figure 6a, 6b and 6c. The peak of the graphite electrode modified with iron-doped nanocatalyst (ZSM-5/Fe), which has a higher specific surface area, has the maximum current compared to other electrodes. Due to Figure 7, the square wave (Sqw) voltammetric peaks of the G, GZ-5 and GZ-5/Fe electrodes, with the scan rate

of $5\text{mV}\cdot\text{s}^{-1}$ in 50 mM phosphate-buffered saline (PBS) at an ambient temperature and in the potential range of 1 to 90 volts were compared. Comparing the electrode peaks, the G-Z/Fe electrode peak has the highest current ($3500\ \mu\text{A cm}^{-2}$) relative to other electrodes. The graphite electrode peak has the lowest current ($2000\ \mu\text{A cm}^{-2}$), which indicates that the ZSM-5 nanocatalyst doped with iron caused to increase the current of analysis.

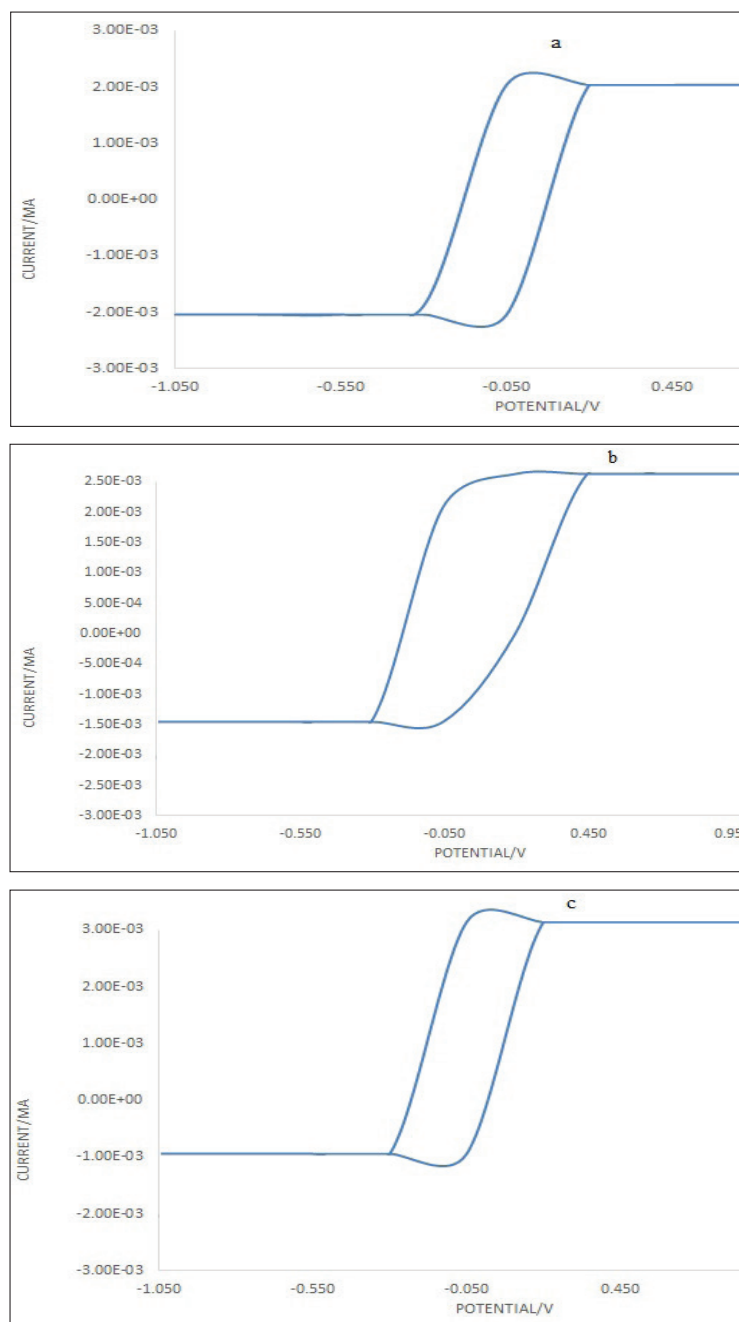


Fig. 6. Cyclic voltammetry (CV) analysis of electrodes prepared in 50 mM phosphate buffered solution (PBS) in room temperature. (a)G, (b)G-Z, (c)G-Z/Fe

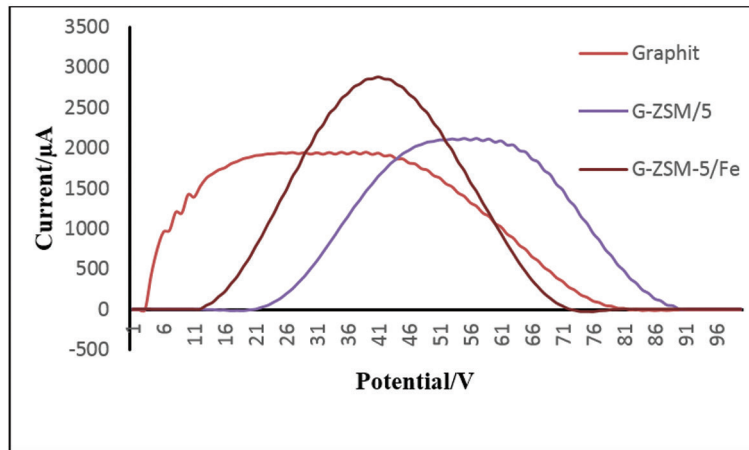


Fig.7. Square wave voltammetry (Sqw) analysis of electrodes prepared in 50 mM phosphate buffered solution (PBS) in room temperature.

According to Figure 7 and 8, the peak related to the output current and removal of COD during 72-hour fuel cell steering, it can be concluded that the produced G-Z/Fe cathode electrode has a higher output efficiency (21/8%) and COD removal

efficiency (36/9%) than G-Z electrode and simple graphite. The electrochemical analyzes (CV and Sqw) show higher efficiency of this electrode and Figure 9 showed the chemical oxygen demand (COD) for graphen, G-Z and G-Z/Fe electrodes..

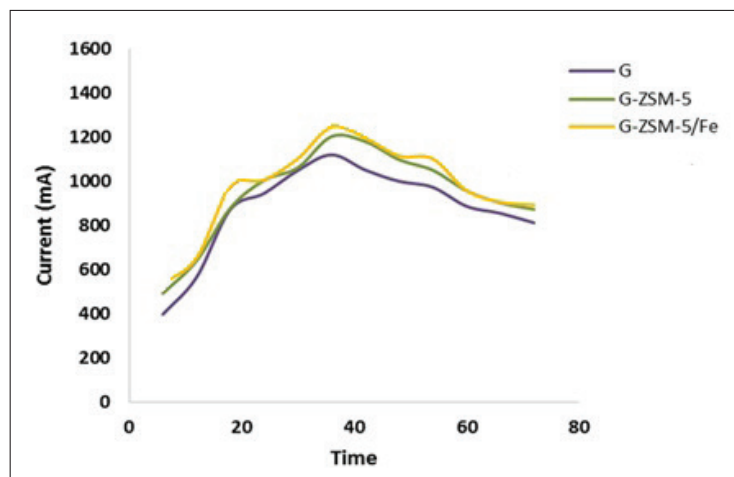


Fig.8. Cell current output per time for G, GZSM-5 and GZSM-5/Fe

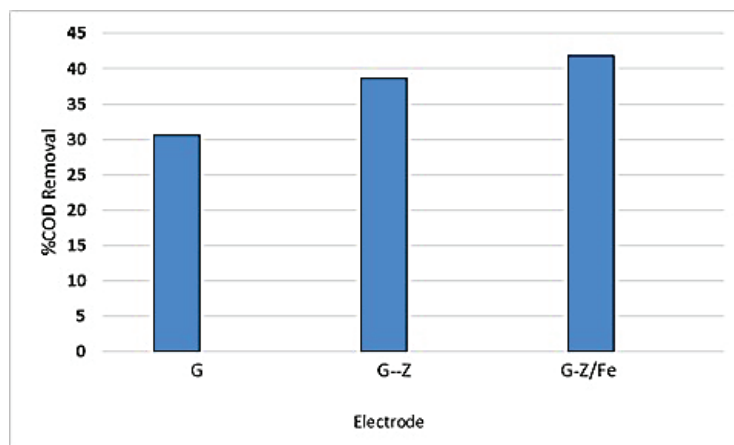


Fig.9. The efficient removal of COD for G,G-Z and G-Z/Fe electrodes

4. Conclusions

By procedure, a new microbial fuel cell was made by graphite rod electrodes. The surface of the cathode was modified by ZSM-5 and ZSM-5 functionalized with iron nanocatalyst. All three electrodes (G, G-ZSM and G-ZSM/Fe) were analyzed by square wave and cyclic voltammetry. Both analyses were introduced that the G-Z/Fe electrode had the higher efficiency as compared to others (Fig. 6-7). Experimental results of fuel cell steering was also studied as the Figure 8 and 9 by the G, G-Z and G-Z/Fe electrode, the results showed that the efficiency of fuel cell output current (I) and residual chemical oxygen demand (%COD) based on this electrode increased up to 21.8% and 36.9%, respectively as compared to other graphite electrode. The high efficiency of G-ZSM/Fe nanocatalyst electrode is due to high specific surface area and the presence of iron particles with high electrical conductivity.

5. Acknowledgments

The authors would like to thank and appreciate Mr. Mojtaba Azemi Motlagh, Laboratory Technical Manager of Arman Shimi Palayesh Gostar Company, as well as Mr. Hoshang Asadi, Personnel of Chemistry Laboratory at Islamic Azad University, South Tehran Branch, for providing laboratory facilities and equipment.

6. References

- [1] B. Min, S. Cheng, B.E. Logan, Electricity generation from swine wastewater using microbial fuel cells, *J. Water Res.*, 39 (2005)1675–1686.
- [2] Z. Lu, D. Chang, J. Ma, G. Huang, L. Cai, L. Zhang, Behavior of metal ions in ioelectrochemical systems: A review, *J. Power Sour.*, 275 (2015) 243–260.
- [3] S.S. Kumar, V. Kumar, Microbial fuel cells (MFCs) for bioelectrochemical treatment of different wastewater streams, *Fuel*, 254 (2019)115526.
- [4] C. Munoz-Cupa, Y. Hu, An overview of microbial fuel cell usage in wastewater treatment, resource recovery and energy production, *Sci. Total Energy Prod.*, 754 (2021) 142429.
- [5] W.W. Li, H.Q. Yu, Z. He, Towards sustainable wastewater treatment by using microbial fuel cells-centered technologies, *Energy Environ. Sci.*, 911 (2014)7-24.
- [6] S.K. Chaudhuri, D.R. Lovley, Electricity generation by direct oxidation of glucose in mediatorless microbial fuel cells, *Nat. Biotechnol.*, 21(2003)1229–1232.
- [7] B. Logan, S. Cheng, V. Watson, G. Estadt, Graphite fiber brush anodes for increased power production in air-cathode microbial fuel cells, *Environ. Sci. Tech.*, 41 (2007) 3341–3346.
- [8] X. Gao, Y. Zhang, X. Li, J. Ye, Novel graphite sheet used as an anodic material for high-performance microbial fuel cells, *Mat. Lett.*, 105 (2013) 24–27.
- [9] E.Y. Emori, F.H. Hirashima, C.H. Zandonai, C.A. Ortiz-Bravo, N.R.C. Fernandes-Machado, M.H.N. Olsen-Scaliante, Catalytic cracking of soybean oil using ZSM5 zeolite, *Catal.Today*, 279 (2017)168–176.
- [10] Q. Zhang, G. Liu, L. Wang, X. Zhang, G. Li, Controllable decomposition of methanol for active fuel cooling technology, *Energy Fuels*, 28 (2014) 4431–4439.
- [11] W. Li, G. Li, C. Jin, X. Liu, J. Wang, One-step synthesis of nanorod-aggregated functional hierarchical iron-containing MFI zeolite microspheres, *J. Mater. Chem., A*, 3 (2015) 14786–14793.
- [12] A. Valipour, S. Ayyaru, Y. Ahn, Application of graphene-based nanomaterials as novel cathode catalysts for improving power generation in single chamber microbial fuel cells, *J. Power Sour.*, 327 (2016) 548-556.
- [13] G.G. Kumar, C.J. Kirubakaran, D.J. Yoo, A.R. Kim, Graphene, poly(ethylenedioxythiophene), Fe₃O₄ nanocomposite: An efficient oxygen reduction catalyst for the continuous electricity production from wastewater treatment microbial fuel cells, *Int. J. Hydrogen Energy*, 41 (2016)13208e13219.

- [14] S.A.A. Yahia, L. Hamadou, M.J. Salar-García, A. Kadri, V.M. Ortiz-Martínez, F.J. Hernández-Fernández, A. Pérez de los Ríos, N. Benbrahim, TiO₂ nanotubes as alternative cathode in microbial fuel cells: Effect of annealing treatment on its performance, *Appl. Sur. Sci.*, 387 (2016) 1037–1045.
- [15] S.S. Manickam, U. Karra, L.W. Huang, N.N. Bui, B.K. Li, J.R. McCutcheon, Activated carbon nanofiber anodes for microbial fuel cells, *Carbon*, 53 (2013) 19–28.
- [16] J. Liu, Y. Qiao, C.X. Guo, S. Lim, H. Song, C.M. Li, Graphene/carbon cloth anode for high-performance mediatorless microbial fuel cells, *Bioresour. Technol. Rep.*, 114 (2012) 275–280.
- [17] S. Kalathil, S. Patil, D. Pant, Microbial fuel cells: electrode materials, encyclopedia of interfacial chemistry, *Sur. Sci. Electrochem.*, Elsevier, 309-318, 2018.
- [18] M. Jose Salar-Garcia, O. Obata, H. Kurt, K. Chandran, Impact of Inoculum Type on the Microbial Community and Power Performance of Urine-Fed Microbial Fuel Cells, *Microorgan.*, 8 (2020) 1921. <http://doi:10.3390/microorganisms8121921>.
- [19] L. Yang, Y. Tang, D. Yan, T. Liu, C. Liu, S. Luo, Polyaniline-reduced graphene oxide hybrid nanosheets with nearly vertical orientation anchoring Palladium nanoparticles for highly active and stable electrocatalysis, *ACS Appl. Mater. Interfaces*, 8 (2016) 169–176.
- [20] P. Pattanayak, F. Papiya, V. Kumar, N. Pramanik, P.P. Kundu, Deposition of Ni–NiO nanoparticles on the reduced graphene oxide filled polypyrrole: Evaluation as cathode catalyst in microbial fuel cells, *Sustain. Energy Fuels*, 3 (2019) 1808–1826.
- [21] P. Mishra, R. Jain, Electrochemical deposition of MWCNT-MnO₂/Ppy nano-composite application for microbial fuel cells, *Int. J. Hydrogen Energy*, 41 (2016) 22394-22405.
- [22] Y. Hou, H. Yuan, Z. Wen, S. Cui, X. Guo, Z. He, J. Chen, Nitrogen-doped graphene/CoNi alloy encased within bamboo-like carbon nanotube hybrids as cathode catalysts in microbial fuel cells, *J. Power Sour.*, 307 (2016) 561-568.
- [23] Q. Wena, Y. Wua, D. Cao, L. Zhao, Q. Sun, Electricity generation and modeling of microbial fuel cell from continuous beer brewery wastewater, *Bio. Tech.*, 100 (2009) 4171-4175.
- [24] S. Fatemi, A.A. Ghoreyshi, G.H. Najafpour, M. Rahimnejad, Investigation of bioelectricity production in dual chamber microbial fuel cell by mixed culture as active biocatalyst, *Iran. J. Biol.*, 27 (2013) 546-554.



Speciation and removal of selenium (IV, VI) from water and wastewaters based on dried activated sludge before determination by flame atomic absorption spectrometry

Mahdiyeh Ghazizadeh^{a,*}, Abdollah Abbasloo^a and Farzaneh Bivar^b

^a Department of Chemistry, Kerman Branch, Islamic Azad University, Kerman, Iran, P. O. Box 167-7635131

^b Department of Chemical engineering, Sirjan Branch, Islamic Azad University, Kerman, Iran, P.O. Box 187-78185

ARTICLE INFO:

Received 4 Dec 2020

Revised form 9 Feb 2021

Accepted 30 Feb 2021

Available online 30 Mar 2021

Keywords:

Selenium,
 Water and wastewater,
 Speciation,
 Activated sludge,
 Biosorption,
 Isotherms.

ABSTRACT

In recent decades, large amount of pollutants enters to the environment due to development of technology. Therefore, it is necessary to use ecofriendly sorbent to eliminate pollutants. In this research, 0.5 g of a dried activated sludge (DAS) was used for speciation selenium and removal of selenite [Se(IV)] from water and wastewater samples. The effect of operating parameters such as solution pH, the amount of bio-sorbent, contact time, temperature and initial concentration of selenium were studied by flame atomic absorption spectrometry (F-AAS). Kinetic data was adjusted to the Langmuir and Freundlich kinetic equations. The resulted showed that the Langmuir equation with a correlation coefficient of 0.9825 has the best match to tetravalent selenium biosorption on DAS. The FT-IR results showed that the biosorption mechanism of Se(IV) on DAS is due to functional groups on the DAS surface (Se(IV)... DAS). For reduction of soluble selenate [Se(VI), SeO₄²⁻] to selenite [Se(IV), SeO₃²⁻], the concentrated HCl was used at 70°C (30 min). So, the Se(VI) reduced to Se(IV) and total selenium (TSe) was determined and the Se (VI) was simply calculated by difference of TSe from Se(IV) content. The method was validated based on spiking samples in water and wastewater samples by F-AAS and using HG-AAS.

1. Introduction

Recently, the selenium studies are considered strongly because of the direct correlation between biological functions and the amount of selenium in the body [1, 2]. Selenium is an essential bioelement and has an important role in the proper biological functioning of many organisms [3, 4], although it becomes toxic when the concentration is more than 1.7 µg L⁻¹ [5]. Modern industrial processes such as the oil refining, the electrolytic copper refining, the

glass manufacturing, the agriculture and mining activities increase the selenium concentration in the environment matrixes [6-8]. Selenium is also used in thermal power stations, the solar panels, insecticides, semiconductors and rectifiers [9]. Two species of this element exist in aqueous systems contain Se(IV) and Se(VI) in the form of selenite (SeO₃²⁻) and selenate (SeO₄²⁻), respectively. Se(IV) is more toxic than Se(VI) [2, 10]. World Health Organization (WHO) proposed the permissible limit of selenium concentration in drinking water should be below 10 µg L⁻¹ [11-14]. Therefore, removal of selenium from wastewaters by an

*Corresponding Author: [Mahdiyeh Ghazizadeh](mailto:Mahdiyeh.Ghazizadeh@iaukerman.ac.ir)

Email: ghazizadeh1385@gmail.com

<https://doi.org/10.24200/amecj.v4.i01.119>

economic and effective methods is necessary. The most appropriate methods for removing selenium from contaminated water include catalytic reduction, chemical precipitation, electrochemical process, evaporation, floatation, ion exchange, membrane processes, biosorption and adsorption [2, 15]. Most of these techniques are expensive and improper for removal of selenium from aqueous samples. However, biosorption can be an effective and ecofriendly method for this purpose. Low cost and availability are two major factors for using biomass to remove the environmental pollutant [15, 16]. Biosorption of selenium by several sorbents such as seaweed, crustacean shell, peanut shell, rice barn, maize, wheat and dry yeast biomass is reported [17-20]. Recently the usage of DAS for removing selenium is extended [21, 22]. In addition, the different instrumental analysis was used for determination of selenium and other metals in different matrixes [23-27]. In this study, the removal of selenium by DAS from aqueous solutions were studied by F-AAS and validated by HG-AAS. The effect of pH, concentration, temperature and contact time was investigated. Kinetic models and thermodynamic parameters were determined.

2. Experimental

2.1. Chemicals

Sodium selenite (Na_2SeO_3) with a purity of 98%, was purchased from Merck (India) and used as a source of Se(IV) ions in the aqueous samples for analytical purpose, sodium hydroxide (NaOH) with a purity of 98% was purchased from Merck (Darmstadt, Germany, <http://www.merck.com>), hydrochloric acid (HCl) with a purity of 37% was purchased from Merck (Darmstadt, Germany, <http://www.merck.com>), dried activated sludge was obtained from Kerman Zamzam refinery, Iran. The different concentration of Selenium was prepared by dilution of deionized water (DW) and ultrapure water was purchased from Millipore Company. The acetate and phosphate buffer was used to adjust the pH between 2.6–6.4 and 6.4–8.0, respectively.

2.2. Apparatus

Flame atomic absorption spectrometer (F-AAS, Varian spectra 220 model, Australia) with wavelength 196.0 nm; slit 1.0 nm; current 10 mA was used ($10\text{-}200\text{ mg L}^{-1}$). The hydride generation atomic absorption spectrometer (HG-AAS, $1\text{-}100\text{ }\mu\text{g L}^{-1}$) and electro thermal atomic absorption spectrometer (ET-AAS, $15\text{-}400\text{ }\mu\text{g L}^{-1}$) were applied as ultra-trace analysis for Se (IV). The analytical pH meter (Benchtop meter inoLab pH 7110 model, WTW company, Germany), analytical balance (ALC model, Acculab company, America), magnetic hitted stirrer (IKA RH basic 2 model, IKA company, Germany), and centrifuge (EBA 20 model, Hettich company, Germany) were used for this study.

2.3. Preparation of dried activated sludge as a biosorbent

The activated sludge obtained from Zamzam company was suspended in a beaker containing 500 ml of deionized water on a magnetic stirrer for a day at 25°C . Let the suspension to precipitate. Then the upper liquid was decanted and the remaining suspension was centrifuged. The resulted sludge was washed with deionized water several times to be neutralized. The collected sample was dried in oven at 80°C for 36 h. The dried biomass was powdered and sieved with mesh No. 25.

2.4. Preparation of sample and selenium solutions

All glass or PCV tubes were cleaned with a 2M of HNO_3 solution for at least one day and then washed for ten times with ultrapure water. As low concentrations of Se(IV) and Se(VI) in water samples, the ion contamination effected on results of analysis, so, we used ultra-trace reagents for sampling processes. Sodium selenite was used to prepare a selenium stock solution with concentration of 1000 ppm (mg L^{-1}). The desired solutions obtained of diluting stock solution. The diluted solutions with concentrations in the range 2-9.5 ppm were used for calibration.

2.5. SPE procedure and Batch experiments

Biosorption of Se(IV) by DAS was achieved in optimized experimental conditions such as pH, contact time, amount of biosorbent and temperature. The experiments were carried out in 100 ml Erlenmeyer flasks. Experiments were achieved with pH 2 to 9, contact time 2 to 35 minute, amount of biosorbent 0.5 to 3 g, temperature 10 to 40°C and selenium concentration 10 to 140 mg L⁻¹. To adjust required pH of aqueous solution, HCl 0.2 M and NaOH 0.1 M were added. Finally, the kinetic models and isotherms were studied. The absorption capacity of DAS for Se(IV) was obtained 124.2 mg g⁻¹ by 140 mg L⁻¹ selenium concentration and 1 g of DAS.

By solid phase extraction procedure (SPE), 0.5 g of biosorbent of DAS added to 100 mL of water and wastewater solution and shaken for 15 min at pH=5. After adsorption, based on chemical bonding between DAS with Se(IV) [$-\text{NH}^+:-\text{NH}_2^+ \text{---} \text{SeO}_3^{2-}$] the solid phase separated/collected in bottom of tube and removed upper liquid phase of water/wastewater. Finally, the Se(IV) determined with F-AAS after desorption Se(IV) from DAS by adding of HNO₃ (0.5 M, 5 mL). The concentration Se(IV) validated by HG-AAS after dilution with DW. For reduction of Se(VI) to Se(IV) the concentrated HCl (50%) was used at 70°C for 30 min. After reduction, the total selenium (TSe) was determined and the Se (VI) was simply calculated by difference of TSe

from Se(IV) content. The linear range(LR), LOD, perconcentration factor (PF) and recovery were obtained 0.5-10.2 mg L⁻¹, 0.12 mg L⁻¹ and 19.8, and 96.5%, respectively

3. Results and discussion

3.1. FT-IR analysis

Fourier Transform Infrared (FT-IR) spectrum of DAS was recorded (Fig. 1) to gain the information about surface functional group. As seen in this spectrum, the stretching vibrations of hydroxyl group (-OH) on DAS surface gives the broad and strong band at 3443 cm⁻¹. The weak peaks at about 2300 cm⁻¹ show the stretching vibrations of -NH, -NH⁺, -NH₂⁺ functional groups of DAS. The band peak at 1646 cm⁻¹ refers to stretching vibrations of -C=O group. The stretching vibrations of -C-O group appears at 1088 cm⁻¹. The band peak at 876 cm⁻¹ is concerned to carbonate group.

3.2. Effect of pH

The effect of pH on the biosorption of Se (IV) by DAS were studied at pH in the range of 2 to 11 for SPE. First, 100 mL selenium solution with concentration 2-9.5 ppm (mg L⁻¹) and 0.5 g DAS at temperature of 25°C (15 min) was used. The results were shown in Figure 2. Three species of selenium in these aqueous solutions include selenite (SeO₃²⁻), biselenite (HSeO₃⁻) and selenious

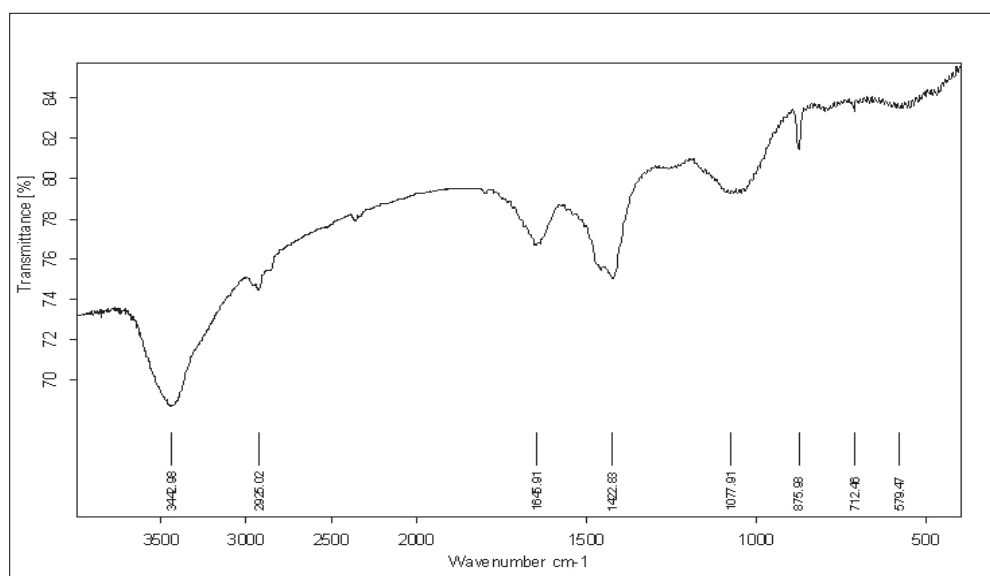


Fig.1. Fourier Transform Infrared (FT-IR) spectrum of DAS

acid (H_2SeO_3) [28, 29]. The selenious acid prevails when pH decreases below 3.5, biselenite prevails when pH is in the range of 3.5 to 9 [2]. The lowest selenium biosorption at pH less than 3.5 is because of inability of neutral selenious acid to interact electrostatically with the DAS. In this work, the highest chemical biosorption of Se(IV) based on DAS was achieved with high recovery more than 95% for batch system and SPE procedure at pH=5.

3.3. Effect of contact time

The effect of contact time, as the next parameter was investigated in the range of 2 to 35 minute at pH=5. As observed in Figure 3, the most proper contact time for selenium biosorption was obtained 15 minutes for SPE. After this contact time, equilibrium occurred. The best time for batch system was obtained 30 min (2 g) for selenium concentration 10 to 140 mg L⁻¹.

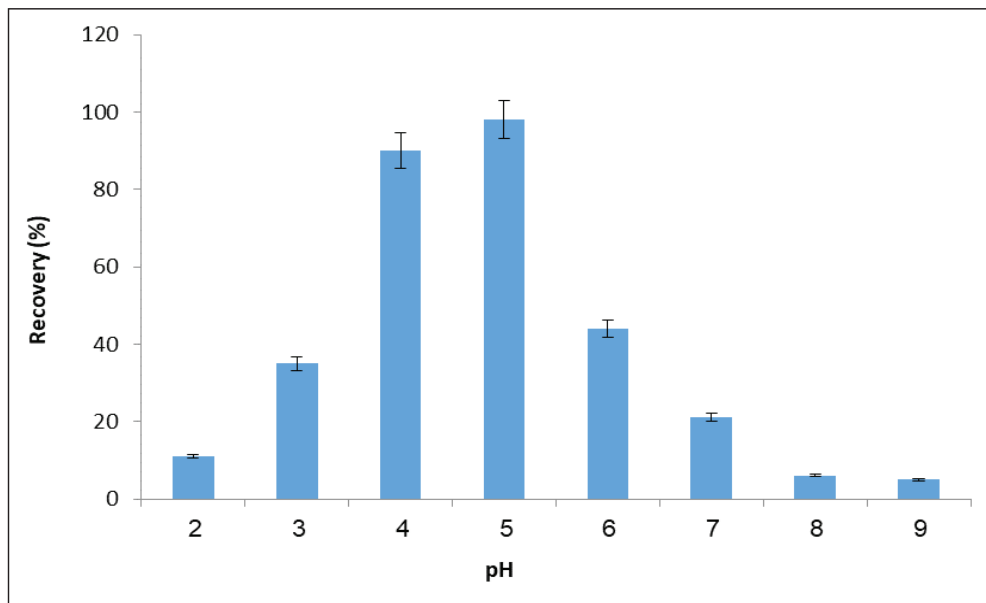


Fig.2. The effect of pH on Se(IV) removal from water and wastewater by DAS

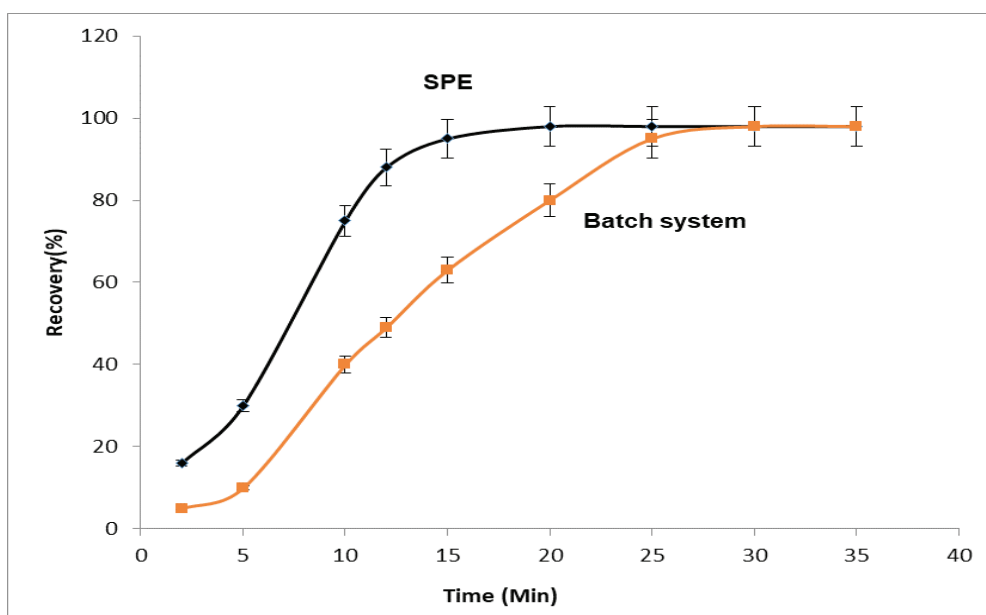


Fig.3. The effect of contact time for removal of Se(IV) from water and wastewater by DAS

3.4. Effect of amount of biosorbent

The effect of amount of biosorbent was investigated under optimized conditions (pH=5 and contact time: 30 min.). As shown in Figure 4, the selenium biosorption increased slowly with the DAS amount up to 2 g for batch system. The DAS surface becomes saturated with the extra Se(IV) ions in

optimized amount of DAS. Therefore, a number of Se(IV) ions remain in solution and biosorption yield decreased. At higher amount of DAS, biosorption yield is almost unchanged. Because most of Se(IV) ions interact with DAS surface. For SPE, the 0.5 g of DAS is favorite mass for removal of Se (IV) in water samples with high recovery more than 95%.

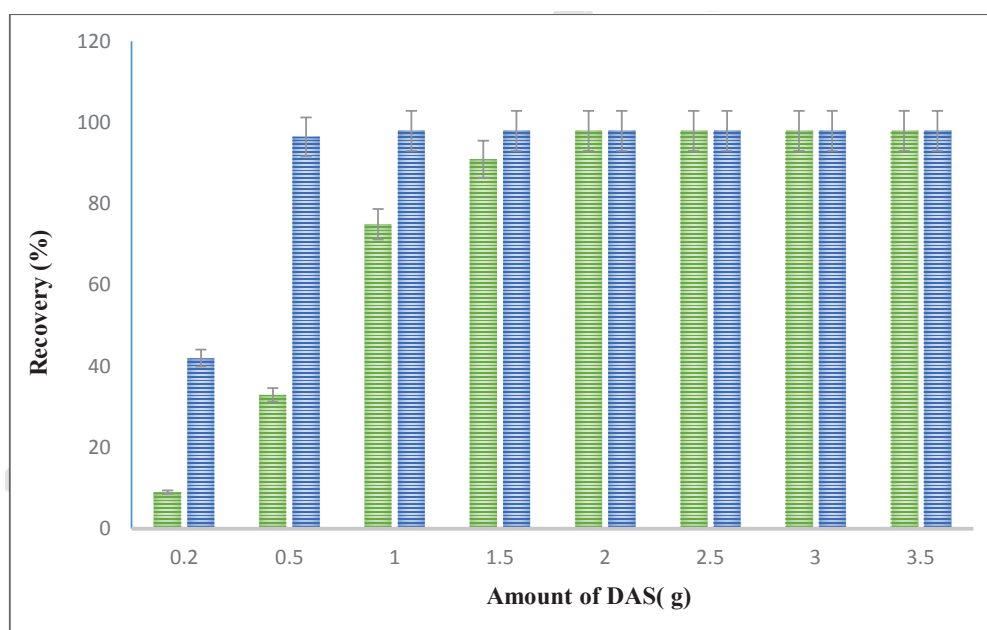


Fig. 4. The effect of biosorbent amount on Se(IV) removal in batch system (green) and SPE procedure(blue) in water and wastewater by DAS

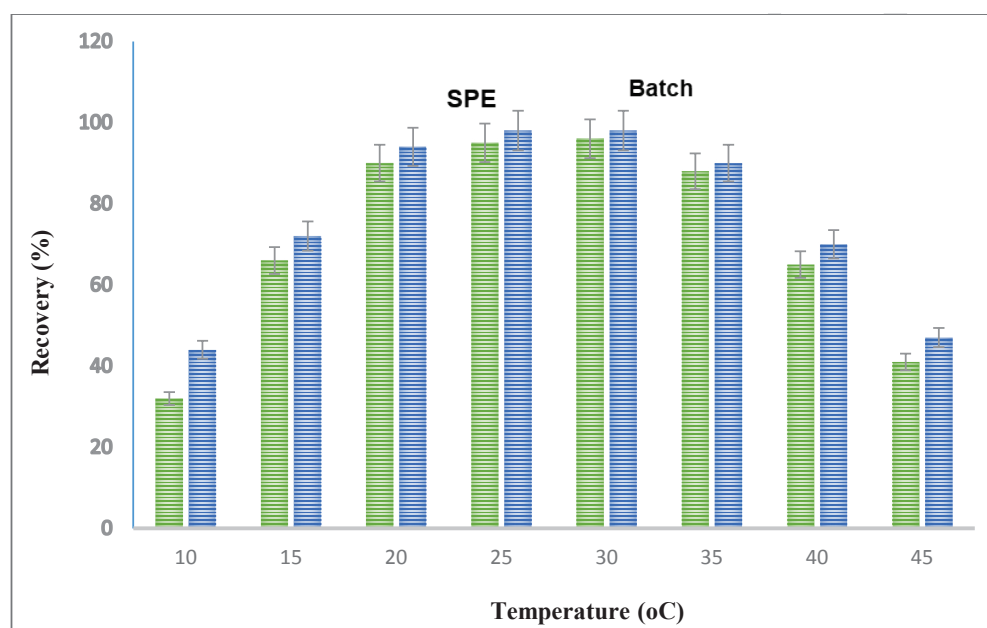


Fig. 5. The effect of temperature on Se(IV) removal in batch system (blue) and SPE procedure(green)from water and wastewater samples by DAS

3.5. Effect of temperature

The effect of temperature on selenium biosorption was investigated between 10-45°C in optimized condition. The results showed us, the optimum temperature was achieved 30°C in optimized condition (pH, contact time and amount of biosorbent DAS were 5, 30 minute and 2 g, respectively). Due to Figure 5, by increasing temperature, the selenium biosorption decreased. It indicated the biosorption by DAS is an exothermic reaction. The best temperature for SPE procedure for DAS was 25-30°C.

3.6. Effect of initial concentration of selenium

Effect of initial concentration of selenium in the range of 20-250 ppm was investigated for absorption capacity. The results indicated that increasing selenium concentration caused to more absorb of the selenium on DAS and decreased the selenium concentration in the solution. The number of sites on DAS were interacted with Se(IV) ions and can be saturated at high concentrations of selenium ions. According to obtained results, the adsorption capacity of Se(IV) ions on DAS increased up to 124.2 mg g⁻¹ [AC; mg per gram]. The results have presented in Figure 6.

3.7. Kinetic isotherms for Se(IV) and Se(VI)

The most popular isotherms are Langmuir [21,30] and Freundlich [21, 31] models. The Langmuir model describes monolayer adsorption, however Freundlich model show heterogeneous surface. The linear form of Langmuir model is given by following equation I:

$$\frac{C_e}{q_e} = \frac{1}{(K_L q_m)} + \frac{C_e}{q_m} \quad (\text{Eq. I})$$

where C_e (mg L⁻¹) is the equilibrium concentration of the solution, q_e (mg g⁻¹) is the amount of metal adsorbed per specific amount of adsorbent, q_m (mg g⁻¹) is the maximum amount of metal ions required to form monolayer, K (L mg⁻¹) is the adsorption equilibrium constant.

The linear form of Freundlich model is given by following equation II:

$$\log(q_e) = \log(K_F) + \left(\frac{1}{n}\right) \log C_e \quad (\text{Eq. II})$$

where n is the adsorption intensity and K_F is the adsorption capacity.

The amount of Se(VI) adsorbed on DAS at equilibrium (q_e , mg g⁻¹) was calculated by Equation (III):

$$q_e = (C_0 - C_e) \times V/m \quad (\text{Eq. III})$$

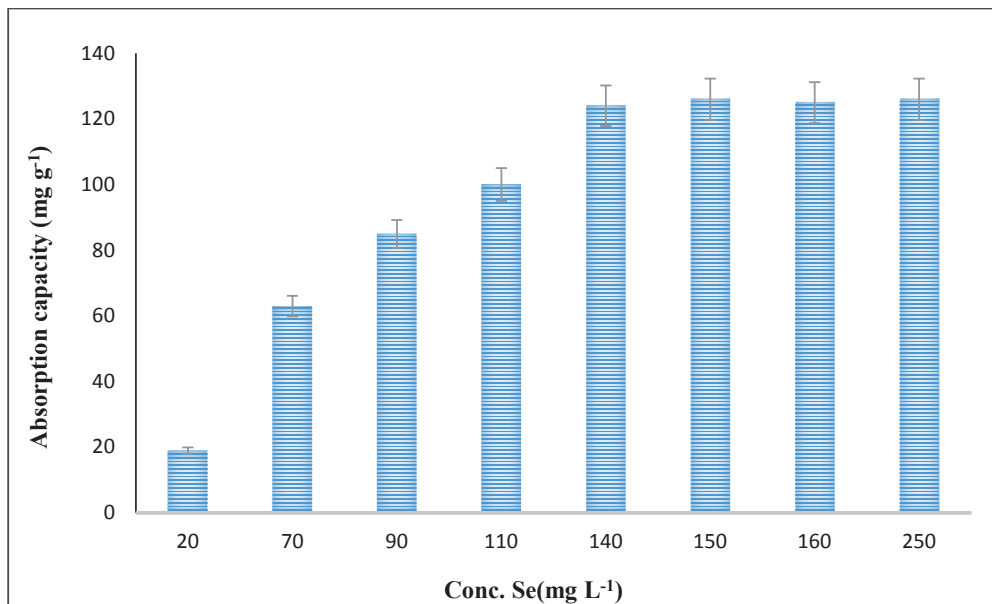


Fig. 6. The effect of initial concentration of Se(IV) ions on absorption capacity of DAS in water and wastewater samples

where C_0 and C_e (mg L^{-1}) are the initial and equilibrium Se(VI) concentrations, respectively, V (L) is the volume of the solution and m (g) is the mass of the adsorbent. ($C_0 = 10\text{-}250 \text{ mg L}^{-1}$, $C_0 = 250 \text{ mg L}^{-1}$ and $C_e = 190 \text{ mg L}^{-1}$, $V = 0.1 \text{ L}$, $m = 0.05 \text{ g}$). So the q_e , q_{max} and C_e/q_e was obtained as 120 mg g^{-1} , 120 mg g^{-1} and 2.08 , respectively. As different concentrations, the C_e/q_e were calculated based on Langmuir model between $0.02\text{-}2.08$.

Linear Langmuir equation was considered to gain

isotherm (Fig. 7). The Se(VI) in solutions with different initial concentrations ($C_0 = 10\text{-}250 \text{ mg L}^{-1}$) were used. Langmuir constants, K_L and q_m were calculated from the slope and intercept of the plot C_e/q_e versus C_e .

As Figure 8, the linear Freundlich isotherm of Se(IV) and Se(VI) is another kinetic model for DAS. Freundlich isotherm parameters, K_F and $1/n$ were calculated from the slope and intercept of linear plot.

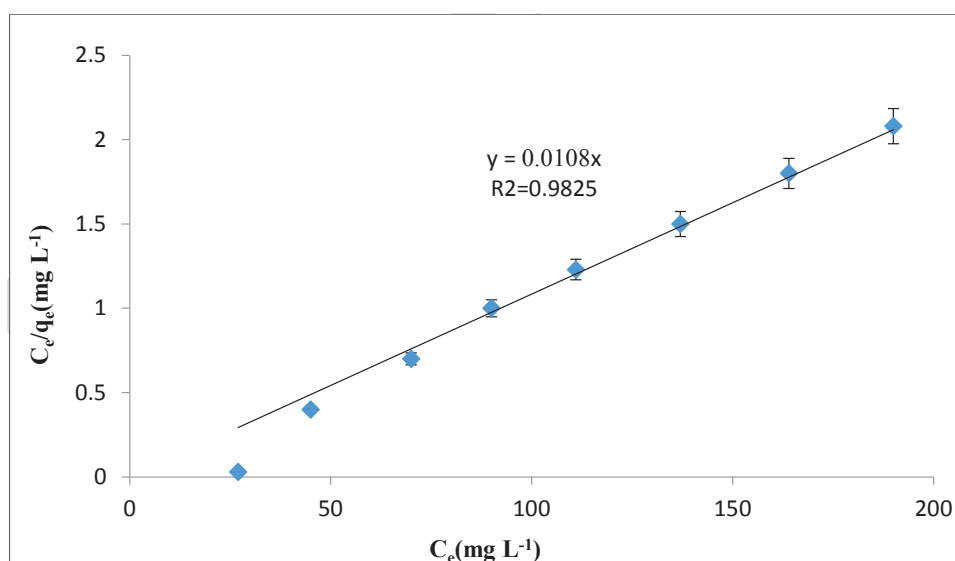


Fig. 7. Linear Langmuir equation for selenium removal by DAS biosorbents from water and wastewater samples

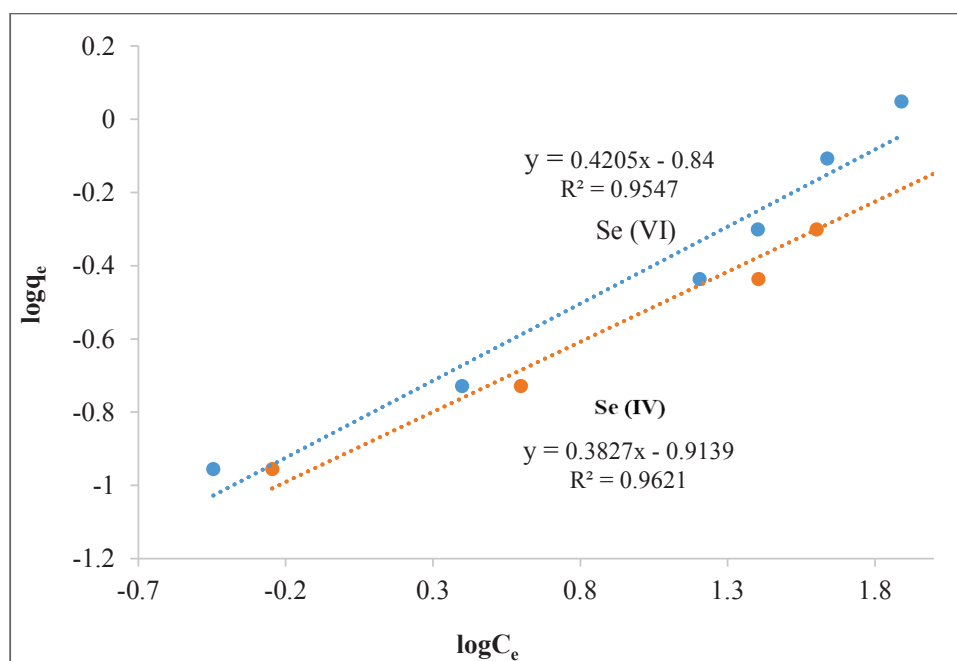


Fig. 8. Linear Freundlich isotherm for selenium removal by DAS biosorbents from water and wastewater samples

3.8. Validation of SPE procedure

The selenium was removed and determined in 100 mL of water and wastewater samples based on DAS with SPE procedure at pH=5. The mean concentration of Se(IV) more than Se(VI) in water samples. The spiked water was used to demonstrate the reliability of the method for determination of Se(IV) and Se(VI) in water samples by SPE procedure. The recovery of spiked samples showed

a satisfactorily result for determination of Se(IV) and Se(VI) in water samples (Table 1). Moreover, the real water samples were analyzed with HG-AAS/ET-AAS and used for validation of results of SPE/F-AAS procedure. The results showed, the favorite efficiency and reliability of proposed method for determination selenium in water and wastewater sample which was compared to ET-AAS and HG-AAS (Table 2)

Table 1. Validation of SPE procedure based on DAS for speciation selenium (VI, IV) in water and wastewater samples (mg L^{-1} ; $n=8$)

Sample	Added Se(IV)	Added Se(VI)	*Found Se(IV)	*Found Se(VI)	Total TSe	Recovery Se(IV) (%)	Recovery Se(VI) (%)
Wastewater 1	-----	-----	4.45± 0.19	1.23± 0.05	5.68 ± 0.24	-----	-----
	4.0	0.5	8.29 ± 0.37	1.75 ± 0.07	10.04± 0.45	96.0	104
Wastewater 2	-----	-----	3.86± 0.18	0.56 ± 0.03	4.42 ± 0.22	-----	-----
	4.0	0.5	7.81 ± 0.35	1.03 ± 0.05	8.84 ± 0.42	98.8	94.7
Wastewater 3	-----	-----	1.95 ± 0.14	1.47± 0.08	3.42 ± 0.15	-----	-----
	2.0	1.5	3.98 ± 0.19	2.95 ± 0.14	6.93 ± 0.34	101.5	98.6
River	-----	-----	ND	ND	ND	-----	-----
	2.0	2.0	1.97 ± 0.11	2.07 ± 4.4	4.04 ± 0.21	94.9	103.5

* $\bar{x} \pm ts / \sqrt{n}$ at 95% confidence ($n=8$)

Well water prepared from Varamin agricultural

Wastewater 1 prepared from drug company

Wastewater 2 prepared from petrochemical factory

Wastewater 3 prepared from paint factory

River water prepared from Karaj

Table 2. Comparing of proposed procedure for selenium determination by F-AAS/DAS with HG-AAS and ET-AAS

Sample	F-AAS/DAS(mg L^{-1})	ET-AAS($\mu\text{g L}^{-1}$)*	*HG-AAS($\mu\text{g L}^{-1}$)
Wastewater*	0.55 ± 0.25	ND	5.36 ± 0.52
Water	ND	41.3 ± 13.81	40.9± 13.81

$\bar{x} \pm ts / \sqrt{n}$ at 95% confidence ($n=5$)

*Wastewater 1 prepared from drug company, 1 mL of sample diluted with DW up to 100 (1:100)

4. Conclusions

In this study, the results showed tetravalent selenium ions (Se_{IV}) biosorption were successfully achieved by DAS from contaminated aqueous solutions. The maximum removal of $\text{Se}(\text{IV})$ ions was 96% at optimized experimental conditions by SPE/F-AAS. The interaction between $\text{Se}(\text{IV})$ ions and functional groups of DAS surface was exothermic. The experimental data were fitted to Freundlich isotherm. Also the speciation $\text{Se}(\text{IV})$ and $\text{Se}(\text{VI})$ ions determined based on DAS by SPE procedure for 0.5 g of DAS at $\text{pH}=5$. The method was validated by ET-AAS and HG-AAS. The absorption capacities for $\text{Se}(\text{IV})$ and $\text{Se}(\text{VI})$ ions with DAS were achieved 124.2 mg g^{-1} and 121.8 mg g^{-1} , respectively.

5. Acknowledgments

The authors would like to thank from Department of Chemistry, Kerman Branch, Islamic Azad University, Kerman, Iran.

6. References

- [1] M. Kashiwa, S. Nishimoto, K. Takahashi, M. Ike, M. Fujita, Factors affecting soluble selenium removal by a selenite reducing bacterium *Bacillus* sp. SF-1, *J. Biosci. Bioeng.*, 89 (2000) 528-533.
- [2] M. Tuzen, A. Sari, Biosorption of selenium from aqueous solution by green alga (*Cladophorahutchinsiae*) biomass: Equilibrium, thermodynamic and kinetic studies, *Chem. Eng. J.*, 158 (2010) 200-206.
- [3] M. Rovira, J. Gimenez, M. Martiinez, X. Marttinez-Lladio, J. Pablo, V. Martii, L. Duro, Sorption of selenium(IV) and selenium(VI) onto natural iron oxides: goethite and hematite, *J. Hazard. Mater.*, 150 (2008) 279-284.
- [4] F.M. Fordyce, selenium deficiency and toxicity in the environment, *Essentials of Medical Geology*, Elsevier Academic Press, Amsterdam, Holland, pp.373-416, 2005.
- [5] K. Nettem, A.S. Almusallam, Equilibrium, kinetic, and thermodynamic studies on the biosorption of selenium (IV) ions onto *Ganoderma Lucidum* Biomass, *Sep. Sci. Tech.*, 48 (2013) 2293-2301.
- [6] H. Robberecht, R.V. Grieken, Selenium in environmental water: determination, speciation and concentration levels, *Talanta*, 29 (1982) 823-844.
- [7] J. Lessa, A. Araujo, G. Silva, L. Guilherme, G. Lopes, Adsorption-desorption reactions of selenium (VI) in tropical cultivated and uncultivated soils under Cerrado biome, *Chemosphere*, 164 (2016) 271-277.
- [8] S. Santos, G. Ungureanu, R. Boaventura, C. Botelho, Selenium contaminated waters: an overview of analytical methods, treatment options and recent advances in sorption methods, *Sci. Total Environ.*, 521-522 (2015) 246-260.
- [9] E.I. El-Shafey, Sorption of Cd(II) and Se(IV) from aqueous solution using modified rice husk, *J. Hazard. Matter.*, 147 (2007) 546- 555.
- [10] F.Sahin, M. Volkan, A.G. Howard, O.Y. Ataman, Selective preconcentration of selenite from aqueous samples using mercapto-silica, *Talanta*, 60 (2003) 1003-1009.
- [11] G. Kallis, D. Butler, The EU water framework directive: measures and implications, *Water Policy*, 3 (2001) 125- 142.
- [12] O.Y. Bakather, A. Kayvani fard, Ihsanullah, M. Khraisheh, M.S. Nasser, M.A. Atieh, Enhanced adsorption of selenium ions from aqueous solution using iron oxide impregnated carbon nanotubes, *Bioinorg. Chem. Appl.*, 2017 (2017) 1-12.
- [13] M. Kieliszek, S. Blazejak, K. Piwowarek, K. Brzezicka, Equilibrium modeling of selenium binding from aqueous solutions by *Candida atilis* ATCC 9950 yeasts, *Biotech.*, 8 (2018) 388: doi: 10.1007/s13205-018-1415-8.
- [14] F.A. Bertolino, A.A.J. Torriero, E. Salinas, R. Olsina, L.D. Martinez. J. Raba, Speciation analysis of selenium in natural water using square-wave voltammetry after preconcentration on activated carbon, *Anal. Chim. Acta*, 572 (2006) 32-38.

- [15] S. Dev, A. Khamkhash, T. Ghosh, S. Aggarwal, Adsorptive removal of Se(IV) by Citrus peels: Effect of adsorbent entrapment in calcium alginate beads, *ACS Omega*, 5 (2020) 17215-17222.
- [16] R.H.S.F. Vieira, B. Volesky, Biosorption: a solution to pollution, *Int. Microbiol.*, 3 (2000) 17-24.
- [17] D.A. Roberts, N.A. Paul, S.A. Dworjanyn, Y. Hu, M.I. Bird, R. de Nys, Gracilaria waste biomass (sampah rumput laut) as a bioresource for selenium biosorption, *J. Appl. Phycol.*, 27 (2015) 611-620.
- [18] S.H. Hasan, D. Ranjan, Agro-industrial waste: a low-cost option for the biosorptive remediation of selenium anions, *Ind. Eng. Chem. Res.*, 49 (2010) 8927-8934.
- [19] S. Beeram, A. Morris, C.J. Hardway, J.C. Richert, J. Sneddon, Studies of whole crawfish shells for the removal of chromium, lead and selenium ions in solution, *Instrum. Sci. Technol.*, 40 (2012) 618-639.
- [20] H. Khakpour, H. Younesi, M. Mohammadhosseini, Two-stage biosorption of selenium from aqueous solution using dried biomass of the baker's yeast *Saccharomyces cerevisiae*, *J. Environ. Chem. Eng.*, 2 (2014) 532-542.
- [21] H. Zare, H. Heydarzadeh, M. Rahimnejad, A. Tardast, M. Seyfi, S.M. Peyghambarzade, Dried activated sludge as an appropriate biosorbent for removal of copper (II) ions, *Arab. J. Chem.*, 8 (2015) 858-864.
- [22] L. Bennamoun, P. Arlabosse, A. Leonard. Review on fundamental aspect of application of drying process to wastewater sludge, *Renew. Sust. Energ. Rev.*, 28 (2013) 29-43.
- [23] H. Shirkhanloo, F. Golbabaie, H. Hassani, F. Eftekhar, M.J. Kian, Occupational exposure to mercury: air exposure assessment and biological monitoring based on dispersive ionic liquid-liquid microextraction, *Iran. J. Public Health*, 43 (2014) 793.
- [24] S. Golkhah, H. Zavvar Mousavi, H. Shirkhanloo, A. Khaligh, Removal of Pb (II) and Cu (II) Ions from Aqueous Solutions by Cadmium Sulfide Nanoparticles, *Int. J. Nanosci. Nanotechnol.*, 13 (2017) 105-117.
- [25] H. Shirkhanloo, A. Khaligh, H.Z. Mousavi, A. Rashidi, Graphene oxide-packed micro-column solid-phase extraction combined with flame atomic absorption spectrometry for determination of lead (II) and nickel (II) in water samples, *Int. J. Environ. Anal. Chem.*, 95 (2015) 16-32.
- [26] M. Arjomandi, H. Shirkhanloo, A review: Analytical methods for heavy metals determination in environment and human samples, *Anal. Methods Environ. Chem. J.*, 2 (2019) 97-126.
- [27] H. Shirkhanloo, S. A. H. Mirzahosseini, N. Shirkhanloo, The evaluation and determination of heavy metals pollution in edible vegetables, water and soil in the south of Tehran province by GIS, *Arch. Environ. Protec.*, 41 (2015) 64-74.
- [28] M. Duc, G. Lefevre, M. Fedoroff, Sorption of selenite ions on hematite, *J. Colloid Interface Sci.*, 298 (2006) 556-563.
- [29] T. Nishimura, H. Hashimoto, M. Nakayama, Removal of selenium(VI) from aqueous solution with poly-amine type weakly basic ion exchange resin, *Sep. Sci. Technol.*, 42 (2007) 3155-3167.
- [30] I. Langmuir, The adsorption of gases on plane surfaces of glass, mica and platinum, *J. Am. Chem. Soc.*, 40 (1918) 1361-1403.
- [31] H. Freundlich, Adsorption in solution. *J. Phys. Chem.*, 57 (1906) 384-410.



Simultaneous adsorption of cationic and anionic dyes using a novel multifunctional mesoporous silica

Amir Vahid ^{a,*}, Majid Abdouss ^b, Shahnaz Nayeri ^b, Aliakbar Miran Beigi ^a

^a Research institute of petroleum industry, Tehran, Iran

^b Faculty of chemistry, Amirkabir University of Technology, Tehran, Iran

ARTICLE INFO:

Received 17 Nov 2020

Revised form 22 Jan 2021

Accepted 15 Feb 2021

Available online 29 Mar 2021

Keywords:

Adsorption,
Multi-Functional,
Dye,
Mesoporous silica,
Synthesis.

ABSTRACT

In the present work a multifunctional nanoadsorbent was synthesized via a well-designed stepwise route, led to the grafting of an amine group on the interior and acidic sites on the exterior of bimodal mesoporous silica nanoparticles (UVM-7). First, amine and thiol groups were grafted on the interior and exterior pores of silica through co-condensation and post synthesis treatment, respectively. Then, the oxidation of thiol on UVM-7 caused to create sulfonic acid and the subsequent template extraction was carried out to obtain the $\text{NH}_2/\text{UVM-7}/\text{SO}_3\text{H}$. The results of XRD, the nitrogen sorption, SEM, TEM, FT-IR and elemental analysis revealed the presence of both types of functional groups on UVM-7. Then, simultaneous adsorption of anionic and cationic dyes (Methylene Blue [MB] and Direct Red 23 [Dr]) using $\text{NH}_2/\text{UVM-7}/\text{SO}_3\text{H}$ was investigated. UV-Vis spectrophotometry was utilized for the determination of dyes in single and binary solutions. Langmuir and Freundlich models were used for the fitting of obtained experimental adsorption data and the constants of both isotherms were calculated for MB and Dr. Moreover, the calculation of thermodynamic parameters revealed that the adsorption of MB and Dr on $\text{NH}_2/\text{UVM-7}/\text{SO}_3\text{H}$ was endothermic and spontaneous. Furthermore, the simultaneous adsorption of both dyes regardless of their different electrostatic charge is the main characteristics of $\text{NH}_2/\text{UVM-7}/\text{SO}_3\text{H}$ which was specially used for treatment of industrial wastewater.

1. Introduction

Dyes as a important raw material were used in different industries including cloth, plastics, tanning, cosmetics and food [1]. Additionally, the dyes are one of the most problematic groups as a results of their environmental impact. Furthermore, the industrial effluents containing dyes may be have a carcinogenic effect in humans when, discharge to waters without any proper treatment.

Methylene Blue (MB) and Direct red (Dr) as the cationic and anionic dyes have harmful effects on human life and environment. Acute exposure to MB causes many health effect such as increased heart rate and cyanosis jaundice quadriplegia in mammals [2,3]. Up to now, the dye adsorption studies have focused on solutions containing single dye and mixture of dyes [4-6]. The most industrial effluents include a mixture of several dyes, so it is necessary to study the simultaneous adsorption of two or more dyes from aqueous solutions [7,8]. However, the dyes are resistance to biodegradation due to their aromatic structure [9]. Many industrial

*Corresponding Author: Amir Vahid

Email: avahid753@gmail.com & vahida@ripi.ir

<https://doi.org/10.24200/amecj.v4.i01.127>

technologies, including chemical oxidation [10], adsorption [11], the coagulation/flocculation [12], the membrane separation and ion exchange [13] was used for the adsorption of dyes from industrial effluents. Among them, adsorption has been known as one of the practical physical processes for the treatment and cleaning of wastewaters, because it is cost effective and very effective. The main problem of this technology is the synthesis of low cost adsorbent possesses with high adsorption capacity [14]. In multi-dye adsorption, the interference of one dye on the other dyes is very important [15]. The liquid chromatography [16], the capillary electrophoresis [17], the spectrometry [18] and the electrochemistry methods [19] are used for the analysis of dyes. Due to advantages of UV-Vis spectrophotometry such as accuracy of results, sensitivity, low cost, easy operation and reproducibility, it was used for analysis of colored samples [20]. The main drawback of this technique is the overlap and interference of broad absorption peaks. So, the simultaneous analysis of mixture dyes could be carried out using derivative spectrophotometry [21]. It was determined based on the derivative values of interest compound while other components have zero value [22].

Also, many applications were used by UVM-7 in different sciences [23-26]. In this work, the synthesis of a multifunctional mesoporous silica contains both acidic and basic functional groups were reported. At the second step, the adsorption of MB / Dr from aqueous solution was carried out simultaneously and the adsorption phenomenon was studied.

2. Experimental

2.1. Reagents and materials

All reagents with ultra-trace analytical grade such as; lead nitrate salt, acids and base solutions were purchased from Merck (Darmstadt, Germany). The structure of MB and Dr are shown in Figure 1. Ultrapure water has been obtained from Millipore continental water system (Bedford, USA). Tetraethyl orthosilicate (TEOS, $(C_2H_5O)_4Si$, CAS N: 78-10-4, Sigma), triethanolamine ($TEAH_3$, $C_6H_{15}NO_3$, CAS N: 102-71-6, Sigma), cetyltrimethylammonium bromide (CTAB, $C_{19}H_{42}BrN$, CAS N: 57-09-0, Merck) and other reagents with analytical grade were prepared from Merck or Sigma Aldrich, Darmstadt, Germany. The pH adjustments were made using appropriate buffer solutions (Merck, Germany).

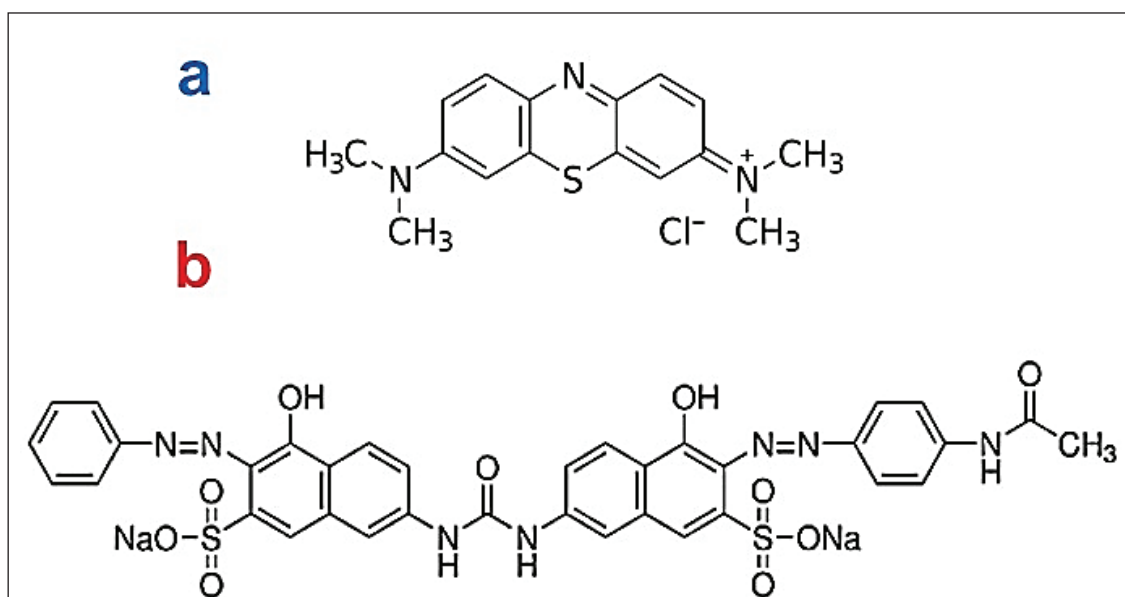


Fig.1. The structure of MB(a) and Dr(b)

2.2. Synthesis of UVM-7

UVM-7 was synthesized via well-known atrane route in which triethanol amine (TEAH3), has effect on the rate of hydrolysis and condensation of tetraethyl orthosilicate (TEOS). In a typical synthesis, mixture of TEOS and TEAH3 heated up to 120 °C and then CTAB (cetyltrimethylammonium bromide) was added when the temperature of the solution reached to 70°C. After addition of water a suspension was formed and aged for 4 hours at ambient temperature. The final molar composition of the synthesis mixture was 1.0 TEOS : 3.5 TEAH3 : 0.25 CTAB : 90 H₂O. The product was filtered, washed with water and acetone and dried in an oven at 80°C overnight and calcined at 550°C for 6 hours.

2.3. Synthesis of NH₂-UVM-7/SO₃H

First, 1.0 g of aminopropyle triethoxysilane (APTES) was added to the aqueous solution of CTAB and after 5 minutes, mixture of TEOS and TEAOH, was added to the micellar solution. The reactants molar ratio was 1.0 TEOS: 3.5 TEAH3 : 0.25 CTAB : 90 H₂O: 0.20 APTES. After aging, the white suspension was filtered and washed thoroughly with water and acetone. The white precipitate dried in oven over night at 80 °C. At the second step, 1.0 g of the as-synthesized NH₂/UVM-7 and 1.0 g of triethoxysilane propanethiol (TPTES) was refluxed in 50 mL of toluene for 12 hours and then, the mixture filtered and dried in oven again. Then, thiol groups grafted on the external surface of the sample was oxidized in 15% H₂O₂ and 1 molar solution of H₂SO₄. Then, CTAB of the as-synthesized NH₂/UVM-7/SO₃H was removed by reflux in 1 molar ethanolic solution of HCL for 24 hours to get access to the internal pores and amine groups. The final product was dried in oven at 80 °C in vacuum oven overnight.

2.4. Batch adsorption procedure

In each test, 0.1 g of adsorbent was added to the 10 mL of a solution containing a known concentration of each dyes while agitating at 250 rpm at 25 °C. After 120 minutes the concentration of residual dyes in supernatant was determined by UV–Vis

spectrophotometer at 502 and 664 nm for Dr and MB, respectively. In binary solution, the best wavelength for each dye was find out utilizing first-order derivative spectrometry.

The adsorption percentage (R%) and adsorption capacity of each dye q_e , (mg dye/g adsorbent) was calculated according to the following equations (Eq.1 and Eq.2):

$$q_e = \frac{(C_0 - C_e)V}{M} \quad (\text{Eq. 1})$$

$$R\% = \frac{(C_0 - C_e)}{C_0} \times 100 \quad (\text{Eq. 2})$$

Where C_0 and C_e (mg L⁻¹) are the initial and equilibrium concentration of dye, respectively. V (L) is the volume of the solution and M (g) is the mass of adsorbent used.

2.5. Characterization

X-ray diffraction (XRD) patterns were recorded using a Philips 1840 diffractometer using nickel-filtered Cu K α (1.5418 Å) X-ray source, operating at 35.4 kV and 28 mA. Textural properties of the synthesized samples were measured by nitrogen adsorption at 77 K using a BELSORP-max apparatus after being out-gassed in vacuum at 120 °C. Elemental analysis was carried out using CHNS-Elementar. FT-IR spectra was recorded using a FT-IR 70 VERTX Bruker spectrophotometer using KBr powder. UV–Vis spectrophotometer was used to measure the concentration of the Methylene Blue and Direct red23 in aqueous solution. FE-SEM images were captured using Mira TESCAN 3-XMU. Samples were sputtered with gold prior to imaging. TEM images were recorded at 150 kV operating voltage using a Zeiss microscope.

3. Results and discussion

3.1. Characterization of NH₂/UVM-7/SO₃H

XRD pattern of NH₂/UVM-7/SO₃H is shown in Figure 2.

A strong and broad diffraction peak can be observed which is characterized in bimodal meso/macroporous material. This peak can be attributed to diffraction of incident X ray from the d_{100} plane. According to the hexagonal symmetry, two weak and broad peaks at higher diffraction angles can be assigned to d_{110} and overlap of d_{200} and d_{210} planes, respectively.

3.2. Nitrogen physisorption

The isotherms of UVM-7 and $\text{NH}_2/\text{UVM-7}/\text{SO}_3\text{H}$ is shown in Figure 3. The isotherms showed the four type of isotherm according to the IUPAC classification. In both isotherms, at low relative

pressure, the inflection is not sharp. By approaching to the saturated relative pressure, increasing of gas uptake led to the sharp increasing of isotherm. This can be attributed to the inter particles of UVM type material which is also present in $\text{NH}_2/\text{UVM-7}/\text{SO}_3\text{H}$ after internal and external grafting of organic moieties. The high BET surface area and pore volume means that the pore structure/size almost preserved after grafting. However, after grafting of organic moieties on UVM-7, the sharpness of these region slightly decreases. The two inflections in $\text{NH}_2/\text{UVM-7}/\text{SO}_3\text{H}$ can be attributed to the presence of two types of pore system.

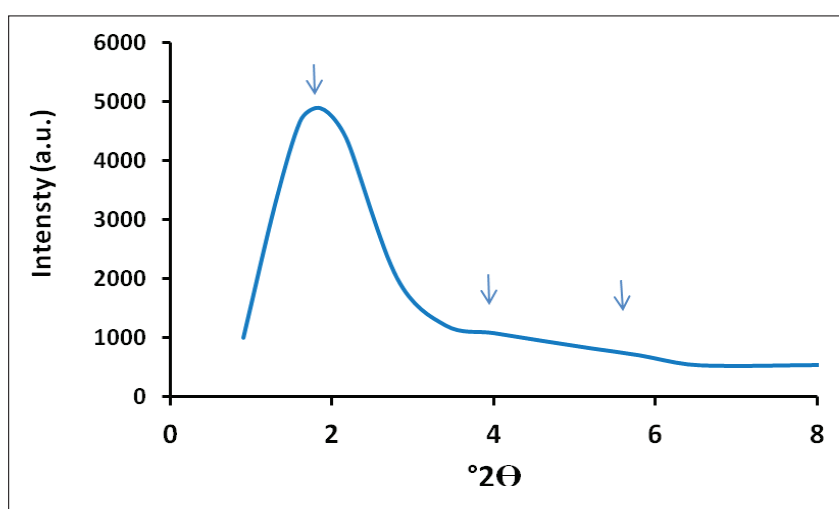


Fig. 2. The XRD pattern of $\text{NH}_2/\text{UVM-7}/\text{SO}_3\text{H}$

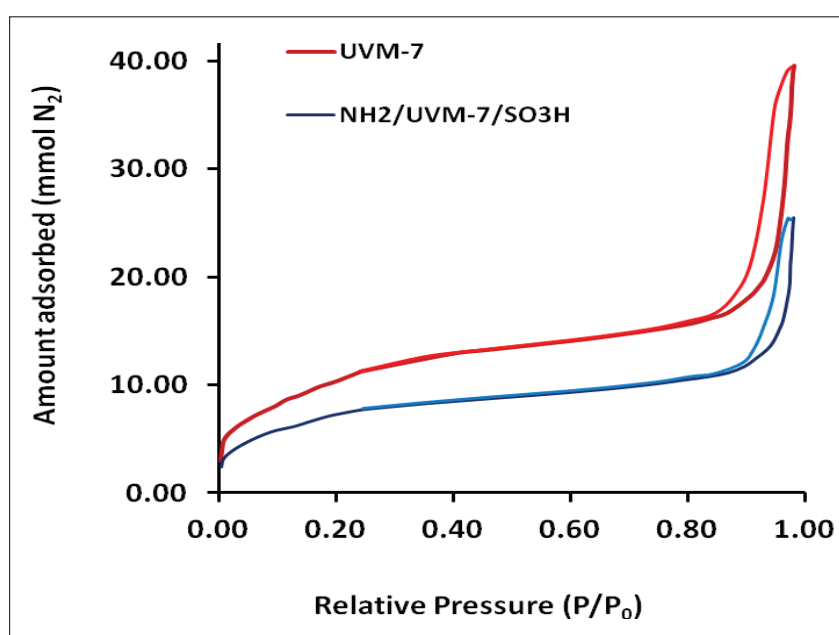


Fig. 3. The isotherms of UVM-7 and $\text{NH}_2/\text{UVM-7}/\text{SO}_3\text{H}$

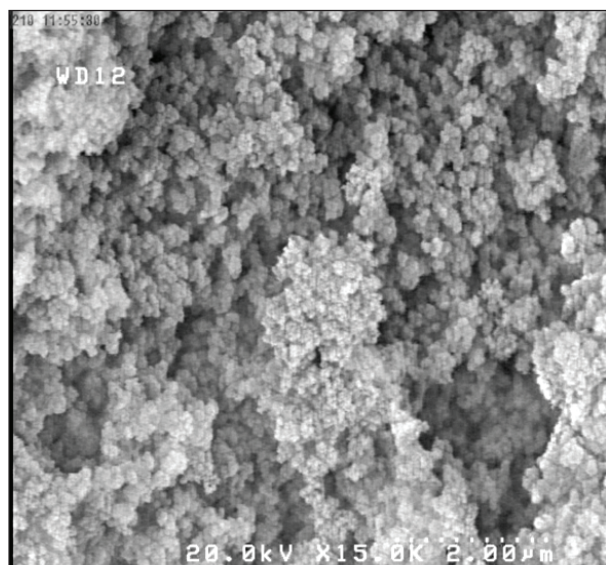


Fig.4. The SEM of NH₂/UVM-7/SO₃H

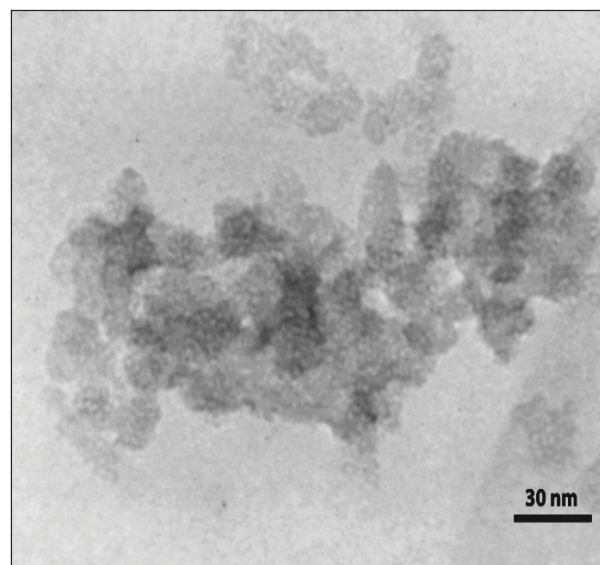


Fig.5. The TEM of NH₂/UVM-7/SO₃H

3.3. TEM and SEM

Electron microscopy is a powerful technique provides a direct view of porous structure, particle morphology and many other information of porous materials at nanoscale. The SEM of NH₂/UVM-7/SO₃H reveals the particle size, shape and morphology of nanomaterials. [Figure 4](#) illustrates the SEM image of NH₂/UVM-7/SO₃H. The sample composed of nanosize particles without presence of large agglomerates. The shape of the nanoparticles is almost irregular. The TEM image of the NH₂/UVM-7/SO₃H is taken perpendicular to d_{100} direction of pores and is displayed in [Figure 5](#). Pore openings are clearly visible. Particle size in sub-ten nanometers and is in agreement with those seen in SEM image.

FT-IR spectra of SO₃H/UVM-7/NH₂ is shown in [Figure 6](#). FT-IR spectroscopy was utilized to indicate the existence of NH₂ and SO₃H functional groups on the UVM-7. Two distinct peaks around 457 cm⁻¹ and 1082 cm⁻¹ is attributed to the symmetric and asymmetric stretching bands of Si-O-Si group in the framework of UVM-7. A broad peak at around 3451 cm⁻¹ is assign to the silanol groups on the surface of UVM-7. A small absorption band at 1558 cm⁻¹ is attributed to the bending vibration of amine group which overlapped with symmetric bending vibrations of O-H. A stretching mode of NH₂ is also overlapped with silanol group's around 3451 cm⁻¹. This indicates that the UVM-7 possess of NH₂ groups. A shoulder, overlapped with asymmetric stretching of Si-O-Si,

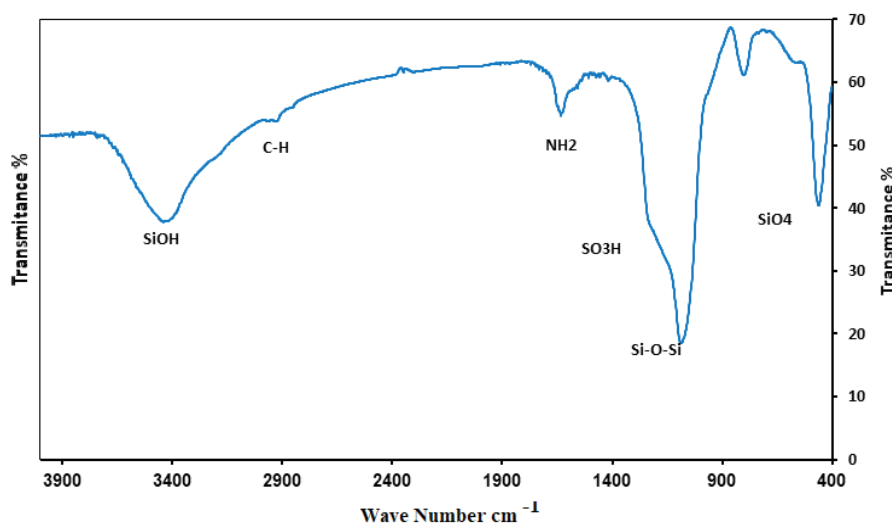


Fig. 6. The FT-IR spectra of SO₃H/UVM-7/NH₂

is attributed to the SO_3^- and $\text{S}=\text{O}$ stretching mode of sulfonic acid functional group. It cannot be seen absorption mode of $\text{S}-\text{H}$ group in the entire spectrum means that thiol groups were fully oxidized to sulfonic acid. Two small absorption peaks at 2852 cm^{-1} and 2926 cm^{-1} is characteristic of the stretching vibration mode of methylene groups of the propyl chain of the APTES and TPDES.

These results approve coexistence of amine and sulfonic acid groups on UVM-7 simultaneously. This statement is supported by elemental analysis of $\text{NH}_2/\text{UVM-7}/\text{SO}_3\text{H}$. Elemental analysis of $\text{NH}_2/\text{UVM-7}/\text{SO}_3\text{H}$ revealed that the sample contains 4.9% (w/w basis) of nitrogen and 5.0% of sulfur.

These results proof presence of amine and sulfonic acid functional groups on $\text{NH}_2/\text{UVM-7}/\text{SO}_3\text{H}$.

3.4. Determination of MB and Dr in single and binary solution

The calibration curve obtained from absorbance spectra of MB and Dr versus concentration at λ_{max} of the corresponding dye and used for the determination of dyes in single solution. The concentration of dyes in binary solution of MB and Dr is obtained by first order derivative spectrophotometry by plotting the change rate of absorbance against wavelength. The obtained spectra for raw and derivative spectra are displayed in Figure 7a and 7b.

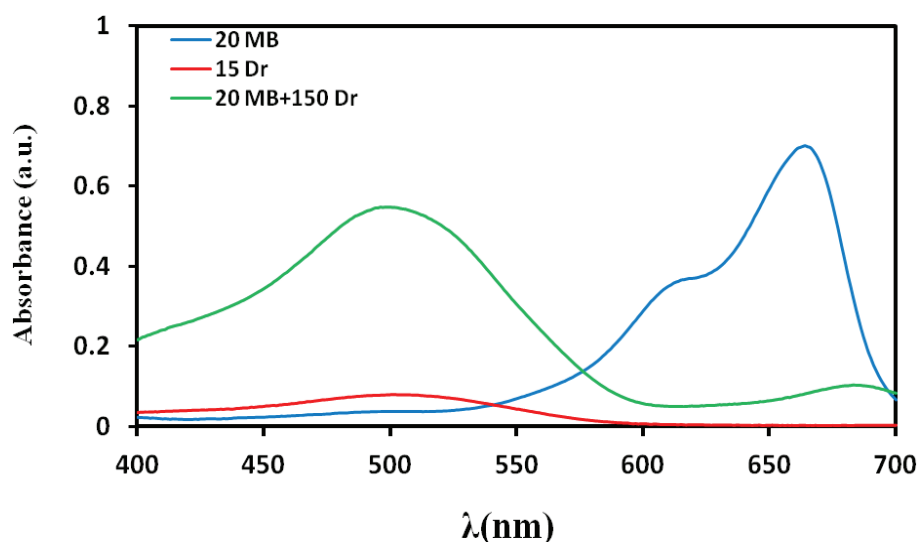


Fig. 7a. The Raw absorption spectra of: MB (20 mg L^{-1}), Dr (15 mg L^{-1}), and their mixture at λ_{max} of the corresponding dye

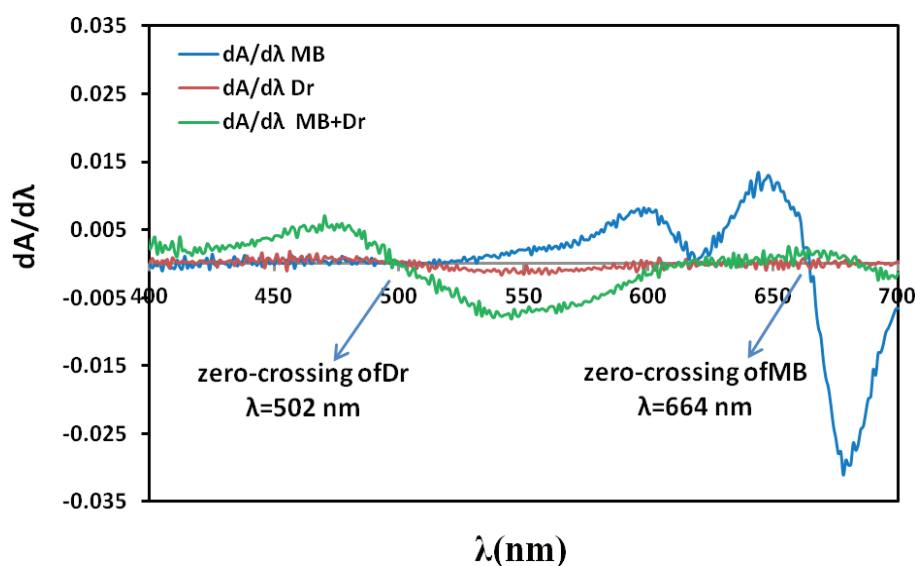


Fig. 7b. The first derivative spectra of MB, Dr, and their mixture by plotting the change rate of absorbance against wavelength

The calibration curves for determination of each dye in the presence of the other one were obtained by measuring of first-order derivative at the zero crossing points of Dr (502 nm) and MB (664nm) [27, 28]. Several standard binary mixtures of MB and Dr were used for the validation of the method. The regression equations and coefficients of determinations, are given in Table 1.

3.5. Equilibrium modeling

3.5.1. Single-component adsorption isotherm

Two well-known adsorption model, Langmuir and Freundlich, were applied to the adsorption data of single-component dye solution (Equation 3 and 4) [29, 30]. In single solution, the R² of Langmuir

isotherm was higher than that of Freundlich, which implies that suggestions of Langmuir model. The homogenous adsorption sites, equal activation energy and monolayer formation, is predominantly determine the mechanism of adsorption. The isotherm constants are presented in Table 2.

$$\frac{C_e}{q_e} = \frac{1}{bq_m} + \frac{C_e}{q_m} \quad (\text{Eq. 3})$$

$$\text{Log } q_e = \text{Log } K_f + \frac{1}{n} \text{log } q_m \quad (\text{Eq. 4})$$

3.5.2. Multi-component adsorption isotherms

In this case, competition for occupation of adsorption sites by adsorbate molecules occur and

Table 1. Determination of MB and Dr in mixture solution using zero-derivative and first-derivative spectrophotometry

Solution No.	*MB(mg L ⁻¹)	*Dr (mg L ⁻¹)	^a Regression equations	R ²
1	1-5	0	S = 0.008C+0.1841	0.9981
2	2-20	10	B = 0.0015C+0.002	0.9890
3	0	1-10	S = 0.0471C+0.021	0.9974
4	2	10-25	B = 0.0001C-0.0006	0.9963

*C is the concentration of the corresponding dye(mg L⁻¹)

^aS and B is the response in single and binary solution

Table 2. Parameters of Langmuir and Freundlich models in single and binary solutions.

Langmuir	q _e (mg g ⁻¹)	b(mg L ⁻¹)	R ²	
MB(sin)	52.63	0.226	0.987	
Dr(sin)	88.33	0.0983	0.996	
MB(bin)	18.86	0.0096	0.876	
Dr(bin)	100	0.1315	0.977	
Freundlich	K _f (mg g ⁻¹)	n	R ²	
MB(sin)	0.0272	3.412	0.947	
Dr(sin)	23.28	3.984	0.950	
MB(bin)	98.24	2.32	0.958	
Dr(bin)	172.60	5.29	0.806	
Extended-Langmuir	q _{max} (mg g ⁻¹)	b ₁	b ₂	R ²
MB(bin)	74.32	0.0021	0.0038	0.999
Dr(bin)	106.78	0.0043	0.0056	0.998

Condition: 10 mL solution, pH: 4 in single and binary solutions.

led to a complex adsorption model. Furthermore, for the design of treatment/refining systems, understanding the mechanism of multi-component adsorption is very important. Despite the difficulty of obtaining of a model for adsorption of binary mixtures, extended-Langmuir model was developed to explain equilibrium adsorption model in such system is as Equation 5:

$$q_{e,i} = \frac{q_i b_i c_i}{1 + \sum b_j c_j} \times 100 \quad (\text{Eq. 5})$$

Using non-linear regression technique, parameters of Equation 5 were obtained given in Table 2. High regression coefficients (R^2 : 96.98–99.86) indicate that the extended Langmuir model has the ability to explain the adsorption equilibrium of binary solution of MB and Dr.

3.6. Adsorption kinetic

The kinetic data of adsorption was obtained with the initial concentrations of 50 mg L⁻¹ and 100 mg L⁻¹ for MB and Dr, respectively. Solutions prepare in 25 mL flask with the stirring rate of 300 rpm and the contact time was changed in the range of 10 to 120 minutes. to evaluate if there are changes/interferences in the adsorption process in the presence of other dyes in the solution.

3.6.1. Pseudo-first order model

The pseudo- first order kinetic model has been

widely used to explain kinetic of adsorption. The model was described by the following Equation 6:

$$\frac{1}{q_t} = \frac{k_1}{q_e} \left(\frac{1}{t}\right) + \frac{1}{q_e} \quad (\text{Eq. 6})$$

Where q_e and q_t are the adsorption capacities (mg g⁻¹) at equilibrium and at time t , respectively. K_1 is the rate constant of pseudo-first order adsorption (L min⁻¹). The pseudo-second order rate equation of McKay and Ho can be represented in the Equation 7.

$$\frac{t}{q_t} = \frac{1}{k_2 q_e^2} + \frac{1}{q_e} t \quad (\text{Eq. 7})$$

Where q_e is the equilibrium adsorption capacity, and K_2 is the pseudo-second order constants (g mg⁻¹.min⁻¹). These terms can be determined experimentally from the slope and intercept of plot t/q_t versus t , shown in Figure 8. The coefficients of both models are shown in Table 3. In all cases including single and binary solutions, the pseudo-second order model has better coefficient of determination, R^2 , which means that kinetic of adsorption of MB and Dr on NH₂/UVM-7/SO₃H can be explained by The difference between two kinetic model can be attributed to the number and accessibility of adsorption sites, specific surface area, pore size, nature of the functional groups of adsorbent and chemical structure of dyes.

Table 3. Kinetics parameters values for the adsorption of MB and Dr on NH₂-SO₃H/UVM-7 in single (sin) and binary (bin) dyes solution

	Pseudo-first order			Pseudo-second order		
	q_e (mg g ⁻¹)	K_1 (min)	R^2	q_e (mg g ⁻¹)	K_2 (g mg ⁻¹ .min ⁻¹)	R^2
MB(sin)	40	3.7	0.867	50	0.0012	0.962
Dr(sin)	4.3	2.43	0.765	5.26	0.372	0.983
MB(bin)	15.87	2.142	0.876	12.98	0.082	0.934
Dr(bin)	66.66	1	0.765	90.9	0.00068	0.826

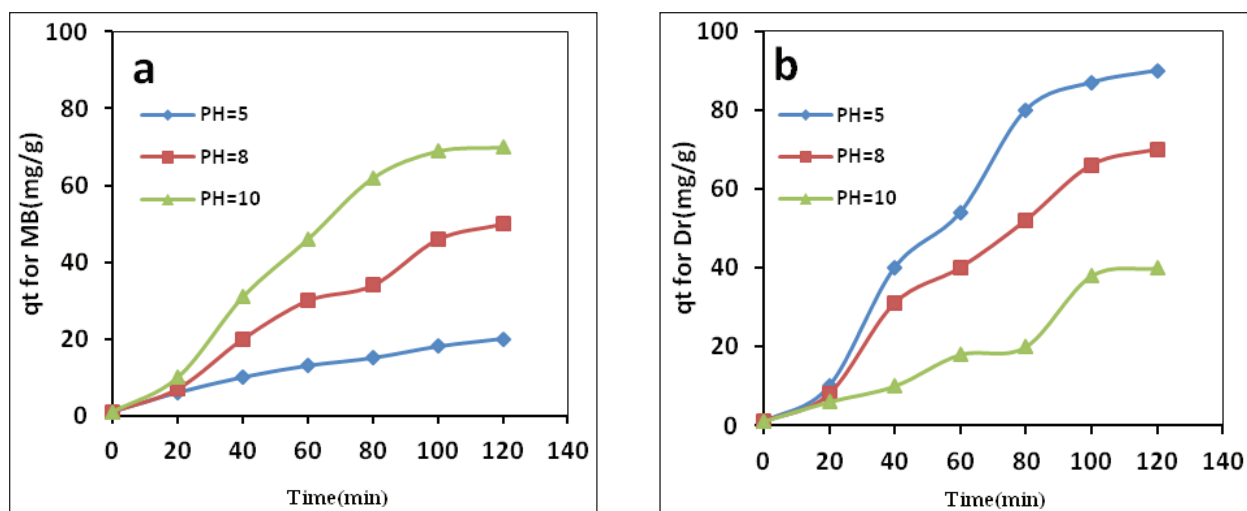


Fig. 8. The effect of pretreatment pH on selective adsorption of MB (a) and Dr (b) on $\text{NH}_2\text{-SO}_3\text{H/UVM-7}$ in binary solution (temperature 30°C , 400 mgL^{-1} initial dye concentration).

3.6.2. Selective adsorption of cationic and anionic dyes

Figure 8 displays that $\text{NH}_2\text{/UVM-7/SO}_3\text{H}$ can selectively adsorb the anionic Dr from the Dr/MB mixture and pretreated at $\text{pH}=5$. While, the $\text{NH}_2\text{/UVM-7/SO}_3\text{H}$ can selectively adsorb the cationic MB dye from the Dr/MB mixture and pretreated at $\text{pH}=10$. This test verifies with the easy, the special treatment and selective adsorption of cationic or anionic dyes by $\text{NH}_2\text{-SO}_3\text{H/UVM-7}$.

3.6.3. Thermodynamic studies

The effect of temperature on the adsorption of MB and Dr onto $\text{NH}_2\text{/UVM-7/SO}_3\text{H}$ was investigated. The obtained results indicate that the amount of equilibrium adsorption (q_e) of MB and Dr on the $\text{NH}_2\text{/UVM-7/SO}_3\text{H}$ slightly increases with increasing temperature which reveals the endothermic nature of adsorption. Main thermodynamic parameters including standard free energy (ΔG), enthalpy (ΔH) and entropy (ΔS) were obtained using Equation 8.

$$\ln kc = \frac{-\Delta H}{RT} + \frac{\Delta S}{R} \quad (\text{Eq. 8})$$

Where R is gas constant ($8.314\text{ Jmol}^{-1}\text{K}^{-1}$) and T

is temperature in Kelvin. The apparent equilibrium constant (K_c) of the adsorption is defined as Equation 9.

$$k_c = \frac{C_a}{C_b} \quad (\text{Eq. 9})$$

Where C_a and C_b is the equilibrium concentration (mg L^{-1}) a of corresponding dye on the adsorbent and in the solution, respectively. The K_c value is used in the Equation 10 to determine the Gibbs free energy of adsorption (ΔG).

$$\Delta G = -RT \ln Kc \quad (\text{Eq. 10})$$

Furthermore, ΔH and ΔS were calculated from the slope and intercept of the linear plot of $\ln Kc$ versus $1/T$, respectively. The obtained thermodynamic parameters are summarized in Table 4. All ΔG values are negative which imply that the spontaneous nature of adsorption. Furthermore, the value of ΔG becomes more negative with increasing of temperature, indicating that the adsorption process is more favorable at higher temperature. As can be seen in Table 4, the positive value of adsorption enthalpy, ΔS , confirms the endothermic nature the adsorption process.

Table 4. Values of thermodynamic parameters for dye adsorption from binary solution onto NH₂/UVM-7/SO₃H

Dye	Temp.(K)	$\Delta G(\text{kJ mol}^{-1})$	$\Delta H(\text{kJ mol}^{-1})$	$\Delta S(\text{kJ mol}^{-1} \text{K}^{-1})$
MB	298	-2.95	8.1	0.038
	308	-3.21		
	318	-3.43		
	328	-3.98		
Dr	298	-4.83	26.3	0.106
	308	-5.82		
	318	-6.98		
	328	-7.83		

4. Conclusions

In This work, a novel synthesis method was developed for the preparation of an adsorbent contains both sulfonic acid and basic amine groups in the exterior and interior pores of UVM-7, respectively. This multifunctional adsorbent, NH₂/UVM-7/SO₃H, can be used for simultaneous removal of multiple dyes with different electrostatic charge. In real aqueous sample and wastewater there are several dyes which differ in their nature. Furthermore, one of the most effective parameters in the removal of dye is its electrostatic charge. On the other hand, large pore size and surface area of UVM-7 can improve the diffusion of the dye toward the adsorption sites. This improved diffusion rate can be accompanied by small size of the adsorbent particles, UVM-7, to improve adsorption yield. However, it would be very useful in terms of industrial point of view, to have a single adsorbent to remove a variety of pollutants. The proposed method can be applied to use a variety of adsorbents and open us a way for treatment of wastewaters which normally contain many types of pollutants.

5. Acknowledgments

The authors would like to thank from Faculty of chemistry, Amirkabir University of Technology, Tehran, Iran.

6. References

- [1] F. I. Vacchi, A. F. Albuquerque, J. A. Vendemiatti, D. A. Morales, A. B. Ormond, H. S. Freeman, G. J. Zocolo, M. V. B. Zanoni, G. Umbuzeiro, Chlorine disinfection of dye wastewater: Implications for a commercial azo dye mixture, *Sci. Total Environ.*, 442 (2013) 302–309.
- [2] M. Anbia, S. A. Hariri, Removal of methylene blue from aqueous solution using nanoporous SBA-3, *Desalination*, 261 (2010) 61–66.
- [3] M. T. Yagub, T. K. Sen, S. Afroze, H. M. Ang, Dye and its removal from aqueous solution by adsorption: a review, *Adv. Colloid Interface Sci.*, 209 (2014) 172–184.
- [4] H. Chaudhuri, S. Dash, A. Sarkar, SBA-15 functionalised with high loading of amino or carboxylate groups as selective adsorbent for enhanced removal of toxic dyes from aqueous solution, *New J. Chem.*, 40 (2016) 3622-3634.
- [5] Z. Wu, Q. Lu, W. H. Fu, S. Wang, C. Liu, N. Xu, D. Wang, Y. M. Wang, Z. Chen, Fabrication of mesoporous Al-SBA-15 as a methylene blue capturer via a spontaneous infiltration route, *New J. Chem.*, 39 (2015) 985-993.

- [6] B. Coasne, Multiscale adsorption and transport in hierarchical porous materials, *New J. Chem.*, 40 (2016) 4078-4094.
- [7] J. F. Gao, J. H. Wang, C. Yang, S. Y. Wang, Y. Z. Peng, Binary biosorption of Acid Red 14 and Reactive Red 15 onto acid treated okara: Simultaneous spectrophotometric determination of two dyes using partial least squares regression, *Chem. Eng. J.*, 71 (2011) 967-975.
- [8] J. F. Gao, Q. Zhang, K. Su, J. H. Wang, Competitive biosorption of Yellow 2G and Reactive Brilliant Red K-2G onto inactive aerobic granules: simultaneous determination of two dyes by first-order derivative spectrophotometry and isotherm studies, *Bioresour. Technol.*, 101 (2010) 5793-5801.
- [9] V. K. Gupta, B. Gupta, A. Rastogi, S. Agarwal, A. Nayak, A comparative investigation on adsorption performances of mesoporous activated carbon prepared from waste rubber tire and activated carbon for a hazardous azo dye--Acid Blue 113, *J. Hazard. Mater.*, 186 (2011) 891-901.
- [10] P. K. Malik, S. K. Saha, Oxidation of direct dyes with hydrogen peroxide using ferrous ion as catalyst, *Sep. Purif. Technol.*, 31 (2003) 241-250.
- [11] M. Anbia, S. A. Hariri, S. N. Ashrafizadeh, Adsorptive removal of anionic dyes by modified nanoporous silica SBA3, *Appl. Surf. Sci.*, 256 (2010) 3228-3233.
- [12] S. Wang, H. Li, L. Xu, Application of zeolite MCM-22 for basic dye removal from wastewater, *J. Colloid Interface Sci.*, 295 (2006) 71-78.
- [13] G. Ciardelli, L. Corsi, M. Marcucci, Membrane Separation for Wastewater Reuse in the Textile Industry, *Resour. Conserv. Recycl.*, 31 (2001) 189-197
- [14] N. Suzuki, J. Liu, Y. Yamauchi, Recent progress on the tailored synthesis of various mesoporous fibers toward practical applications, *New J. Chem.*, 38 (2014) 3330-3335.
- [15] M. Turabik, Adsorption of basic dyes from single and binary component systems onto bentonite: Simultaneous analysis of Basic Red 46 and Basic Yellow 28 by first order derivative spectrophotometric analysis method, *J. Hazard. Mater.*, 158 (2008) 52-64.
- [16] M. Kucharska, J. Grabka, A review of chromatographic methods for determination of synthetic food dyes, *Talanta*, 80 (2010) 1045-1051.
- [17] A. A. Peláez-Cid, S. Blasco-Sancho, F. M. Matysik, Determination of textile dyes by means of non-aqueous capillary electrophoresis with electrochemical detection, *Talanta*, 75 (2008) 1362-1368.
- [18] C. Bosch Ojeda, F. Sanchez Rojas, Recent applications in derivative ultraviolet/visible absorption spectrophotometry: 2009-2011: A review, *Microchem. J.*, 106 (2013) 1-16.
- [19] F. Sánchez Rojas, C. Bosch Ojeda, Recent development in derivative ultraviolet/visible absorption spectrophotometry: 2004-2008: a review, *Anal. Chim. Acta*, 635 (2009) 22-44.
- [20] C. Bosch Ojeda, F. Sanchez Rojas, Recent developments in derivative ultraviolet/visible absorption spectrophotometry, *Anal. Chim. Acta*, 518 (2004) 1-24.
- [21] J. Zolgharnein, M. Bagtash, T. Shariatmanesh, Simultaneous removal of binary mixture of Brilliant Green and Crystal Violet using derivative spectrophotometric determination, multivariate optimization and adsorption characterization of dyes on surfactant modified nano- γ -alumina, *Spectrochim. Acta - Part A Mol. Biomol. Spectrosc.*, 137 (2015) 1016-1028.
- [22] A. Vargas and M. Reyes, Integral solutions to complex problems: climate change, adaptation policies and payment for ecosystem services schemes, *Int. J. Plur. Econ. Educ.*, 3 (2012) 173.
- [23] H. Shir Khanloo, A. Khaligh, F. Golbabaeei, Z. Sadeghi, A. Vahid, A. Rashidi, On-line

- micro column preconcentration system based on amino bimodal mesoporous silica nanoparticles as a novel adsorbent for removal and speciation of chromium (III, VI) in environmental samples, *J. Environ. Health Sci. Eng.* 13 (2015) 1-12.
- [24] H. Shirkhanloo, S.D. Ahranjani, A lead analysis based on amine functionalized bimodal mesoporous silica nanoparticles in human biological samples by ultrasound assisted-ionic liquid trap-micro solid phase extraction, *Journal of pharm. Biomed. Anal.*, 157 (2018) 1-9.
- [25] H. Shirkhanloo, M. Falahnejad, H.Z. Mousavi, On-line ultrasound-assisted dispersive micro-solid-phase extraction based on amino bimodal mesoporous silica nanoparticles for the preconcentration and determination of cadmium in human biological samples, *Biol. Trace Elem. Res.*, 171 (2016) 472-481.
- [26] H. Shirkhanloo, M. Falahnejad, H.Z. Mousavi, Mesoporous silica nanoparticles as an adsorbent for preconcentration and determination of trace amount of nickel in environmental samples by atom trap flame atomic absorption spectrometry, *J. Appl. Spec.*, 82 (2016) 1072-1077.
- [27] C.P. Ye, R. N. Wang, X. Gao, W.Y. Li, CO₂ Capture Performance of supported phosphonium dual amine-functionalized ionic liquids@MCM-41, *Energy Fuels*, 34 (2020) 14379-14387.
- [28] A. Balcha, P.O. Yadav, T. Dey, Photocatalytic degradation of methylene blue dye by zinc oxide nanoparticles obtained from precipitation and sol-gel methods, *Environ. Sci. Pollut. Res. Int.*, 23 (2016) 25485–25493.
- [29] I. Langmuir, THE adsorption of gases on plane surfaces of glass, mica and platinum, *J. Am. Chem. Soc.*, 40 (1918) 1361–1403.
- [30] J. Yu, A. Zou, W. He, B. Liu, Adsorption of mixed dye system with cetyltrimethylammonium bromide modified sepiolite: characterization, performance, kinetics and thermodynamics, *Water*, 12 (2020) 981. doi:10.3390/w12040981



Removal of organic dye compounds in water and wastewater samples based on covalent organic frameworks -titanium dioxide before analysis by UV-VIS spectroscopy

Aida Bahadori^a and Mehdi Ranjbar^{b,*}

^a Student Research Committee, Kerman University of Medical Sciences, Kerman, Iran

^bPharmaceutics Research Center, Institute of Neuropharmacology, Kerman University of Medical Sciences, Kerman, Iran

ARTICLE INFO:

Received 24 Nov 2020

Revised form 5 Feb 2021

Accepted 25 Feb 2021

Available online 30 Mar 2021

Keywords:

Carbon nanostructures,
Carbon organic frameworks,
Dye removal,
Semi degradation-adsorption solid phase extraction,
Titanium dioxide,
UV radiation.

ABSTRACT

A simple and rapid microwave-assisted combustion method was developed to synthesize homogenous carbon nanostructures (HCNS). This research presents a new and novel nanocomposite structures for removal of methylene red (2-(4- Dimethylaminophenylazo) benzoic acid), methylene orange (4-[4-(Dimethylamino) phenylazo]benzenesulfonic acid sodium salt) and methylene blue (3,7-bis(Dimethylamino)phenazathionium chloride) with semi degradation-adsorption solid phase extraction (SDA-SPE) procedure before determination by UV-VIS spectroscopy. A covalent organic frameworks (COFs) with high purity were synthesized and characterized by X-ray diffraction (XRD) and scanning electron microscopy (SEM). The results indicated that the self-assembled carbon nanostructures (COFs) synthesized with the cost-effective method which was used as a novel adsorbent for adsorption of dyes after semi-degradation of methylene red, orange and blue (1-5 mg L⁻¹) as an organic dye by titanium dioxide (TiO₂) nanoparticles in presence of UV radiation. Based on results, the COFs/TiO₂ has good agreement with the Langmuir adsorption isotherm model with favorite coefficient of determination (R²= 0.9989). The recovery of dye removal based on semi-degradation/adsorption of COFs/TiO₂ and adsorption of COFs were obtained 98.7% and 48.3%, respectively (RSD less than 5%). The method was validated by spiking dye to real samples.

1. Introduction

Nanomaterials are particles that are in the size range between 1-100 nm. The importance of nanomaterials in terms of strength is the presence of active sites and their low density. Nanomaterials have a wide range of applications in optical data storage, sensors, light and durable building materials, and wastewater treatment. The gained

importance of the conventional heating methods (CHM) is due to the microwaves interact with the reactants at the molecular level. By CHM, the electromagnetic energy is transferred and converted to heat by rapid kinetics through the motion of the molecules [1-3]. Today, the conservation of water resources has been increasingly considered by various international organizations such as WHO, FDA and EPA. By increasing of population growth as a result of over-exploitation of limited water resources and on the other hand, water pollution due to various biological, agricultural

*Corresponding Author: [Mehdi Ranjbar](mailto:Mehdi.Ranjbar@kmu.ac.ir)

Email: Mehdi.Ranjbar@kmu.ac.ir

<https://doi.org/10.24200/amecj.v4.i01.131>

and industrial activities caused to water crisis in future years. Methylene organic compounds such as methyl red, methyl orange and methyl blue are the photoactive phenothiazine dyes [4-6]. Paints are one of the main and most important pollutants that are used in various industries to dye related products. Therefore, a significant amount of pollution caused by pigments is produced due to their extensive release into the effluent. The presence of these dyes in water is inappropriate even at very low concentrations and causes widespread environmental pollution by pharmaceutical industries[7]. Recently, many methods based on nanostructure materials was used for removal organic compounds. Hence, a simple and rapid microwave assisted combustion technique was used for synthesis of CdO nanospheres for removal pollution in waters [6]. Microwave assisted reverse microemulsion process as an easy, low cost and fast method can be used for synthesis of nano emulsions [8]. Photocatalytic degradation of compounds using nanoparticles with ultraviolet light is one of the advanced oxidation methods that is expanding in recent decades [9, 10]. Photocatalyst as a catalyst activated in the presence of light is which absorbs light to produce a chemical reaction in the environment [11, 12]. When the UV rays reach to a surface covered with a photocatalyst the electron-cavity can react with molecules on the surface of the particles[13]. Bio photocatalytic materials[14] as a kind of photocatalyst was used in water purification based on degradation and adsorption process[15], during the adsorption process, solute molecules are removed from the solution and adsorbed by the adsorbent. Most of the molecules are adsorbed on the surface of the adsorbent pores and small extent on the outer surface of the particles. The adsorption transfer from the solution to the adsorbent continues until the concentration of the solvent remaining in the solution is in equilibrium with the concentration of the solvent adsorbed by the adsorbent. When equilibrium is established, the adsorption transfer stops. Adsorption equilibrium is established in the dynamic sense when the rate of adsorption of the adsorbed component on the surface is equal to its

rate of absorption [16], self-cleaning glasses and organic molecules degradation[17]. Hydrothermal synthesis method has many advantage such as energy storage[18], simplicity[19], low cost[20], better nuclear control[21], pollution-free (because reaction takes place indoors)[22], better diffusivity[23], high reaction speed and better shape control[24]. In recent years, many nanocomposites used for degradation or adsorption of organic dyes[25-27]. The unique structure of the non-ionic surfactant which their unique structure enables them to encapsulate water-soluble and water-repellent materials [28, 29] and organic building constituent units[30]. One of the new techniques in removing emerging pollutants is the use of environmentally friendly modifiers and reducing the bioavailability of pollutants in the environment[31]. In recent years, bio-charcoal has been gradually approbated which as black gold can be used to solve the problem of sustainable development of agriculture and other aspects by the academic community[32], [33], [34], [35]. In this study, the COFs synthesized and used as a novel adsorbent for removal dyes based on SDA-SPE procedure in water samples after semi-degradation of organic dye by titanium dioxide (TiO_2) nanoparticales in presence of UV radiation. The recovery and absorption capacity of dyes with COFs/ TiO_2 were calculated before determined by UV-VIS spectrometer.

2. Experimental

2.1. Instrumental

Varian UV-VIS spectrophotometer was used for this study (Cary 50, USA). UV-VIS spectrophotometer included dual beam, the monochromator, the wavelength ranges between 190–1100 nm, the spectral bandwidth (1.5 nm), the dual Si diode detectors, the quartz over coated optics based on scan rates of $24000 \text{ nm min}^{-1}$ and computer operating system. The Power Consumption of UV-VIS spectrophotometer has supply of 100 - 240 volts AC and frequency 50 - 60 Hz. The condition of UV-VIS spectrophotometers was shown in Table 1. The unique optical design enables to measure dye samples, also, the large or odd-shaped

Table 1. The condition of UV-VIS spectrophotometers

Parameters	Values
Dimensions	477 mm x 567 mm x 196 mm
Height	196 mm
Light Source	Xenon flash lamp (80 Hz)
Maximum Scanning Speed	24,000 nm min ⁻¹
Photometric System	Double beam
Spectral Bandwidth	1.5 nm

samples to be measured. The highly focused beam also provides superior coupling to fiber optics caused to use the UV-Vis in different matrixes. Powder X-ray diffraction (XRD) was prepared by a PRO X-ray diffractometer. Scanning electron microscopy images were obtained using gun design using a point-source cathode of tungsten (SEM, Philips XL 30 FEG). The transmission electron microscope was used for preparation particle size of COFs (TEM, Philips EM 300).

2.2. Materials and Reagents

Reagents were acquired from Sigma Aldrich and Merck companies, Germany. Methanol (HPLC grade), toluene, acetone, hexane and dichloromethane (HPLC grade) were obtained from Merck Ltd. (Germany). More materials used in this study such as methyl red [(CH₃)₂NC₆H₄N-NC₆H₄CO₂H, (2-(4-Dimethylaminophenylazo) benzoic acid, CAS N: 493-52-7], methyl orange [C₁₄H₁₄N₃NaO₃S, 4-[4-(Dimethylamino) phenylazo]benzenesulfonic acid sodium salt, CAS N:547-58-0] and methyl blue [C₃₇H₂₇N₃Na₂O₉S₃, 3,7-bis-Dimethylamino)phenazathionium chloride, CAS N:28983-56-4] were purchased from Sigma company(Germany), C₃H₇NO (DMF) was purchased from Merck company in Germany, without further purification. Benzene-1,4-diboronic acid (95.0 %, CAS N: 4612-26-4) and hexahydroxytriphenylene (C₁₈H₆(OH)₆, CAS N: 4877-80-9, MW 324.3 g mol⁻¹) were purchased Sigma-Aldrich. The B₃O₃ (boroxine, CAS N: 823-96-1)) was prepared From Sigma(Germany). The pH of the water sand wastewater samples were digitally calculated by pH meter of Metrohm (744, Swiss). The pH was

adjusted by favorite buffer solutions (Merck, Germany). The various buffer solutions, the acetate (PH=3.0–6.0), the NaH₂PO₄ / Na₂HPO₄ (pH=6.0–8.0) and NH₃/NH₄Cl (pH=8.0-10) were prepared. After adjusted pH samples, the ultrasonication (Grant, U.K) and the centrifuging (3000-10000 rpm, 3K30 model) was used for extraction and separation nanoparticles from water samples(Sigma, Germany).

2.3. Synthesis of COFs

Covalent organic frameworks (COFs) has two/three dimensional structures(2D,3D) which was generated by reactions between organic precursors. The covalent bonds depended on porous and crystalline form. The COFs is an improvements of organic material based on coordination chemistry. We synthesis COFs was done based on the Yaghi method and COFs framework scaffolds were prepared by the boronate linkages using solvothermal synthetic methods [36-37]. In fact, the synthesis of COFs was obtained by condensation reactions of C₆H₄[B(OH)₂]₂ with C₁₈H₆(OH)₆ and finally the carbon structure of C₉H₄BO₂ (COF₅) produced. Moreover, the two nozzles electrospinning was used to fabricate the scaffolds. The electrospinning experimental setup was a nano model (Tehran, Iran) with two nozzles. The voltage applied at the tip of the needle was 18 kV. The mass flow rates were 0.5 ml h⁻¹, and distance between the tip of the needle and the collector was maintained at 15 cm. The speed of the rotary collector was 400 rpm and scanning distance was 10 cm. Experimental conditions for the preparation of self-assembled carbon nanostructures was shown in Table 2.

Table 2. Experimental conditions of self-assembled carbon nanostructures.

Sample	DMF: H ₂ O (D.R*)	Time (min)	Temp. (°C)	Morphology
1	2:1	4	180	NPs**+ Agglomerate
2	2:1	8	180	NPs+ Agglomerate
3	2:1	8	200	NPs+ Agglomerate
4	2:1	8	200	NPs+ Agglomerate

*Dilution Ratio, **Nanoparticles

2.4. Removal procedure

For each experiment, a dye solution with a concentration of 5 mg per 1000 mL (5 mg L⁻¹) was prepared and 0.5 g of COFs as catalyst was added to it in presence of TiO₂/UV. Then the pH of the solution was adjusted with buffer solution between 3-9 and irradiated with UV radiation. Then, the all samples, was stirred with a magnetic stirrer for 15 min. By SDA-SPE procedure, the amount of dye (5 mg L⁻¹) removed by COFs/TiO₂/UV. First, the dye semi-degradation was obtained in presence of TiO₂/UV and intermediate forms of dyes created in water samples. The dye and intermediate dye were absorbed on COFs with high recovery up to 98.7%. The nanoparticles of adsorbent separated from water solution by centrifuging. Then the dye concentration in remained solution was directly determined by UV-VIS spectrometry. To prevent the reaction of hydroxyl radicals in the sample, some ethanol was added to the test tubes. Validation of methodology was obtained by spiking of real samples by proposed procedure. The recovery of proposed method based on COFs/TiO₂ was achieved for dyes extraction by the below equation. The C_i is the primary concentrations of dye in sample and C_f is the final concentration of dye by SDA-SPE procedure coupled to UV-VIS (n=5, Eq. 1).

$$\text{Recovery (R\%)} = (C_i - C_f) / C_i \times 100 \quad (\text{EQ.1})$$

3. Results and Discussion

3.1. Structural Analysis

By full width of the half maximum (FWHM) based

on the Debay-Scherer equation, the particle size of COFs nanocomposites was obtained approximately 50-100 nm. Figure 1 shows the X-ray diffraction analysis (XRD) of self-assembled carbon nanostructures in different conditions. The results show that by increasing of temperature based on solvothermal method from 180°C to 220°C, the crystallized amount of synthesized carbon nanostructures (COFs) gradually increases. The sharper peaks without any noisy peaks was seen. Interestingly, the position (2θ) of the peaks have not changed, and only the intensity of the peaks increased, which indicates an increase in the degree of purity in products.

3.2. Measurement size (DLS)

By increasing of temperature for COFs nanocomposites with solvothermal method, the sintering process and crystallization of COFs was increased and caused to smaller size of nano structures. DLS analysis was displayed in Figure 2.

3.3. Morphological and pore characteristics

Microscopic morphology and particle-size distribution (PSD) of the products were visualized by scanning electron microscopy (SEM) images. The Figures 3 displays the SEM images of carbon nanostructures of COFs. The morphology of COFs nanocomposites under the influence of biochar concentration change into rods with quantum particles-like on its surface. Results show which biochar concentration has a great impact on particle size of final products.

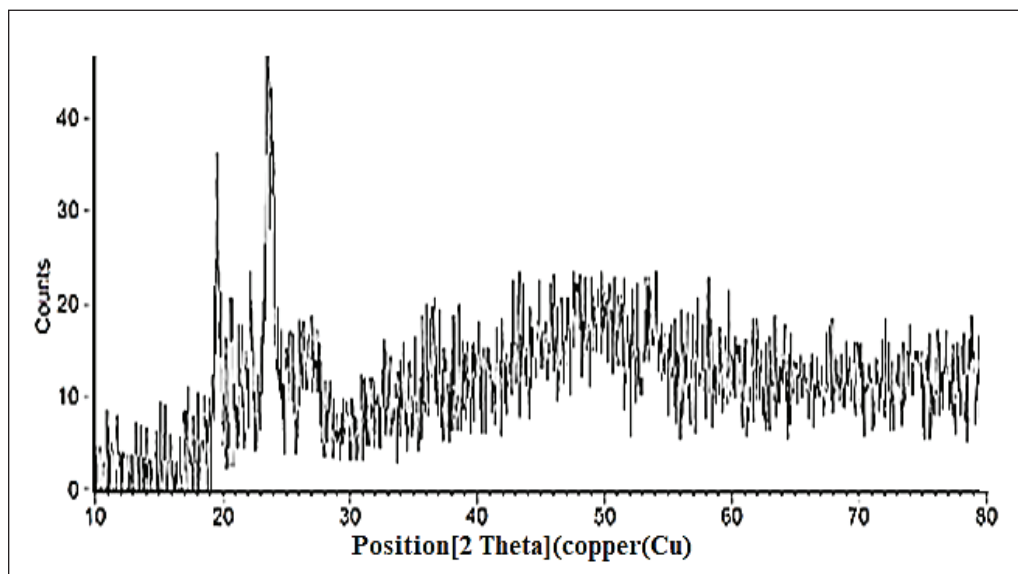


Fig. 1. X-ray diffraction analysis of synthesized self-assembled carbon nanostructures

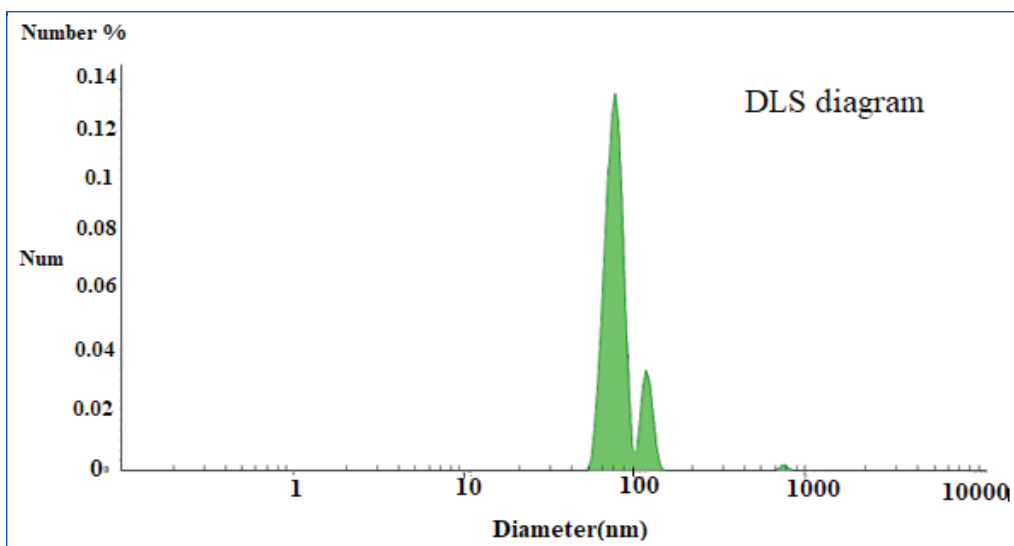


Fig. 2. The DLS diagram related to carbon nanostructures of COFs

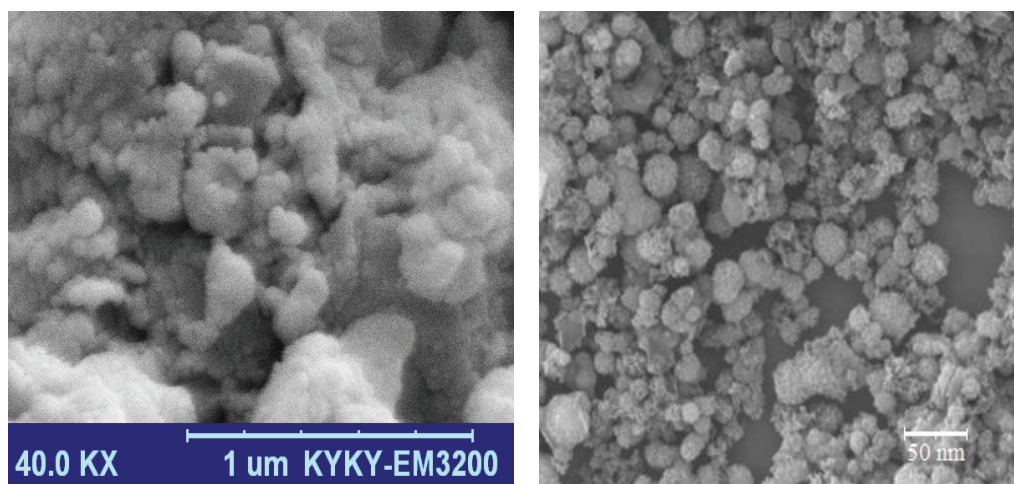


Fig. 3. SEM images of carbon nanostructures of COFs

3.4. Photocatalytic semi-degradation/adsorption and mechanism

The Figure 4 demonstrate the photocatalytic semi-degradation of methylene red, methylene blue and methylene orange organic dyes using COFs/TiO₂ modified with biochar in time cycles (0 min-40 min). The results show that the percent degradation /adsorption of MO is more than 99 % which can be depended on the low steric hindrance of MO structure. Also amount the percent degradation/adsorption of MR is a little more than MB which can also be related to low steric hindrance of MR structure ratio to MB. By reducing of time contact of photocatalyst with organic dyes, the extraction recovery of dyes decreased up to 40-54 % by SDA-SPE procedure. TiO₂ a highly efficient photocatalyst has a small band gap energy and relatively positive valance band edge under UV-light irradiation. TiO₂ caused to photogenerated electron-hole pairs and the transfer of the charge carriers. The charge carriers

transferred to the surface of the TiO₂ and react with O₂, H₂O, or OH groups and generated radicals. The decomposition of Dyes was initiated by the attack of •OH on the methyl group of the benzene ring of dye, leading to make a new compound. On the other hand, the presence of COFs can enhance the adsorption ability of the Dye via π - π stacking interaction between the π -electrons of the benzene rings in dye molecules and π -electron rich region of COFs nanostructure.

The effect of pH on the photocatalytic degradation/adsorption of MB, MR and MO organic dyes were revealed in Figure 5. As results the pH don't effected on extraction dyes on COFs/TiO₂ based on UV radiation by SDA-SPE procedure. By procedure, π - π stacking interaction between the π -electrons of the benzene rings in dye molecules and π -electron rich region of COFs nanostructure caused to efficient adsorption after semi degradation process.

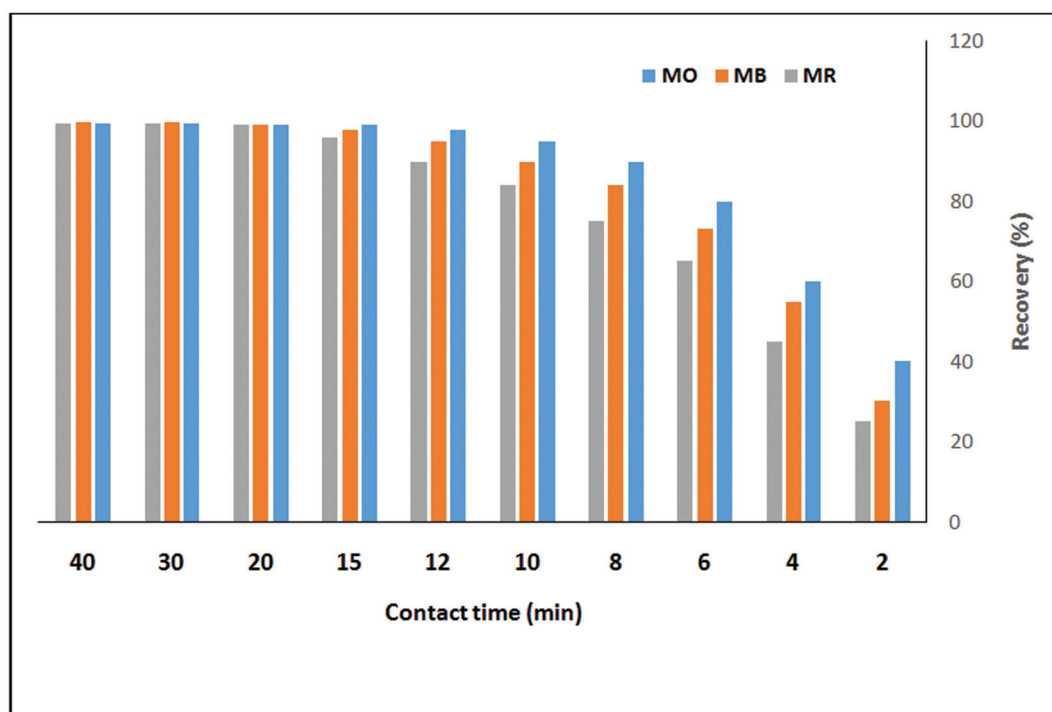


Fig. 4. The effect of time on recovery of adsorption/ photocatalytic degradation of methylene red, methylene blue and methylene orange organic dyes (0 min-40 min)

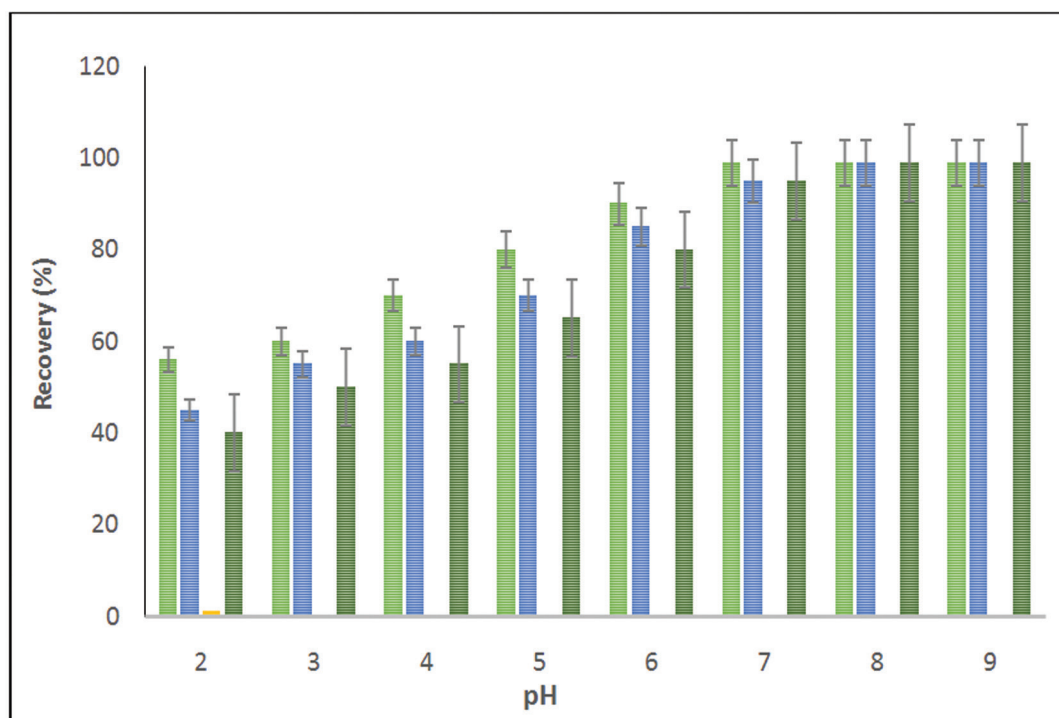


Fig. 5. The effect of pH on the photocatalytic semi-degradation/adsorption of MB(blue), MR(green dark) and MO(green) organic dyes

By increasing of time contact of carbon nanostructures(COFs) with organic dyes for all three dye structures, the degradation/adsorption of dyes initially increased due to high surface area of carbon nanostructures of COFs for photoreaction.

3.5. Kinetic study

Adsorbents in nano sizes of COFs have been shown to have better adsorption performance compared to other materials due to their high specific surface area, small size, and lack of internal penetration resistance. The most widespread models of surface adsorption isotherms for discontinuous systems are the Langmuir and Freundlich models. By the proposed procedure the R^2 for COFs/TiO₂ was achieved about 0.9988 and 0.9575 for the Langmuir and Freundlich models. So, the Langmuir model selected and used for this work. Most nanosorbents follow the Langmuir adsorption isotherm model, which can be evidence of the homogeneity of their surfaces and the fragmentation of the adsorption process. Quasi-first-order and quasi-second-order synthetic models were well used to describe the dye

adsorption process on the surface of nanosorbents. Large amounts of adsorption rate constants in both models can indicate rapid adsorption of dye molecules. After desorption, the nanosorbent can be used for several cycles (23 N).

3.6. Validation of method

The validation of SDA-SPE method based on COFs and COFs/TiO₂ in present of UV irradiation is important to evaluate the correct statistical results for extraction dye from waters. In SDA-SPE method, 5 mg L⁻¹ of dyes was made and used for extraction dyes from water samples and validated by spiking of standard solution to real samples (Table 3).

4. Conclusions

In this study, COFs and COFs-TiO₂ as a novel sorbent based on UV radiation was used for dye removal/extraction from water samples by SDA-SPE procedure. Based on results, the applied, fast, sensitive method based on COFs/TiO₂/UV was demonstrated. The semi degradation/adsorption

Table 3. Validation dye extraction based on COFs/TiO₂ and COFs by spiking of real samples

Sample	Added	Dye	Conc. COFs	Conc. COFs/TiO ₂	Recovery (%) COFs	Recovery (%) COFs/TiO ₂
Wastewater	----	MO	1.12 ± 0.07	1.86 ± 0.11	----	----
	1.5	MO	2.59 ± 0.13	3.39 ± 0.17	0.98	102
Wastewater	----	MR	2.64 ± 0.12	3.83 ± 0.19	----	----
	2.5	MR	5.11 ± 0.23	6.26 ± 0.27	98.8	97.2
Wastewater	----	MB	0.95 ± 0.04	1.74 ± 0.08	----	----
	1.0	MB	1.96 ± 0.12	2.70 ± 0.14	101.2	0.96

of dyes based on COFs/TiO₂/UV had efficient extraction in the optimized conditions. According to the evidence of morphological and COFs characterization such as, XRD, SEM and DLs, the dyes were efficiently removed from water samples. The results showed us, the activity and reaction of COFs/TiO₂/UV were more than COFs, primary carbon structure and TiO₂ in optimized conditions. Therefore, the fast, simple and efficient method based on SDA-SPE was used for removal of dye from waters by nanotechnology.

5. Acknowledgments

Authors are grateful to council of Chemistry and Pharmaceutical Sciences and Cosmetic Products Research Center, Kerman University of Medical Sciences, Kerman, Iran with grant number 98000651.

6. References

- [1] S.A. Khayyat, Photocatalytic oxidation of phenolic pollutants and hydrophobic organic compounds in industrial wastewater using modified nonosize titanium silicate-1 thin film technology, *J. Nanosci. Nanotechnol.*, 14 (2014) 7345-7350.
- [2] C.D. Raman, S. Kanmani, Textile dye degradation using nano zero valent iron: a review, *J. Environ. Manage.*, 177 (2016) 341-355.
- [3] Z.A. Mirian, A. Nezamzadeh-Ejhieh, Removal of phenol content of an industrial wastewater via a heterogeneous photodegradation process using supported FeO onto nanoparticles of Iranian clinoptilolite, *Desalin. Wat. Treat.*, 35 (2016) 16483-16494.
- [4] K. Ordon, Functionalized semiconducting oxides based on bismuth vanadate with anchored organic dye molecules for photoactive applications, Le Mans, 2018.
- [5] I.A. Packiavathy, Antibiofilm and quorum sensing inhibitory potential of Cuminum cyminum and its secondary metabolite methyl eugenol against Gram negative bacterial pathogens, *Int. Food Res. J.*, 1 (2012) 85-92.
- [6] R. Saravanan, Visible light degradation of textile effluent using novel catalyst ZnO/ γ -Mn₂O₃, *J. Taiwan Ind. Chem. Eng.*, 45 (2014) 1910-1917.
- [7] J. Xu, Magnetic properties and methylene blue adsorptive performance of CoFe₂O₄/activated carbon nanocomposites, *Mater. Chem. Phys.*, 147 (2014) 915-919.
- [8] Y. Xu, Holey graphene frameworks for highly efficient capacitive energy storage, *Nat. communications*, 5 (2014) 1-8.
- [9] G. Matafonova, V. Batoev, Recent advances in application of UV light-emitting diodes for degrading organic pollutants in water through advanced oxidation processes: A review, *Water Res.*, 132 (2018) 177-189.
- [10] M. Borges, Photocatalysis with solar energy: Sunlight-responsive photocatalyst based on TiO₂ loaded on a natural material for wastewater treatment, *Solar Energy*, 135 (2016) 527-535.

- [11] M. Pelaez, A review on the visible light active titanium dioxide photocatalysts for environmental applications, *Appl. Cat. B: Environ.*, 125 (2012)331-349.
- [12] T.P. Yoon, M.A. Ischay, J. Du, Visible light photocatalysis as a greener approach to photochemical synthesis, *Nat. Chem.*, 2 (2010) 52-57.
- [13] X. Yu, Controllable preparation, characterization and performance of Cu₂O thin film and photocatalytic degradation of methylene blue using response surface methodology, *Mater. Res. Bull.*, 64 (2015) 410-417.
- [14] J. Cao, In situ preparation of novel p-n junction photocatalyst BiOI/(BiO) 2CO₃ with enhanced visible light photocatalytic activity, *J. Hazard. Mater.*, 239 (2012) 316-324.
- [15] H. Aziz, Biomaterials supported with titania as photocatalyst in peat water purification, *J. Chem. Pharm.*, 7 (2015) 192-197.
- [16] P.A.F. Rodrigues, M.J. Galdes, N.J. Belino. Legionella: Bioactive nano-filters for air purification systems. in 1st portuguese biomedical engineering meeting, IEEE, 2011.
- [17] T. Choi, J. S. Kim, J.H. Kim, Transparent nitrogen doped TiO₂/WO₃ composite films for self-cleaning glass applications with improved photodegradation activity, *Adv. Powder Technol.*, 27 (2016) 347-353.
- [18] H. Hayashi, Y. Hakuta, Hydrothermal synthesis of metal oxide nanoparticles in supercritical water, *Mater.*, 3 (2010) 3794-3817.
- [19] J.Wen, High-temperature-mixing hydrothermal synthesis of ZnO nanocrystals with wide growth window, *Curr. Appl. Phys.*, 14 (2014) 359-365.
- [20] C.-Y.Cao, Low-cost synthesis of flowerlike α -Fe₂O₃ nanostructures for heavy metal ion removal: adsorption property and mechanism, *Langmuir*, 28 (2012) 4573-4579.
- [21] H. Wan, Hydrothermal synthesis of cobalt sulfide nanotubes: The size control and its application in supercapacitors, *J. Power Sour.*, 243 (2013) 396-402.
- [22] X. Xu, Hydrothermal synthesis of cobalt particles with hierarchy structure and physicochemical properties, *Mater. Res. Bull.*, 72 (2015) 7-12.
- [23] J. Chen, S. Wang, M.S. Whittingham, Hydrothermal synthesis of cathode materials, *J. Power Sour.*, 174 (2007) 442-448.
- [24] X.Li, J. Zang, Facile hydrothermal synthesis of sodium tantalate (NaTaO₃) nanocubes and high photocatalytic properties. *J. Phys. Chem. C*, 45 (2009) 19411-19418.
- [25] S. Farhadi, F. Siadatnasab, A. Khataee, Ultrasound-assisted degradation of organic dyes over magnetic CoFe₂O₄@ ZnS core-shell nanocomposite, *Ultrasonics Sonochem.*, 37 (2017) 298-309.
- [26] M. Eghbali-Arani, Ultrasound-assisted synthesis of YbVO₄ nanostructure and YbVO₄/CuWO₄ nanocomposites for enhanced photocatalytic degradation of organic dyes under visible light, *Ultrasonics Sonochem.*, 43 (2018) 120-135.
- [27] E. Costa, P.P. Zamora, A.J. Zarbin, Novel TiO₂/C nanocomposites: synthesis, characterization, and application as a photocatalyst for the degradation of organic pollutants, *J. Colloid Interface Sci.*, 368 (2012) 121-127.
- [28] J. Zhu, Two-dimensional porous polymers: from sandwich-like structure to layered skeleton, *Accounts Chem. Res.*, 51 (2018) 3191-3202.
- [29] Y. Song, A novel ascorbic acid electrochemical sensor based on spherical MOF-5 arrayed on a three-dimensional porous carbon electrode, *Anal. Methods*, 8 (2016) 2290-2296.
- [30] H. Furukawa, The chemistry and applications of metal-organic frameworks, *Sci.*, 341 (2013) 123-146.
- [31] A.U. Czaja, N. Trukhan, U. Müller, Industrial applications of metal-organic frameworks, *Chem. Soc. Rev.*, 38 (2009) 1284-1293.
- [32] M. Larsson, Bio-methane upgrading of pyrolysis gas from charcoal production, *Sustain. Energy Technol. Assess.*, 3 (2013) 66-73.

- [33] B. Shen, Elemental mercury removal by the modified bio-char from medicinal residues, *Chem. Eng. J.*, 272 (2015) 28-37.
- [34] Y.S. Ok, SMART biochar technology: a shifting paradigm towards advanced materials and healthcare research, *Environ. Technol. Innov.*, 4 (2015) 206-209.
- [35] J. Lehmann, J. Gaunt, M. Rondon, Bio-char sequestration in terrestrial ecosystems—a review, *Mitig. Adapt. Strateg. Glob. Chang.*, 11 (2006) 403-427.
- [36] O.M. Yaghi, Reticular Chemistry: Construction, properties, and precision reactions of frameworks, *J. Am. Chem. Soc.*, 138 (2016) 15507–15509.
- [37] O.M. Yaghi, M. O-Keeffe, N.W. Ockwig, H.K. Chae, M. Eddaoudi, J. Kim, Reticular synthesis and the design of new materials, *Nat.*, 423 (2003) 705-714.



Benzene extraction in environmental samples based on the mixture of nanoactivated carbon and ionic liquid coated on fused silica fiber before determination by headspace solid-phase microextraction-gas chromatography

Afsaneh Afzali^{a,*}, Hossein Vahidi^b and Saeed Fakhraie^c

^a Department of Environment, Faculty of Natural Resources and Earth Sciences, University of Kashan, Kashan, Iran

^b Department of Environment, Institute of Science and High Technology and Environmental Sciences, Graduate University of Advanced Technology, Kerman, Iran

^c Chemistry Department, Yasouj University, P.O. Box 7483-75918, Yasouj, Iran

ARTICLE INFO:

Received 2 Nov 2020

Revised form 8 Jan 2021

Accepted 11 Feb 2021

Available online 29 Mar 2021

Keywords:

Soil and vegetables,
Nano activated carbon,
Ionic liquid,
Headspace solid phase microextraction,
Gas chromatography spectrometry

ABSTRACT

In this study, the mixture of nano activated carbon (NAC) and ionic liquid (3-triphenylphosphonio-propane-1-sulfonate; $C_{21}H_{21}O_3PS$) was coated on fused silica fiber of SPME holder (NAC-IL-FSF/SPME). Then NAC/IL was used for determining of benzene in soil and vegetables samples (1.0 g, $n=50$) surrounding a chemical industry zone. After benzene adsorption on NAC-IL based on head space solid phase microextraction (HS-SPME), the concentration of benzene was simply determined by introducing probe to injector of gas chromatography with flame-ionization detection (GC-FID). All effected parameters such as the sorbent mass, the amount of sample, the temperature, and the interaction time were optimized in glass chromatography vials by static procedures. The benzene vapor was absorbed from soil and vegetables samples with NAC-IL-FSF/SPME holder for 10 min at 80°C (10 mg of NAC and 0.1 g of ionic liquid in 0.5 mL of acetone coated on FSF). Then the benzene was desorbed and determined by GC-FID spectrometry. The extraction efficiency and absorption capacity of adsorbent were obtained 98.5% and 127.2 mg g⁻¹, respectively. The high surface area of NAC and favorite interaction of aromatic chain in IL (π - π), caused to efficiently remove of benzene vapor by HS-SPME procedure as compared to other nanostructures.

1. Introduction

Recently different sources of volatile organic compounds (VOC's) such as benzene released in atmospheric air. VOC's consist of dangerous compounds which were produced due to the leaking gasoline vapor from the car engine or

other chemical activity [1-4]. The main material of refrigerants, plastics, adhesives, paints, and petroleum products is composed of VOCs [5]. VOC's such as benzene effect on human health and caused cancer in human body [6-8]. For many years, the analysis of trace volatile organic compounds (VOCs) in exhaled breath could potentially provide rapid screening procedures to diagnose and monitor the diseases of the lungs. The previous research showed that the earlier detection VOCs with GC-

*Corresponding Author: [Afsaneh Afzali](mailto:Afsaneh.Afzali@kashanu.ac.ir)

Email: a.afzali@kashanu.ac.ir

<https://doi.org/10.24200/amecj.v4.i01.134>

MS caused to decrease the different types of cancer in human body. The most diagnostic tools cannot detect the cancer disease in primary stages. Various types of biomarkers including peptides, DNA, RNA, and cells are used in the diagnosis of cancer in human body [9]. The high concentration of BTEX (benzene, toluene, Ethylbenzene, Xylenes) can be absorbed by skin, lungs and gastrointestinal system from air, waters and foods. The VOCs can be accumulated in liver, renal, and CNS and caused to dysfunction in human organs. Benzene vapor cause to lymphoma, anemia, the acute leukemia in humans and classified as high risk factor material which was reported by international agency for research on cancer (IARC) [10,11]. The different cancers may be generated by exposure to benzene in the indoor air. Among the BTEX compounds, benzene is the most dangerous material and cause to bone damage, dysfunction of CNS, damage of liver and respiratory tract. Based on US occupational safety and health administration (OSHA) and centers for disease control and prevention, national institute for occupational safety and health(NIOSH), the average of 1.0 ppm benzene in air was selected as the permissible exposure limit (PEL) [12]. Many techniques such as extraction, adsorption, degradation, the catalytic oxidation, the adsorptive concentration-catalytic oxidation, the photocatalytic oxidation, and the plasma catalytic oxidation were used for removal and determination of VOCs in water samples [13]. The important sources of benzene include, the petroleum company, benzene tanks, petrochemical factories and gas pipes [14]. Moreover, the low value of BTEX compounds in the water, soil and vegetables is very hazardous and must be controlled [15]. Nanoparticles (NPs) have been highly used for removal of environmental pollutants such as VOCs from air and waters. Due to the unique properties of NPs, the adsorption process was obtained with high efficiency and recovery [16]. The cupric oxide nanoparticles (CuONPs) have been used for adsorptive removal of benzene and toluene from aqueous environments [17]. Due to previous studies, the different methods such as, adsorption [18,19], the photo-catalytic oxidation and thermal

oxidation [20] were used for removal of VOC's or BTEX in environment matrixes. Teimoori et al (2020) showed that the benzene can be extracted and determined in waters and wastewater samples based on functionalized carbon nanotubes (R-CNTs) using GC-FID. They observed that under optimal conditions, the adsorption efficiency of CNTs@PhSA and CNTs for benzene was obtained 97.7% and 20.6 % in water samples, respectively [15]. Recently, the activated carbon based on micro pores and heterogeneous surface functional groups was used for benzene extraction in environmental samples such as water and wastewater samples [21, 22]. Also, the activated carbon was most commonly used as absorbent for VOC's removal from air and waters. By previous researches, the adsorption capacity of activated carbon was reported and depended on its surface area, pore volume, porosity and chemical functional groups. In addition, the other nano-carbon structures such as MWCNTs, graphene (NG) and carbon quantum dots (CQDs) were used for BTEX removal from environment matrixes [23, 24].

In this study, the novel adsorbent based on NAC-IL coated on FSF/SPME holder was used for benzene extraction/separation/determination in soil and vegetables samples by HS-SPME procedure coupled to GC-FID. Validation methodology was confirmed by spiking of samples.

2. Experimental

2.1. Apparatus

Gas chromatography based on air /gas loop injection with flame ionization detector was used for benzene analysis in air (Agilent GC, 7890A, GC-FID, Netherland). The sampling valves introduced a sample into the carrier gas stream and valves were also used to inject sample gases/ liquids in gas streams. The split/split less injector, FID detector, and a column of PDS (50 m × 0.2 mm; poly dimethyl siloxane) were selected for benzene determination by Agilent GC. The ultra-pure hydrogen gas (H₂) with flow rate of 1.0 mL min⁻¹ was used as a carrier gas. For batch or static system, the different volumes of PTFE vials (parker) were purchased from Sigma, Germany.

2.2. Reagents and Materials

All chemicals were purchased from Merck, and Sigma Aldrich companies, Germany. The stock solution of benzene (ppm, mgL^{-1}) was prepared (0.1, 0.2, 0.5, 1.0, 1.5, 2.0, 2.5, 3.0 ppm) and placed on vials as calibration curve of benzene by HS-SPME-GC-FID procedure. Benzene solution (99.7%) was purchased from Sigma and then, the eight solutions of benzene as standard calibration were prepared before proposed procedure. The other chemicals such as HNO_3 , HCl, acetone, methanol and ethanol with high purity (99%, GC grade) were purchased from Merck (Germany). The sorbent of NAC was synthesized by RIPI Nano laboratory. The NAC (≈ 50 nm), with 80% purity were synthesized. The characterizations of NAC were achieved by different spectra such as XRD, SEM and TEM. Ionic liquid (3-triphenylphosphonio-propane-1-sulfonate; $\text{C}_{21}\text{H}_{21}\text{O}_3\text{PS}$; CAS N: 116154-22-4, MW:384.43, 5 g) Was purchased from Sigma Aldrich, Germany (Fig. 1).

2.3. Synthesis of Nano activated carbon (NAC)

Activated carbons (ACs) was synthesized by the carbonized method for 2.0 h at 600 °C by activating at 900 °C in a furnace. The carbonized chars were followed by typically heats biomass feedstock in a kiln (pyrolysis) at temperatures between 300-800°C by Ar gas. The produced material was also known as charcoal (porous). Firstly, 20 g of raw powders prepared and placed in the porcelain crucible, then was heated up to 600°C per minute and hold for 2.0 hours. By decreasing temperature up to 25°C, the product is ready for weight. The activation of ACs based on microwave heating method caused to create the Nano activated carbon (NAC) by previous works. First, the carbonized sample was mixed with KOH (CS/KOH; ratio 1:3; wt/wt). By heating, the NAC was carried out at 800 °C (rate: 25 °C/min; hold: 1h) in a tube furnace and cooling down to room temperature under N_2 flow rate (0.5 Lmin^{-1}) [25,26].

2.4. Characterization

X-ray diffraction (XRD) patterns were recorded on a Seifert TT 3000 diffractometer (Ahrensburg, Germany) using nickel filtered $\text{Cu-K}\alpha$ radiation of wavelength 0.1541 nm. The textural properties of the sorbent including surface area, pore volume, and pore size distribution were determined by nitrogen adsorption-desorption isotherms using BELSORP-mini porosimeter (Bell Japan, Inc.). Prior to analysis, the samples were degassed under vacuum at 300 °C for 4 hours until a stable vacuum of 0.1 Pa was reached. The specific surface areas and pore volume of the sorbents were calculated by the Brunauer-Emmett-Teller (BET) and Barrett-Joyner-Halenda (BJH) methods, respectively. The BET surface area of NAC was determined using a Micrometrics ASAP 2010 system. Scanning electron microscopy (SEM, Phillips, PW3710, Netherland) was used for surface image analysis of the sorbents. The morphology of sorbent was examined by transmission electron microscopy (TEM, CM30, Philips, Netherland).

2.5. Benzene Extraction Procedure

By procedure, 10 mg of NAC and 0.1 g of ionic liquid in 0.5 mL of acetone were mixed in glass tube. Then FSF was put into mixture and temperature increased up to 55°C. After vaporization of acetone, the NAC/IL was coated on FSF/SPME holder. When the probe of NAC-IL-FSF/SPME fixed in head space of GC vial, 1 g of powder samples (soil, vegetables) were placed in the bottom of vial and were closed in glass vial, tightly. The temperature of vial was increased up to 80°C by heat power accessory and benzene in soil and vegetables samples which were vaped/adsorbed by NAC/IL-SPME in head space of vial for 10 min. Then, the probe of NAC/IL introduced to injector of GC and benzene was determined by GC-FID (Fig. 1). The temperatures of GC injector and detector were tuned up to 200°C and 240°C, respectively. The temperature programming of oven was adjusted between 50- 220°C for 20 min. Based on results, benzene can be efficiently absorbed on the NAC/IL adsorbents with high recovery of more than 95%. The concentration of benzene according to the calibration curve was calculated and evaluated.

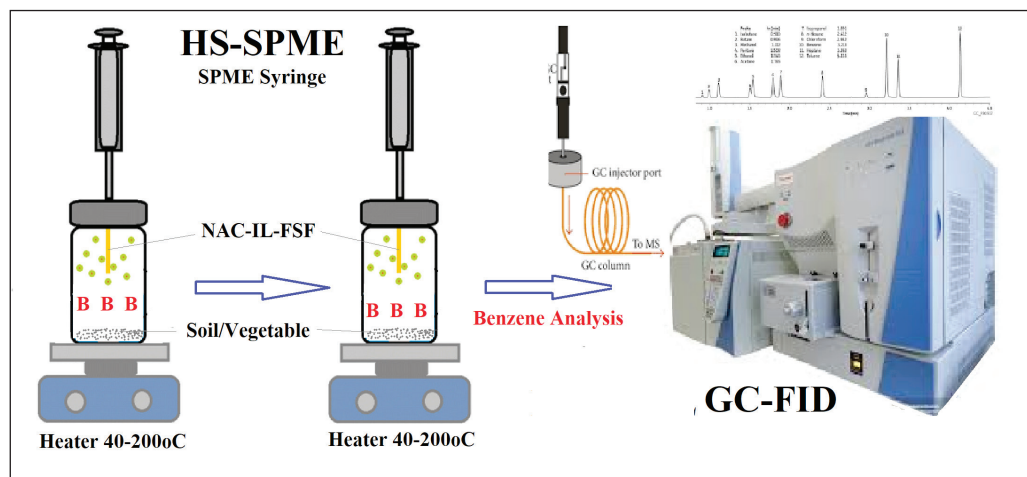


Fig.1. The procedure of benzene extraction in soil and vegetables samples based on NAC-IL-FSF/SPME by HS-SPME/GC-FID

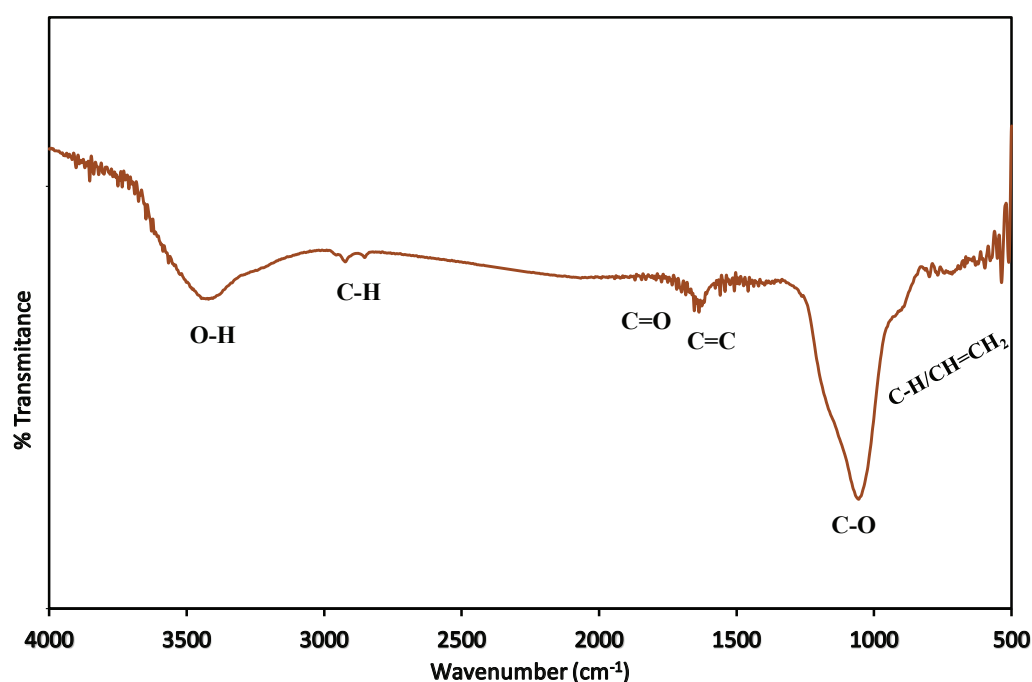


Fig.2. The FTIR spectrum of NAC

3. Results and Discussion

3.1. FTIR of ACNPs

The FTIR spectrum of NAC was shown in Figure 2. The band at 3430 cm⁻¹ was related to the stretching vibration of OH group. The band at 2909 cm⁻¹ and 2839 cm⁻¹ were related to asymmetric and symmetric C-H stretching vibration of CH₂ bond.

The C=O stretching of COOH group shown in Figure 2 at 1710 cm⁻¹ bond and peak at 1058 cm⁻¹ was related to the C-O vibration mode. The peak at 1613 cm⁻¹ belonged to C=C bond in benzene rings which was characterized by stretching vibration. The bands from 500 cm⁻¹ to 850 cm⁻¹ belonged to C-H and CH=CH₂ vibrations in aromatic rings.

3.2. SEM and TEM of NAC

FE-SEM and HR-TEM were used for morphological study of prepared NAC. The FE-SEM images of the synthesized NAC sample was shown in Figure 3. The FE-SEM images of NAC sample displayed small broken pieces of particles with irregular shapes, which can significantly affect the pore characteristics (e.g., pore size distribution and average pore diameter, Fig.3a). The NAC appeared to have many different sizes of pores, indicating that the structure had been destroyed and a dense porosity was formed through KOH activation. In order to observe the structure of NAC adsorbents, HR-TEM imaging was used. The HR-TEM image (Fig.3b) clearly shows the graphene-like structure with a 2D morphology, and the image with 50 nm scale confirms the existence of intermittent graphitic layers and porous structure.

3.3. Optimization of benzene extraction

All effected parameters such as the sorbent mass, amount of sample, the temperature, kind of ionic liquid, and time interaction were optimized in glass vials by static procedures. The benzene vapor was absorbed/extracted from 1 g of soil and vegetables samples with NAC-IL-FSF/SPME prob.

3.3.1. The effect of NAC and IL amount

As high extraction, the amount of NAC and IL coated on FSF has been optimized for benzene concentration between 0.1- 3.0 mg g⁻¹. Therefore, 2-25 mg of NAC and 0.02-0.2 g of ionic liquid in 0.5 mL of acetone were coated on FSF for benzene extraction in food, vegetable, and soil samples by the HS-SPME procedure which was coupled to GC-FID. The results showed the high recovery for soil/food /vegetable samples were obtained by 8 mg of NAC and 80 mg of ionic liquid for benzene adsorption by purposed procedure. So, 10 mg of NAC and 100 mg of ionic liquid coated on SFS was used for further work (Fig.4). The extra amount of NAC and ionic liquid had no effect on the extraction/adsorption efficiency of benzene from soil, food and vegetable samples.

3.3.2. The effect of temperature

The temperature is the main parameter for adsorption and desorption benzene from adsorbent by HS-SPME/GC-FID. The results showed the best adsorption of benzene from 1 g of powder soil and vegetables was achieved at 60-80°C in batch system for 10 min. After 10 min, extra time had no effect on the adsorption efficiency of benzene by NAC-IL-FSF. Also, increasing temperature more than 80°C caused to reduce adsorption efficiency by NAC/

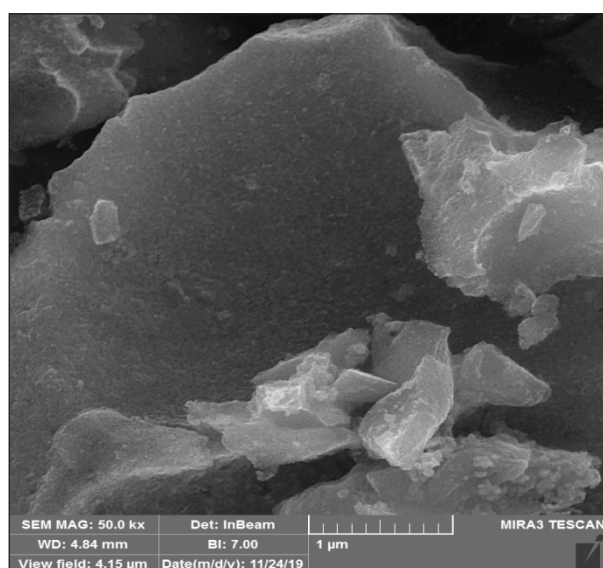


Fig.3a. The FE-SEM images of NAC sample

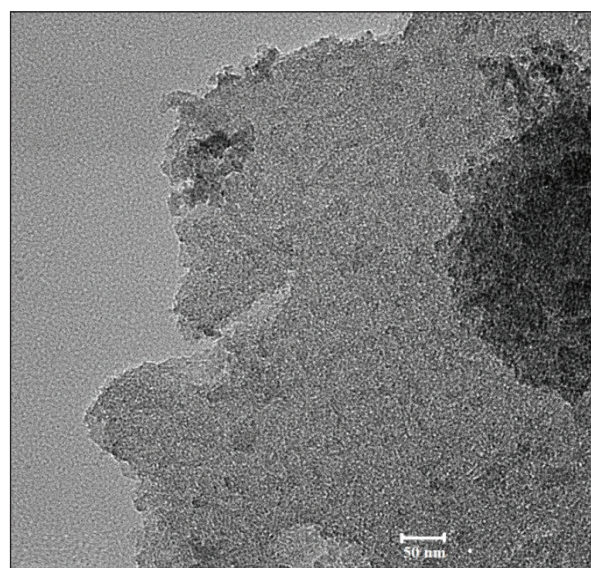


Fig.3b. The HR-TEM images of NAC sample

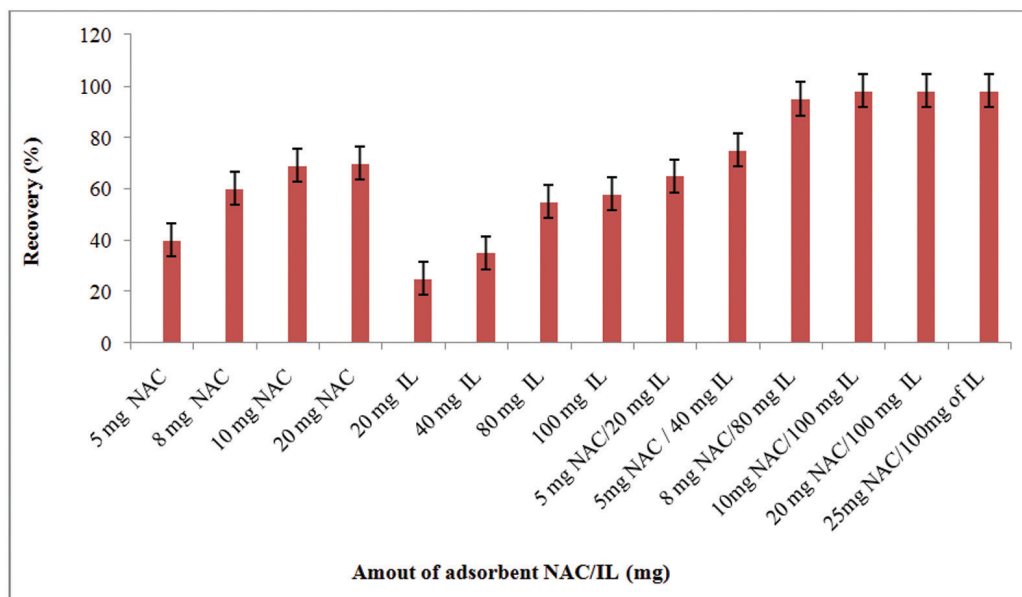


Fig. 4. The effect of NAC- IL amount for benzene extraction based on NAC-IL-FSF/SPME in soil/food /vegetable samples by HS-SPME/GC-FID

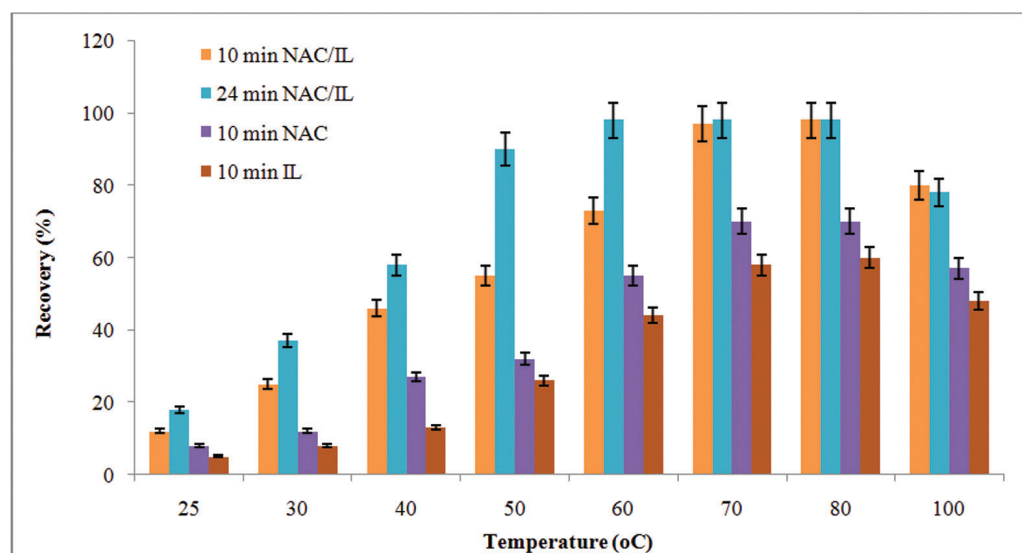


Fig. 5. The effect of temperature for benzene extraction in soil/vegetable samples based on NAC-IL-FSF/SPME by HS-SPME/GC-FID

IL. So, 70°C was selected as optimum temperature for benzene adsorption by NAC/IL in batch system (Fig. 5). Moreover, the adsorbed benzene on NAC-IL-FSF based on HS-SPME can be desorbed in injector of GC-FID at 200°C in presence of N₂ or Ar gas. The temperature programming of oven was adjusted between 50-220°C for 20 min. The results showed that by decreasing temperature less than 60°C, the recovery decreased up to 72.2% for 10 min and increased more than 95% for 24 min. In addition, after vaporization benzene in vial air hold for 2-3 min at 70-80°C and

then the temperature in batch system reduced up to 50°C for 7 min. Finally, the absorbed benzene on SFS probe was desorbed and determined by introducing to injector of GC-FID. The extraction efficiency and the absorption capacity of NAC/IL were obtained more than 95% and 127.2 mg g⁻¹, respectively. The results showed that the absorption capacity of NAC and IL were separately achieved at 72.6 mg g⁻¹ and 58.3 mg g⁻¹, respectively. So, in dynamic system, the values depended on flow rate of gas which was lower than batch system and must be optimized.

3.3.3. The effect of reaction time

Due to boiling point of benzene and vaporization at low temperature, it can adsorb on NAC/IL adsorbent in different time. The results showed that at low and favorite temperature the reaction time between benzene and adsorbent decreased and increased, respectively. By optimization, the minimum time for efficient recovery was obtained for 10 min at 70-80°C. When, the temperature reduced up to 50°C, all of benzene mass can be adsorbed on NAC/IL at 24.5 min. Therefor the reaction time depended on π - π interaction in aromatic chain of IL or NAC and physical adsorption of NAC. On the other hand, there is relationship between temperature and π - π interaction and best recovery was obtained for 10 min at 70-80°C.

3.3.4. The effect of different ionic liquids

The effect of different ionic liquids for benzene extraction from soil and vegetables was evaluated. So, the different ionic liquids such as [EMIM][PF6], [BMIM][PF6], [HMIM][BF4] and [PPP][S] as (3-triphenylphosphonio-propane-1-sulfonate; C₂₁H₂₁O₃PS) were mixed with NAC and dilution diluted with 0.5 mL of acetone. Then, the acetone was vaped at 55°C and IL/NAC were coated on fused silica fiber of SPME holder (NAC-

IL-FSF/SPME). The adsorbent was used for benzene extraction by HS-SPME/GC-FID. The results showed that the tri-phenyl of [PPP][S] with power π - π interaction of aromatic chain and different mass has more interaction with benzene aromatic cycles as compared to imidazolium rings in [EMIM][PF6], [BMIM][PF6] and [HMIM][BF4]. Therefore, [PPP][S]/NAC with ratio of 100 mg/10 mg was used for further work in optimized conditions which was shown in Figure 6.

3.3.5. Validation in real samples

The validation of HS-SPME/GC-FID method based on NAC-FSF/SPME and NAC-IL-FSF/SPME is important factor for extraction of benzene from soil and vegetables. By procedure, 0.1-3 mg L⁻¹ of benzene concentration was used for validation of methodology and the probe of SPME fixed in head space of GC vial. The 25 number of soil, vegetables powders (rice, cabbage, spinach) and standard solution of benzene were placed in the bottom of vial and were closed in the glass vial, tightly. All samples were validated by spiking of real samples with standard solutions based on NAC/IL-FSF/SPME probe by HS-SPME/GC-FID (Table 1 and 2). Finally, extraction efficiency was calculated by

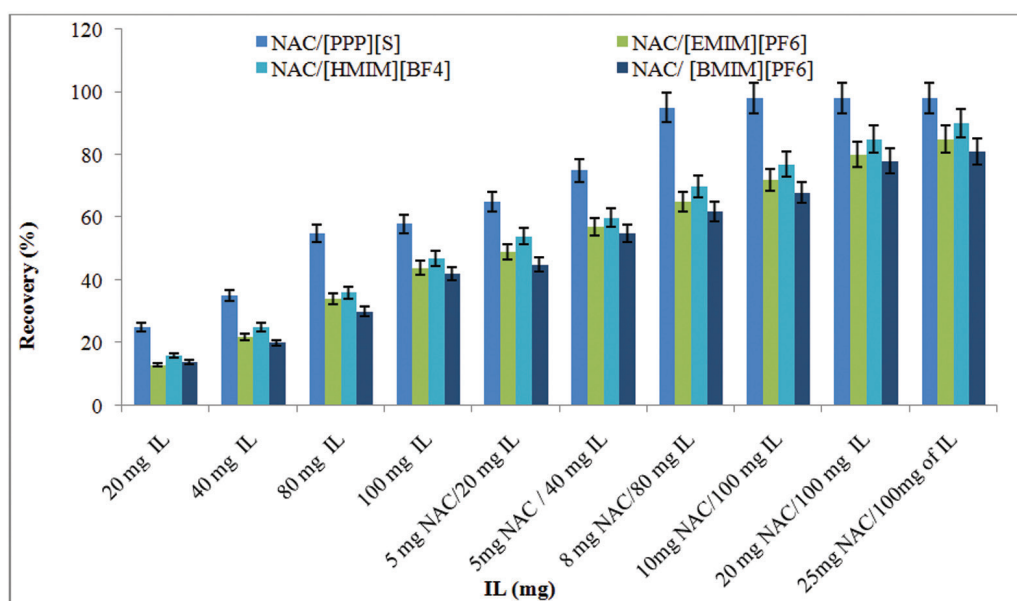


Fig. 6. The effect of different ionic liquids for benzene extraction in soil/food /vegetable samples based on NAC-IL-FSF/SPME by HS-SPME/GC-FID

Table 1. Validation of HS-SPME/GC-FID method based on NAC/IL-FSF/SPME for benzene extraction from soil and vegetables (1 g) near chemical industry

Samples	Benzene std. (mg L ⁻¹)	*Found Method (mg L ⁻¹)	Recovery (%)
A-Soil	----	2.45 ± 0.09	----
	2.0	4.40 ± 0.23	97.5
B-Rice	----	0.84 ± 0.05	----
	0.5	1.35 ± 0.06	102.2
C-Cabbage	----	1.32 ± 0.07	----
	1.0	2.28 ± 0.13	96.0
D-Spinach	----	0.76 ± 0.04	----
	0.5	1.24 ± 0.07	95.8
E-Eucalyptus	----	1.85 ± 0.11	----
	2.0	2.83 ± 0.14	98.3

* Mean of three determinations ± confidence interval (P = 0.95, n = 5)

Table 2. Validation of HS-SPME/GC-FID method based on NAC-FSF/SPME for benzene extraction from soil and vegetables (1 g) near chemical industry

Samples	Benzene std. (mg L ⁻¹)	*Found Method (mg L ⁻¹)	Recovery (%)
A-Soil	----	1.72 ± 0.08	----
	1.5	3.19 ± 0.16	98.2
B-Rice	----	0.59 ± 0.03	----
	0.5	1.07 ± 0.05	96.0
C-Cabbage	----	0.91 ± 0.06	----
	1.0	1.93 ± 0.12	102
D-Spinach	----	0.52 ± 0.03	----
	0.5	1.01 ± 0.07	98.0
E-Eucalyptus	----	1.27 ± 0.12	----
	1.5	2.83 ± 0.14	98.3

* Mean of three determinations ± confidence interval (P = 0.95, n = 5)

determining of benzene concentration by GC-FID in soil and vegetables. The efficient recovery of spiked samples had satisfactorily results with high accuracy and precision, which indicated the ability of HS-SPME/GC-FID method based on NAC/IL-FSF/SPME adsorbent for benzene extraction from

environmental samples. After desorption of benzene from NAC/IL-FSF/SPME probe in GC injector, the concentration of benzene was simply determined by GC-FID. For validation, the results based on NAC/IL-FSF/SPME probe with GC-FID were compared to high resolution GC-MS (Table 3).

Table 3. Comparing of proposed procedure with GC-MS based on NAC/IL-FSF/SPME for benzene extraction from soil and vegetables (1.0 g) near chemical industry

Samples	GC-MS (mg L ⁻¹)	*Found Method (mg L ⁻¹)	Recovery (%)
A-Soil	2.52 ± 0.08	2.42 ± 0.12	96.1
B-Rice	0.81 ± 0.04	0.83 ± 0.06	102.4
C-Cabbage	1.35 ± 0.06	1.34 ± 0.07	99.3
D-Spinach	0.80 ± 0.03	0.76 ± 0.05	95.0
E-Eucalyptus	1.88 ± 0.08	1.83 ± 0.13	97.3

* Mean of three determinations ± confidence interval (P = 0.95, n = 5)

4. Conclusions

In this study, NAC/IL-FSF/SPME as a new adsorbent was used for benzene extraction from soil, and vegetables powders by HS-SPME/GC-FID procedure. Based on results, the simple, fast, sensitive and accurate results based on NAC/IL adsorbent were demonstrated. The absorption of benzene based on NAC/IL-FSF/SPME probe had efficient recovery in the optimized conditions (more than 95%). The parameters such as the amount of NAC/IL, the amount of soil and vegetables, the temperature, kind of ionic liquid, and time were studied. In optimized conditions, the maximum adsorption capacity of 127.2 mg g⁻¹, 72.6 mg g⁻¹ and 58.3 mg g⁻¹ for NAC/IL, NAC and IL were obtained respectively, by HS-SPME/GC-FID. The results showed that the activity and reaction of NAC/IL for benzene extraction from soil/vegetables samples were more than NAC and IL in optimized conditions. Therefore, the applied and efficient procedure based on NAC/IL-FSF/SPME probe was used for extraction of benzene in environmental samples.

5. Acknowledgments

The authors would like to thank from Amin Mokhtari Kheirabadi, Research Center for Nuclear Medicine, Tehran University of Medical Sciences, Tehran, Iran, and Hajar Bahrami and Atefeh Rasekh from Faraz Exir Samin Company, Isfahan, Iran.

6. References

- [1] S. Sun, Z. Zhao, J. Shen, Effects of the manufacturing conditions on the VOCs emissions of particleboard, *Bioresour.*, 15 (2020) 1074–1084.
- [2] G.H. Li, W. Wei, X. Shao, L. Nie, H.L. Wang, A comprehensive classification method for VOCs emission sources to tackle air pollution based on VOCs species reactivity and emission amounts, *J. Environ. Sci.*, 67 (2018) 78–88.
- [3] G.D. Thurston, Outdoor air pollution: sources, atmospheric transport, and human health effects, *international encyclopedia of public health*, 2nd ed., Elsevier: Cambridge, MA, USA, 5 (2017) 367–377.
- [4] A.R. Schnatter, DC. Glass, G. Tang, RD. Irons, L. Rushton, Myelodysplastic syndrome and benzene exposure among petroleum workers: an international pooled analysis, *J. Natl. Cancer Inst.*, 104 (2012) 1724-1737.
- [5] K. Zhou, QG. Zhang, GL. Han, AM. Zhu, L. Liu, Pervaporation of water–ethanol and methanol–MTBE mixtures using poly (vinyl alcohol)/cellulose acetate blended membranes, *J. Membrane Sci.*, 448 (2013) 93-101.
- [6] J.E. Chang, D.S. Lee, S.W. Ban, J. Oh, M.Y. Jung, S.H. Kim, S.J. Park, K. Persaud,

- S. Jheon, Analysis of volatile organic compounds in exhaled breath for lung cancer diagnosis using a sensor system, *Sens. Actuators B Chem.*, 255 (2018) 800–807.
- [7] Y. Sun, Y. Chen, C. Sun, H. Liu, Y. Wang, X. Jiang, Analysis of volatile organic compounds from patients and cell lines for the validation of lung cancer biomarkers by proton-transfer-reaction mass spectrometry, *Anal. Methods*, 11 (2019) 3188–3197.
- [8] J. Rudnicka, T. Kowalkowski, B. Buszewski, Searching for selected VOCs in human breath samples as potential markers of lung cancer, *Lung Cancer*, 135 (2019) 123–129.
- [9] T. Ahmad Mir, S. Ibrahim Wani, Early detection of lung cancer biomarkers through biosensor technology: a review, *J. Pharm. Biomed. Anal.*, 164 (2019) 93–103.
- [10] M. Aivalioti, I. Vamvasakis, E. Gidarakos, BTEX and MTBE adsorption onto raw and thermally modified diatomite, *J. Hazard. Mater.*, 178 (2010) 136–143.
- [11] International Agency for Research on Cancer (IARC) monographs on the evaluation of carcinogenic risks to humans. overall evaluations of carcinogenicity, 1–42, 1987.
- [12] T.J. Lentz, M. Seaton, P. Rane, S.J. Gilbert, L.T. McKernan, C. Whittaker, Technical Report: the NIOSH occupational exposure banding process for chemical risk management, US, 2019.
- [13] S. KP Veerapandian, N. De Geyter, J.M. Giraudon, J.F. Lamonier, R. Morent, The use of zeolites for VOCs abatement by combining non-thermal plasma, adsorption, and/or catalysis: a review, *Catalysts*, 9 (2019) 98.
- [14] J.M.M.D. Mello, H. deLimaBranda, A.A.U. deSouza, A. daSilva, Biodegradation of BTEX compounds in a biofilm reactor-Modeling and simulation, *J. Petrol. Sci. Eng.*, 70 (2010) 131–139.
- [15] S. Teimoori, A. Hessam Hassani, M. Panaahie, Extraction and determination of benzene from waters and wastewater samples based on functionalized carbon nanotubes by static head space gas chromatography mass spectrometry, *Anal. Method Environ. Chem. J.*, 3 (1) (2020) 17–26.
- [16] M.J. Lashaki, J.D. Atkinson, Z. Hashisho, J.H. Phillips, J.E. Anderson, M. Nichols, The role of beaded activated carbon's pore size distribution on heel formation during cyclic adsorption/desorption of organic vapors, *J. Hazard. Mater.*, 315 (2016) 42–51.
- [17] L. Mohammadi, E. Bazrafshan, M. Noroozifar, A. Ansari-Moghaddam, F. Barahuie, D. Balarak, Adsorptive removal of benzene and toluene from aqueous environments by cupric oxide nanoparticles: kinetics and isotherm studies, *J. Chem.*, 2017 (2017) 1–10. <https://doi.org/10.1155/2017/2069519>
- [18] J. Cheng, L. Li, Y. Li, Q. Wang, C. He, Fabrication of pillar arene-polymer-functionalized cotton fibers as adsorbents for adsorption of organic pollutants in water and volatile organic compounds in air, *Cellulose*, 26 (2019) 3299–3312.
- [19] R. Ashouri, H. Shir Khanloo, A.M. Rashidi, S.A.H. Mirzahassemi, N. Mansouri, Dynamic and static removal of benzene from air based on task-specific ionic liquid coated on MWCNTs by sorbent tube-headspace solid-phase extraction procedure, *Int. J. Environ. Sci. Technol.*, (2020) 1–14. <https://doi.org/10.1007/s13762-020-02995-4>
- [20] M. Mao, Y. Li, J. Hou, M. Zeng, X. Zhao, Extremely efficient full solar spectrum light driven thermocatalytic activity for the oxidation of VOCs on OMS-2 nanorod catalyst, *Appl. Catal. B*, 174 (2015) 496–503.
- [21] I. Ghouma, M. Jeguirim, S. Dorge, L. Limousy, C. Matei Ghimbeu, A. Ouederni, Activated carbon prepared by physical activation of olive stones for the removal of NO₂ at ambient temperature, *Comptes Rendus Chim.*, 18 (2015) 63–74.

- [22] O. Yahya Bakather, Adsorption of benzene on impregnated carbon nanotubes, *Ain Shams Eng. J.*, 11 (2020) 905-912.
- [23] M. Bagheri, H. Shirkhanloo, J. Rakhtshah, Air pollution control: The evaluation of TerphApm@ MWCNTs as a novel heterogeneous sorbent for benzene removal from air by solid phase gas extraction, *Arab. J. Chem.*, 13 (2020) 1741-1751.
- [24] Y. Liu, J. Zhang, X. Chen, J. Zheng, G. Wang, and G. Liang, Insights into the adsorption of simple benzene derivatives on carbon nanotubes, *RSC Adv.*, 4 (2014) 58036-58046.
- [25] Y. Kan, Q. Yue, B. Gao, Q. Li, Preparation of epoxy resin-based activated carbons from waste printed circuit boards by steam activation, *Mater. Lett.*, 159 (2015) 443-446.
- [26] J.M. Valente Nabais, P.J.M. Carrott, M.M.L. Ribeiro Carrott, J.A. Menéndez, Preparation and modification of activated carbon by microwave heating, *Carbon*, 42 (2004)1315-20.